INTERSTELLAR ABSORPTION BANDS

by

Gordon Ernest Bromage

Ph. D.

University of Edinburgh

1971

Abstract.

New observational profiles of the broad interstellar 'bands' '4430', '4760' and '4890' have been derived by automated spectrophotometry of image tube spectra, for ten reddened late B type supergiants. The presence of an apparent emission wing (that is, a region of decreased interstellar extinction) in the '4430' profile has been confirmed. There is a slight indication of a similar feature on the '4760' profile.

Profiles for diffuse interstellar features in the red have been obtained from photographic spectra of two very heavily reddened stars in the Cygnus OB2 association. One of these is the most heavily reddened star known, Schulte No.12. These spectra show the strongest interstellar features in the red so far reported in any stellar spectra : the unidentified line at λ 628.3 nm. attains a central depth of nearly 50%.

The possibility that the interstellar bands arise from impurities in dust grains has been considered in detail. The classical theory of extinction by small particles containing impurities has been applied to a wide range of grain types, including (for the first time) 'core-mantle' grains, size distributions of absorbing grains, and spheroidal particles. The application to spheroids was made using the 'Second Range of Validity' of the Rayleigh approximation. In addition, combined profiles of blended lines have been calculated, also for the first time.

Direct comparison has been made with the observed profiles of seven diffuse features. Taking into account current opinion as to the composition of interstellar dust, the observations may be explained by the presence of impurities in either silicate grains with effective

radii of about 120 nm., or possibly graphite grains about 50 nm. in radius coated with a thin dielectric condensate. None of the observed profiles are at variance with the hypothesis that all the lines arise from the same impurities in the same type of grains. The concentration of such impurities needed to reproduce the observed line profiles and strengths is only about one in 10^4 atoms in the grain.

Contents.

Contents (contd.)

Contents (contd.)

1. Introduction

1.1 Discovery of the Interstellar Bands

The optical spectrum of starlight is modified by the presence of interstellar material : atoms, molecules and ions absorb light at characteristic wavelengths, giving sharp, narrow lines in the spectra of distant stars; and clouds of tiny solid particles called interstellar grains absorb and scatter light of all wavelengths (and especially short wavelengths) giving a general dimming and reddening of the starlight.

Interstellar lines are usually easily distinguishable from those of stellar origin by their very small width, due to the very low temperature and pressure of the interstellar gas, The first line to be identified as interstellar was the Fraunhofer K line of ionised calcium. J. Hartmann (1904) showed that, of all the lines visible in the spectrum of δ Orionis (a spectroscopic binary), the K line alone remained 'stationary', unaffected by the periodic motion of the star. Fifteen years after Hartmann, Miss M.L. Heger (1919) discovered interstellar sodium D lines, and since then optical line absorptions of the interstellar gas have been identified with many different types of atoms, ions, and molecules, including: Na, K, Fe, Ca, CH, CN, Ca^+, Ti^+ and CH^+. In addition, radio observations have suggested the presence of various molecules, ions, and radicals, including some six-atom molecules. The molecular bands in the optical region are resolved into only one or two sharp, narrow lines under interstellar conditions: for example, the Fraunhofer G

band of CH is seen as only one line, at λ430.03 nm. (McKellar, 1940).

Some interstellar lines, however, are not at all sharp and narrow, but rather diffuse and usually wider than even the stellar lines. These diffuse lines - now called 'Interstellar Absorption Bands', or 'Diffuse Interstellar Absorption Features' (DISAFs) - were discovered and investigated by P.W. Merrill and his colleagues at Mount Wilson in the 1930's. Merrill's first report (Merrill, 1934) proposes an interstellar origin for four lines at λλ 578.0, 579.9, 628.4, and 661.4 nm., all of which are a few tenths of a nanometre in width. An exceptionally broad line near λ443 nm. was pointed out by Merrill two years later (Merrill, 1936), and C.S. Beals and G.H. Blanchet (1938) verified its existence. This line -- usually called '4430' after its wavelength in Ångstrom units -- is undoubtedly the most famous and most discussed DISAF of all. In 1938, Merrill and M.L. Humason demonstrated its 'stationary' nature in the spectrum of a binary, thus locating its origin as extra-stellar. This proof followed similar ones for λλ 578.0, 579.7, and 628.4 nm. lines (Merrill, 1936).

Some of the lines had in fact been seen before 1934, as Merrill and O.C. Wilson (1938) pointed out, but their interstellar nature had not been realised. Miss Heger (1921) saw the lines at λλ 578.0 and 579.7 nm. in the spectra of ξ Persei and (less certainly) ρ Leonis, and noted that they were "possibly stationary". In fact,

even before Hartmann's discovery of the interstellar 'K' line, Miss A.J. Cannon (1901) saw absorption lines at λλ 578.2 and 579.7 nm. in the spectrum of γ Velorum. A.D. Code (1958) thinks that the compilers of the Henry Draper catalogue also saw '4430', but mistook it for Hγ, in the spectrum of HD 80077.

The λ628.4 nm. line in the spectrum of Deneb was separated from the bandhead of the atmospheric oxygen 'α band' at λ627.8 nm. by Wright (1921) for the first time, but again its interstellar nature was not realised. Then, finally, in 1930 Merrill encountered the spectrum of the heavily reddened star HD 183143, and his curiosity was aroused by a number of unidentifiable lines which seemingly could not be interstellar because they were not narrow enough.....

In addition to the five lines already mentioned, Merrill and Wilson (1938) pointed out two more, at λλ620.3 and 627.0 nm.; and an eighth one, in the blue at about λ476 nm., was tentatively proposed by Merrill in private correspondence with Beals (See Beals, 1942).

1.2 Observations of '4430'.

Since 1950 both theoretical and observational work in connection with the unidentified interstellar bands has concentrated on '4430'. Many authors have published lists of '4430' strengths, usually in terms of the maximum absorption, or central depth, A_c, as a percentage of the local stellar continuum intensity.

L. Binnendijk (1952) reviewed the earlier results and combined them all in a graph of $A_c(4430)$ against colour excess.

The first extensive catalogue was that of D. Duke (1951), who measured $A_c(4430)$ in over 400 stars. Duke confirmed the result of W.W. Morgan (1939) that $A_c(4430)$ is correlated best with colour excess. Other important contributions have been made by G.A.H. Walker (1963), R. Stoeckly and K. Dressler (1964), H. Kristenson and M. Rudkjøbing (1965), E.J. Wampler (1966), Walker and Hodge (1966) and by the contributors to the Edinburgh spectrophotometric survey (Baker, 1949; Butler and Seddon, 1958, 1960; Butler and Thompson 1961). Stoeckly and Dressler (1964) restated an earlier suggestion of Morgan's (1944) that an observed deficiency of '4430' in the spectra of the very hottest stars may be due to preferential evaporation near these stars of the particular grains containing the '4430' line-carriers. Wampler (1963, 1966) and S.A. Kellmann (1970) have found systematic variations of the ratio of Ac(4430) to colour excess with galactic longitude, and between clusters and surrounding fields.

Seven published lists of '4430' strength have been subjected to an interesting statistical analysis by T.J. Deeming and Walker (1967). These authors find that correlations between '4430' and colour excess E_{B-V} are improved substantially if the choice of stars is restricted in spectral type. The strength and shape of '4430' may therefore be much more dependent on the various stellar

lines within and near the band than has often been assumed.

The strongest '4430' ever reported is A_C= 26%, for Cygnus OB2 no. 8A (Svolopoulos, 1963). This result, however, must be considered doubtful since Wampler (1966) gives a value of only 14% for the same star. For the most heavily reddened star known, Cygnus OB2 no. 12, Wampler gives A_C= 19%.

Virtually all the results from photographic spectra - from Beals and Blanchet (1938) to Greenstein and Aller (1950) to Seddon (1967) - indicate a symmetrical absorption profile for '4430'. A slight asymmetry was, however, reported by G.H. Herbig (1966) for the star HD 183143. The photoelectric measurements of Wampler (1966) indicate various asymmetries including emission wings. The most recent photographic determinations, from direct comparisons of spectra of reddened and unreddened stars (Wickramasinghe et al., 1968; Walker et al., 1970; York, 1971) confirm Wampler's general result. Finally, image-tube observations at Edinburgh (Brück and Nandy, 1968) suggest that the presence of a violetward emission wing in the '4430' profile may be quite general. These findings open up again many questions that were once thought finally resolved.

1.3 Observations of Other Lines

In contrast with the abundance of accumulated data on '4430', there have been very few studies of the other lines.

The most comprehensive list of strengths of the lines at λλ 578.0, 579.7, and 628.3 nm. is still that of Merrill, R.F. Sanford, Wilson and C.G. Burwell (1937). Equivalent widths are given in this list for about 130 stars. Strengths of λλ 476.4, 578.0, 579.7, 628.3 and 661.4 nm. for 15 stars are given in the Edinburgh survey (Butler and Seddon, 1958, 1960; Butler and Thompson, 1961). It was during this survey that two new broad DISAFs were discovered, at λ618 nm. (Wilson, 1956) and at λ489 nm., (Butler and Seddon, 1958). The latter was also discovered independently by Wilson (1958a). Equivalent widths of λ618 for 15 stars, and of λ489 for ten of these are given in the papers of Butler and Seddon, and Butler and Thompson, cited above.

A few measurements of λλ578, 618, 620.3, 628.4, and 661.4 nm. lines for four moderately reddened stars of southerly declination have been reported by W. Buscombe and P.M. Kennedy (1968); and D.G. York (1971) has published equivalent widths of the same lines and also λ579.7, for up to thirteen stars. York's values for λλ578, 579.7, and 628.4 are about twice or thrice the earlier estimates of Merrill et al. (1937). The integration regions used by York were much wider, however, and his errors are larger.

The star that originally aroused Merrill's curiosity, HD 183143, has recently been studied spectroscopically in great detail by G.H. Herbig. A total of fifteen new DISAFs, mostly very faint indeed, have been reported by Herbig (1966, 1967; and in private correspondence with F.M. Johnson (1965, 1970)). Five of these can be seen

Table I A summary of the strengths and widths of the known diffuse features, as given in, or deduced from, published papers.

A_c is the central depth of the apparent absorption, W is the equivalent width expressed in picometres (= 0.01 Å), and δ is the half-width in nanometres. Mean values are usually unweighted averages of the individual contributions listed. Approximate values for the interstellar D, G, and K lines are included for comparison.

(a) The '4430' line.

A_c/E_{B-V} (% per mag.)		W/E_{B-V} (pm. per mag.)		δ (nm)		Profile
12	B	500:	B	2.2	BB	Symmetric (BB)
14	D	190	GA	2.1	GA	Wide wings (B)
13	Sl	230	BS+BT	2.8	Ws	Symmetric (GA)
8	SD	380	S	1.8	BS	Symmetric; wide wings (Ws)
6-12	Wp	200:	BN	2.0	Wp	Slight asymmetry; weak emission wings (Wp)
13	WH	120	BK	2.1	S	Symmetric, gaussian (S)
14	S	280	Y	1.9	BN	Slight asymmetry, degraded red (H)
7	BN			1.9	H	Asymmetric, degraded to violet(W+)
13	BK					Emission to violet (BN)
12	H					Strong emission wings (WHY)
6-12	K					Varying strengths of emission wings (Y)
11	Mean	270	Mean	2.1	Mean	

(continued)

(Table I continued)

(b) Other lines.

λ_{A_C} (nm)	A_C/A_C('4430')		MEAN	W/W('4430')		MEAN	δ (nm)		MEAN
450.2 ± .1	0.2:	Ws	0.3	0.03:	S	0.03:	0.3	BS +Ws	0.3
	0.2	BS							
	0.3	S							
	0.4	H					0.3	H	
472.8 ± .2	0.2:	BS	0.3	0.05	BS	0.04	0.3	BS	0.4
	0.35	H		0.03	BT		0.4	H	
476.3 ± .2	0.2-0.3	Ws	0.3	0.14	BS	0.10	0.3-4.0	Ws	0.8:
	0.4	BS		0.07	BT		0.8	BS	
	0.3	H		0.1	S		0.4	H	
488.5 ± .3	0.3-0.4	Ws	0.4	0.57	BS	0.52	2.5	Ws	3.3
	0.4	BS		0.48	BT		3.5	S	
	0.4	S		0.52	S		4.0	H	
	0.5	H							

(continued)

(Table I continued)

λ_{A_c}	$A_c/A_c('4430')$		MEAN	$W/W('4430')$		MEAN	δ (nm)		MEAN
570.6 ± .2	0.2	Ws	0.3	--		0.04?	0.6	BS	0.4
	0.2:	BS					0.4	H	
	0.4	H							
577.8 ± .3	0.2:	BS	0.2:	0.5	M+	0.55	~1	BS	1.7:
				0.56	BS		1.7	H	
				0.54	BT				
578.0 ± .1	1.2	M+	1.2	1.1	BK		0.25	H	0.3:
	1.0	Ws		0.4	Y				
	0.9	BS							
	1.9	H							
579.7 ± .1	0.5	M+	0.7	0.13	M+	0.18	0.12	H	0.1:
	0.5	BS		0.24	BS				
	1.1	H		0.15	BT				
				0.2	Y				
617.5 ± .2	0.4	Ws	0.4	0.54	S		4.0	Ws	3.0
	0.4	BS		0.4	BK		~2	BS	
	0.4	S					2.9	S	
	0.4	H					3.0	H	
619.6 ± .1	0.6	H	0.6			0.81	0.1	H	0.1:
620.3 ± .1	0.2	Ws	0.4	0.14	S		0.2	H	0.2:
	0.3	BS		0.4	BK				
	0.7	H							

(continued)

(Table I continued)

627.0 ± .1	0.2 0.9	BS H	0.6	0.14	M+	1.05 0.88 0.7 1.8 1.0	BS BT S BK Y	1.0	0.15	H	0.2:
628.3 ± .1	1.7 1.6 3.6 1.9	M+ BS BK H	2.0	1.0	M+				0.4	H	0.4:
637.9 ± .1	0.2 0.3 0.8	Ws BS H	0.6	0.11	BS			0.1	0.6 0.1	BS H	0.1:
661.4 ± .1	0.5 0.4 1.7	Ws BS H	1.0:	0.16 0.04 0.4	BS BT BK			0.2:	1: 0.1	BS H	0.2:

(c) Some identified lines for comparison.

Ca II 'K' (λ393.37)	10:	0.5:	
CH I 'G' (λ430.03)	1:	0.05:	
Na I 'D' (sum) (λλ589.00, 589.59)	10:	1.0:	≲ 0.02

(continued)

(Table I continued)

Key

	References	Notes
B	Baker (1949)	7 stars ; O type.
BB	Beals and Blanchet (1938)	46 stars ; O to B3 types.
BK	Buscombe and Kennedy (1968)	30 stars for '4430' ; 4 stars otherwise ; southerly stars.
BN	Brück and Nandy (1968)	9 stars ; B type supergiants.
BS	Butler and Seddon (1958, 1960)	11 stars ; B2I and B3I types.
BT	Butler and Thompson (1961)	4 stars ; B5I and A0I types.
D	Duke (1951)	400 stars.
GA	Greenstein and Aller (1950)	38 stars.
H	Herbig (1966, 1967, and see also Johnson, 1970)	One star (HD 183143, B7I) ; unconfirmed lines also recorded at λλ536.2, 542, 545, 584.4, 585, 601, 637.6, 666.1.
K	Kellmann (1970)	150 stars.
M+	Merrill et al. (1937), Merrill and Wilson (1938)	130 stars for λλ578, 628.3 ; 60 for λ579.7 ; 5 for λ627. All entries calculated via assumed values for '6283'/'4430' ratios.
S	Seddon (1967,1968)	15 stars ; B1 to A0 supergiants.

(continued)

(Table I continued)

SD	Stoeckly and Dressler (1964)	60 stars.
Sl	Svolopoulos (1963)	5 stars ; O type.
WH	Walker and Hodge (1966)	450 stars ; O to B5 type.
WHY	Walker, Hutchings and Younger (1970)	
Wp	Wampler (1966)	100 stars.
Ws	Wilson (R.) (1956, 1958a)	5 B1I stars ; and HD 183143 (B7I).
W+	Wickramasinghe et al. (1968)	3 pairs of stars.
Y	York (1971)	13 stars.

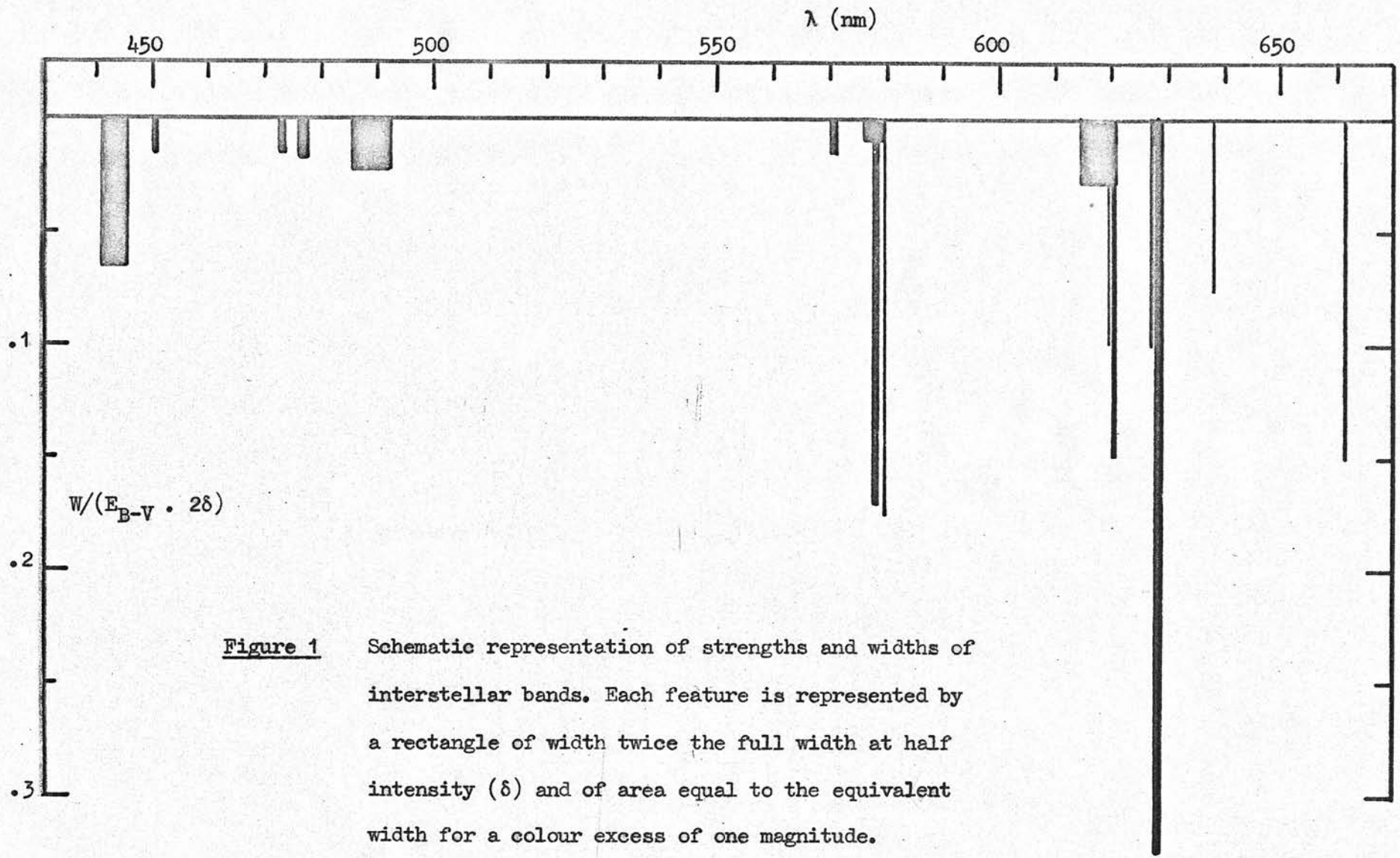

Figure 1 Schematic representation of strengths and widths of interstellar bands. Each feature is represented by a rectangle of width twice the full width at half intensity (δ) and of area equal to the equivalent width for a colour excess of one magnitude.

in the 'atlas' of Butler and Seddon (1958, 1960), and these authors actually tentatively suggested the interstellar nature of the λ637.9 nm. line (Butler and Seddon, 1960, page 205).

York (1971) is convinced that at least some of the DISAFS vary considerably in wavelength from star to star: this is at variance with the results of Merrill and Wilson (1938) and Herbig (1966, 1967), who have used higher resolution than York.

The present state of our knowledge about the DISAFs is summarised in Table I.

A schematic representation of the strengths and widths of these features is shown in Figure 1.

Figure 2 shows two sections of the spectrum of the very reddened star HD 50064. The ordinate is photographic density. Many of the DISAFs listed in Table I are indicated. (This spectrum was obtained with the Isaac Newton Telescope, Herstmonceux; full details are given in Chapter 4.)

1.4 Early Theories.

Because of the width of the DISAFs they were at first thought to be molecular bands (Russell, 1935; Swings, 1937; Saha, 1937). But E.H. Eyster (1937) and Beals (1942) pointed out that this would be very unlikely since in interstellar space only the very lowest rotational-vibrational levels would be populated and laboratory 'bands' of diatomic and triatomic molecules would be reduced to just a few isolated lines. The CH, CN, and

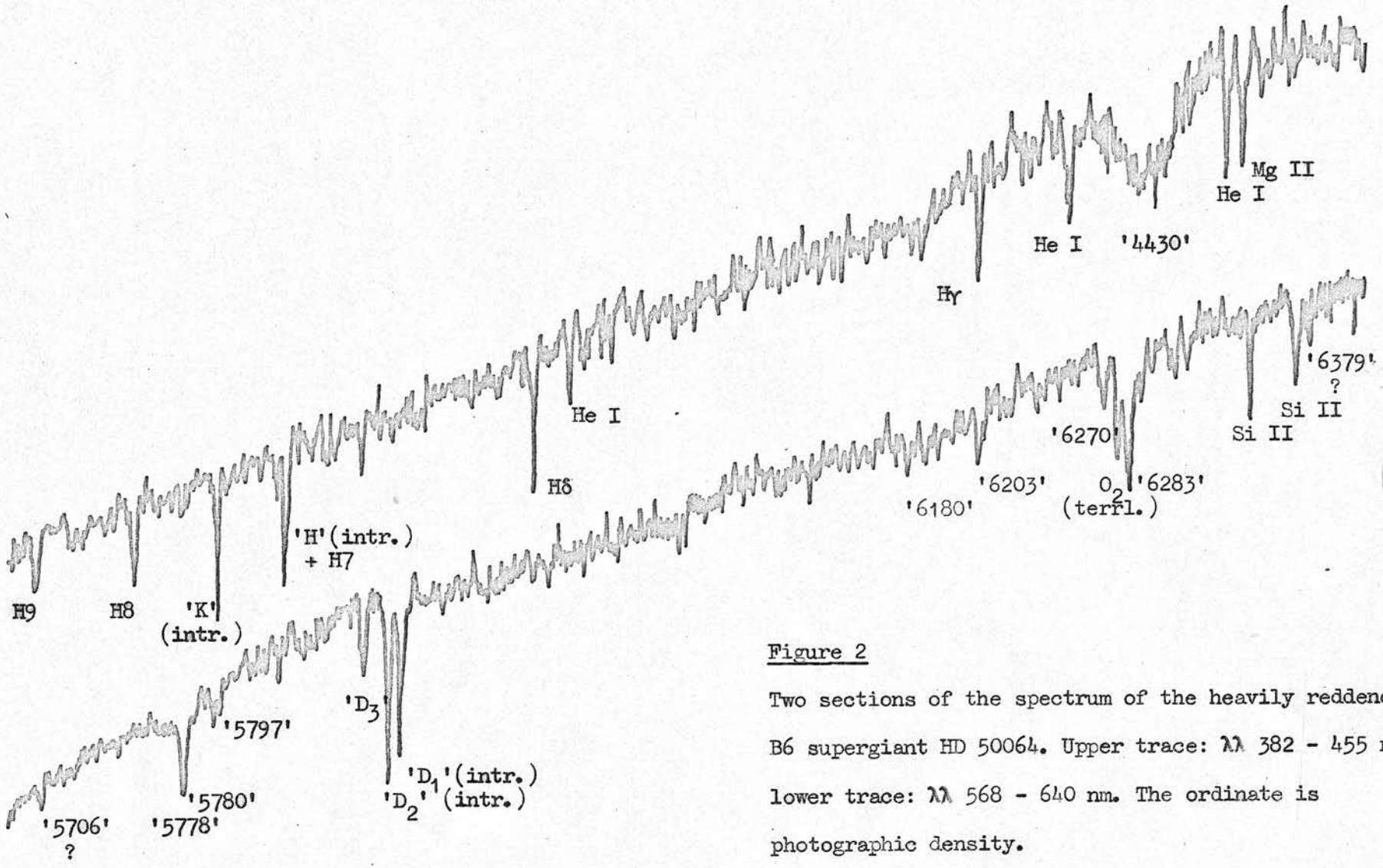

Figure 2

Two sections of the spectrum of the heavily reddened B6 supergiant HD 50064. Upper trace: λλ 382 - 455 nm.; lower trace: λλ 568 - 640 nm. The ordinate is photographic density.

CH^+ narrow lines identified by A. McKellar (1940) and others all correspond to only the two lowest rotational levels in the respective molecules. Moreover, no accurate wavelength coincidences with leading systems of laboratory molecular bands could be found (Eyster, 1937).

Thus, Beals and Blanchet (1938) and P. Swings and Y. Öhman (1939) suggested the only other obvious possibility, namely that the DISAFs were selective absorptions by the interstellar dust grains -- or, in other words, that the 'continuous' extinction was not continuous at all but included absorption lines. Such absorptions had been seen in the laboratory, ranging from considerably less than one nanometre to over a hundred nanometres in width, which of course includes the DISAFs, but the available laboratory data were too meagre to permit detailed investigations.

The grain-origin hypothesis was supported a little by the observed correlations between interstellar line strength and continuous extinction, the latter represented by the amount of reddening, the colour excess. Merrill and Wilson (1938) found that the correlation between strength of the λ628.4 nm. line and colour excess was better than between λ628.4 and D line strengths, and Morgan (1939) found a similar result for λ443 and the interstellar K line. The origin of the DISAFs seemed to be physically closer to the dust grains than to the free atoms of the interstellar gas.

But the grain-origin hypothesis suffered a major setback with the results of some calculations by

Van de Hulst (1948, 1949). He assumed that the features arose from atoms dispersed evenly throughout the volume of the interstellar grains, and that the grains were composed of ice, and were of sizes that best fitted the observations of continuous extinction. Using an approximate form of the classical dispersion formula, and his own extinction calculations for ice grains, he then derived theoretical profiles for the two strongest DISAFs, at $\lambda\lambda$443 and 628.4 nm. These theoretical profiles did not match the observations at all well: '4430' in particular was predicted to be highly asymmetric, with apparent emission in the violet wing, whereas the observations suggested nothing of the sort. Van de Hulst concluded that it might be necessary to return to the first hypothesis -- the molecular origin -- or at least to consider the possibility that molecules on the surface of the grains, or in the surface layers, were responsible.

1.5 Recent Attempts at Identification: Free Molecules or Ions.

If the diffuse features arise from free molecules or ions then their broad, diffuse nature can only be explained if:

(i) the molecule is so complex that vibrational structure is still unresolved, or

(ii) the lines are due to predissociation or preionisation (autoionisation).

For many years G. Herzberg has been attempting to

identify the DISAFs with predissociation transitions in his laboratory spectra of various molecules, but so far without success (Herzberg, 1955, 1965, 1967). He at first also considered O^-, C^-, or N^- to be possible candidates and Rudkjøbing (1969) has recently suggested that preionisation transitions to O^- are responsible for the two diffuse lines at λ 578 and 579.7 nm. The same author proposed that the broadest DISAFs are formed by preionisation transitions to H^-, but his tentative identification is open to criticism on the following counts. His extrapolation of wavenumbers of resonance lines along an isoelectronic sequence of ions would seem to be largely arbitrary: certainly the wavelength of the '6180' line would fit the extrapolation of resonance lines better than '4430'. But if '6180' were the resonance line, this would leave '4430' without explanation. In any case, these features are not as wide as the quantum mechanical calculations (quoted by Rudkjøbing in support of his theory) would imply, and '4430' is now known to be well clear of the Whitford-Nandy discontinuity in the continuous extinction curve (Harris, 1970), so that it cannot be broadened further in that respect. An explanation is also wanting as to why no DISAFs are seen in ordinary stellar atmospheres where H^- contributes substantially to continuous opacity.

Of other molecules and ions considered by Herzberg, various triatomic molecules of the general form HXY have been investigated, and rejected; and CH_4^+ and NH_4 (Herzberg, 1967) are now under consideration.

A serious objection to the proposed explanation involving predissociation or preionisation was raised by R. Wilson (1964). There is an abundance problem, in that each molecule or ion can absorb only one photon during its lifetime (or, as Wilson put it, the formation of the absorption line destroys its carrier). The constant replenishment of the source at the rate needed to explain the DISAF strengths is considered rather unlikely (Wilson, 1964; Herbig, 1967). In answer to this, Herzberg (1965, 1967) can only quote another abundance anomaly, in connection with the radio observations of OH sources. T. de Jong (1971) however, has calculated total abundances of H^- under various interstellar conditions, and has found that if there exist hot, low density 'intercloud' regions as in the model of Field et al. (1969) then the H^- density there would be sufficiently high to be able to explain '4430' on Rudkjøbing's theory. But de Jong also found that '4430' formation in HI regions and actual dust clouds would be impossible, so that the DISAF - E_{B-V} correlations may have to be explained away somehow. The recent observations of excess polarisation over '4430' (Nandy and Seddon, 1970) seem to definitely exclude Rudkjøbing's explanation, because he specifically predicts no change in polarisation over this band (Rudkjøbing, 1969b).

As pointed out by Herzberg in 1955, if a molecule is complex enough then even in the interstellar environment sufficient population of higher rotational levels to give diffuse lines is still a possibility. Following a line of

thought and experiment that started with J.R. Platt's proposal (Platt, 1956) of a molecular origin of the continuous extinction and B. Donn's subsequent suggestion (Donn, 1968) that these Platt particles may be 'graphite-precursor' molecules such as aromatic hydrocarbons, F.M. Johnson (1970) has made the startling assertion that the DISAFs are due to the molecule $MgC_{46}H_{30}N_6$ (bispyridyl magnesium tetrabenzoporphine). Johnson has investigated the spectra of many kinds of complex molecules, in both the solid state and in suspension, at both room temperature and liquid nitrogen temperature (77°K). He apparently concentrated on searching for a line at or near λ443 nm.: the most interesting compounds in this respect were the porphyrins.

The search was narrowed down to magnesium tetrabenzoporphine (MgTBP), which in suspension at 77°K exhibits a line in the close vicinity of 443 nm., and also some other lines close to the red DISAFs. By dissolving MgTBP in pyridene, Johnson isolated the molecule $MgC_{46}H_{30}N_6$; and looking at its absorption spectrum at 77°K he recorded sixteen wavelength coincidences with old and new (Herbig's) DISAFs. The strongest feature, the Soret (0,0) band, was at λ442.8nm., the position of the strongest DISAF; and in addition there were an unspecified number of weaker lines (including perhaps a very broad one near λ635 nm.) of which 15 (not necessarily the next strongest 15) corresponded to 15 out of 25 of Herbig's lines. Unfortunately, some of the stronger and more

'established' of these, including the intense λ628.3 nm. line, were not seen in the absorption spectrum of bispyridyl MgTBP. What is more, '4430' was much too strong in the laboratory spectrum compared with the other lines; and also the widths of the lines, and the profile of '4430', are not the same as those observed in the interstellar medium.

York (1971), in criticising this identification, particularly cites the λ628.3 line, which Johnson tentatively assigns to a transition from an energy level 0.03 eV above the ground state of his molecule: this line is so intense that the assignment must surely be very unlikely. If York's wavelength variations from star to star for some DISAFs are in fact real, then presumably no free molecule can be responsible.

It is extremely difficult to envisage the formation of such a complex molecule as Johnson's in the large numbers that are needed, and in such a great preference to other equally complex molecules, which would have absorption lines that are not observed. There is rather a large gap between the most complex molecule so far detected in interstellar space by the radio astronomers (a molecule of six atoms, and molecular weight about 50) and bispyridyl MgTBP (83 atoms, molecular weight 690).

The survival of such molecules on a galactic scale is equally unlikely, considering the apparently loose binding of the pyridene molecules onto the MgTBP.

Yet, having said all this, it is difficult to argue with Johnson's contention that the odds against his

finding such wavelength coincidences by chance must be very long indeed. It is interesting that the infrared spectrum of the same molecule shows emission features corresponding to observed interstellar, circumstellar and cometary emission lines near 10 nm. in wavelength. The conventional interpretation (Woolf and Ney, 1969) is that these lines arise from silicate grain precursors, and recent observations at high resolution of silicon monoxide bands in α Orionis (Cudaback et al., 1971) tend to support this view, rather than Johnson's.

The laboratory conditions under which Johnson recorded his spectra were still rather far removed from interstellar conditions, under which his wavelength coincidences may not be so good. But even so, to his investigation must be accredited the closest approach to a solution of the DISAF problem under the hypothesis of free molecular origins.

1.6 Recent Attempts at Identification: Dust Grains.

Turning next to the hypothesis of grain origins, we find a proposal by A. Unsöld (1963, 1964) that the DISAFs could arise from collective oscillations of free electrons in very small metallic particles. If these are almost precisely spherical in shape and have radii in the range $3 \lesssim a \lesssim 10$ nm., then a critical frequency occurs at $1/\sqrt{3}$ times the well-known macroscopic (plane-surface) volume plasma frequency. Therefore, to identify, say, the '4430'-metal we must look for one with a plasma oscillation wavelength of $443/\sqrt{3} = 256$ nm., that is, for an energy-loss peak at about 4.9 eV. No coincidences have

been reported so far, the plasma frequencies being generally considerably larger than those we are looking for.

Unsöld also suggested that a common source for DISAFs and continuous extinction might be tiny metallic spheres coated with ice. C.A. Whitney (1964) followed up this idea with predictions for alkali metal spheres of 10 nm. radius coated with ice, and seems to have found that the critical wavelength for sodium could be shifted to λ443 nm. by a suitable combination of sodium core size and thickness of ice mantle. His results have apparently still not been published in full -- perhaps because he tried and (presumably) failed to find '4430' in laboratory experiments with such particles. In any case, this particular theory is unlikely in that it requires a considerable overabundance of sodium in the interstellar medium (see Hobbs, 1971).

A basic difficulty with Unsöld's general theory is that one needs a separate metal for each DISAF. Furthermore, since the lines are considered to be broadened principally by deviations from sphericity of the metallic particles, each species must have a precisely constant distribution of shapes, all over the Milky Way. For example, the particles of '4430'-metal, if spheroids, need a constant distribution of the ratio of long to short semi-axes, b/a, in the approximate range 0.95 to 1.05. It is difficult to imagine such conditions being realised in practice.

It is nevertheless interesting to note in this connection that the theoretical ratio of macroscopic volume plasma frequency to surface plasma frequency ($\sqrt{2}$) (Arakawa et al., 1966) is closely similar to the ratio of the observed frequencies of the two principal broad DISAFs, '4430' and '6180' (1.40).

A rather different mechanism, involving H_2^+ ions absorbed onto interstellar grains, was proposed by Herbig in 1963. Unsöld (1964) has criticised the proposal on the grounds that the two basic assumptions of the theory are incompatible: the required metastable level of H_2^+ could not be sufficiently populated if the interaction of the ions and the grain were strong enough to shift and broaden the absorption lines to the required amount. Other criticism has centred on the fact that the proposed absorptions could only take place in the presence of a strong radiation field (for example, near an OB star), whereas observed '4430' is not restricted to such regions. Herbig's theory is really restricted to '4430', and other lines are not explained so well at all. Herbig himself does not mention his own theory in his short 1967 review.

There remains only the possibility that the DISAFs arise from impurities dispersed throughout the interstellar grains. In considering this we are returning to one of the earliest proposals, which has only been seriously contended by Van de Hulst's (1949) calculations of impurity line profiles.

The theme was taken up by Wilson (1964), by Unsöld (1964), and then in more detail by F. Hoyle and N.C. Wickramasinghe (1967) and by J.G. Ireland, K. Nandy, H. Seddon, Wickramasinghe, and R.D. Wolstencroft (Nandy et al., 1968; Wickramasinghe et al., 1968; Wolstencroft et al., 1969). These last authors consider that the commonly observed 'colour centres' arising from defects in crystal lattices will probably give absorption bands that are much wider than DISAFs, but that other types of impurity absorptions could be of the required widths.

K. Dressler (1965), W.W. Duley (1968, 1969) and Duley and W.R.M. Graham (1969) have proposed that matrix shifts of resonant calcium and sodium lines in solid grains could account for '4430' and some of the other DISAFs. As usual, their best fit is with '4430', not only because everyone seems to find this line the most interesting of all, but also, as it turns out, because it is a strong and wide feature.

Duley and Graham (1969) find that, of various hydrocarbon matrices, only benzene can shift the λ422.6 nm. resonance line of calcium to λ443 nm. Unfortunately, the concentration required to produce such a shift gives a line too strong and too wide (about 25 nm. in full width at half intensity). The authors compare their spectra with a tentative identification of '4430' in the spectrum of a Type I supernova (Seddon, 1969), which band has a half-width of about 15 nm. Their results are reproduced in Figure 3, together with the

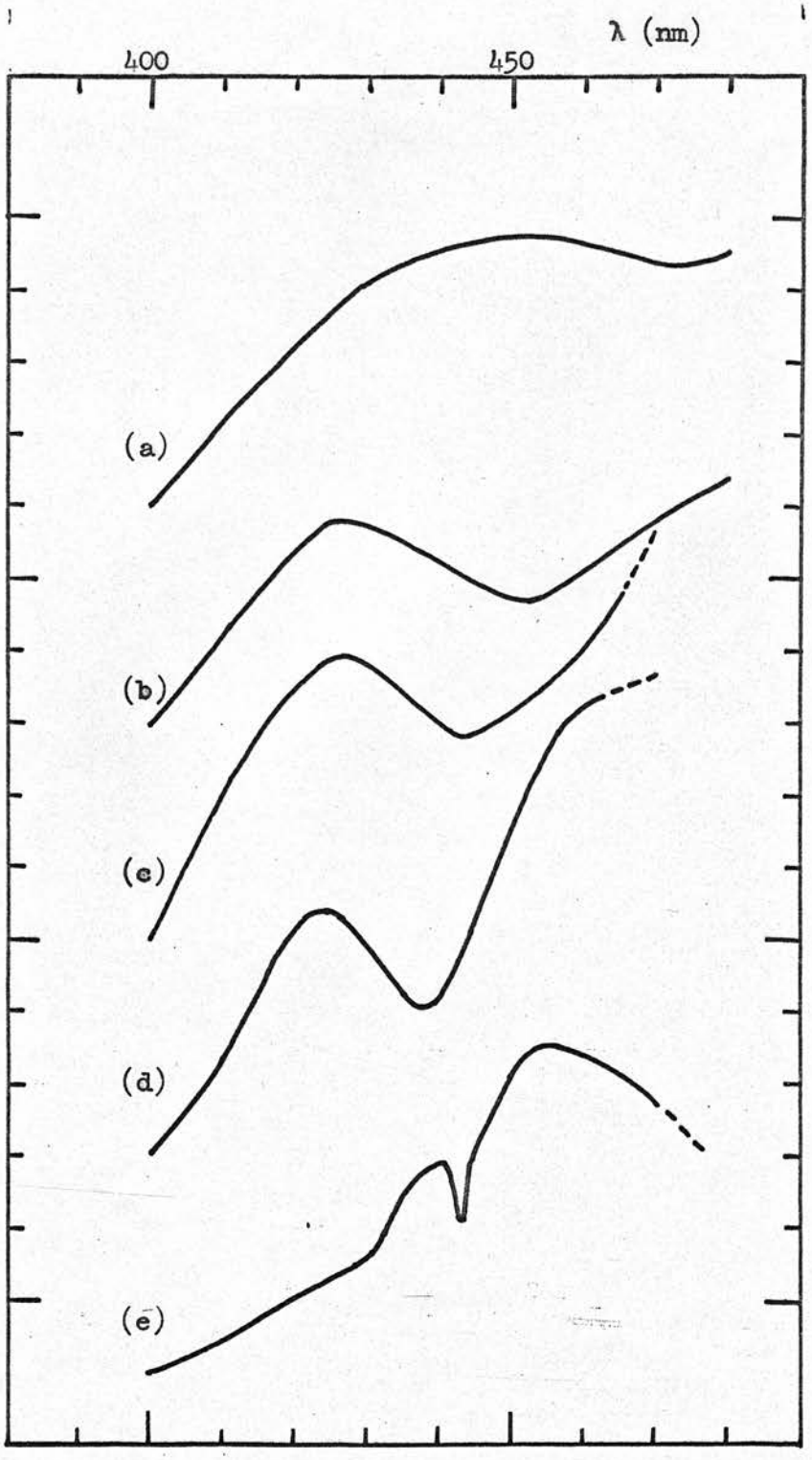

Figure 3 Shift of Ca I λ422.7 in C_6H_6 matrix (Duley and Graham, 1969, decreasing concentration of calcium from (a) to (c)) compared with mean spectrum of SN-NGC-2713 (Seddon, 1969, but corrected for galactic redshift) and a typical strong '4430' band in a stellar spectrum (d and e, respectively)

supernova '4430' and a typical strong interstellar '4430' (the latter adapted from Figure 1). The shift of the calcium line would be substantially less than 20 nm. if the line were only 2 nm. wide, and correspondingly weak, as seen in stellar spectra. Moreover, comparison with the supernova spectra is not straightforward because the observed wavelength of an absorption line is altered by the speed of recession of the galaxy in which the supernova is situated, and by the (unknown) speed of the ejected matter.

But even though the calcium line λ422.6 nm. seemingly cannot be responsible for '4430', this obviously does not mean we must abandon the general hypothesis of impurities in grains. From the above discussion of the work of Duley and Graham, it seems possible that matrix shifts on the scale seen in the laboratory are not feasible for actual interstellar grains and DISAF strengths. We may have to look for lines with 'normal' wavelengths within perhaps only two or three nanometres of the DISAF wavelengths.

Several experimentalists have recently claimed identifications of some of the broader DISAFs with impurity absorptions in samples of terrestrial rocks and crystals. For example, Kunciman (1970) notes a band at λ444 nm. due to ferric ion impurities in chrysoberyl ($BeAl_2O_4$). Manning (1970), in a series of papers, discusses wavelength coincidences between some DISAFs and absorptions due to Fe^{++} and Fe^{+++} impurities in various terrestrial silicate complexes, including pyroxenes and

garnets. But in all these cases, the widths of the bands correspond to the supposed diffuse bands in supernova spectra (Seddon, 1969) and not to the common 'interstellar' ones. Hence these identifications are open to the same kind of criticism as those of Duley and Graham.

The comparisons of laboratory data with the supernova spectra may or may not be valid, but certainly to extrapolate to the problem of the ordinary interstellar DISAFs (especially the narrower features) is little more than intelligent speculation. It is however interesting to note here in connection with laboratory wavelength coincidences a result of A.P. Lenham and D.M. Treherne (1966a). These authors found that many transition metals have optical absorption maxima at about 2.0 eV, that is, very near '6180'. Other common maxima occur at about 0.95, 1.6, 2.2, 5 and 9 μm in wavelength.

Leaving aside specific identifications of the impurities involved, let us consider the more general question of whether Van de Hulst's theoretical profiles for DISAFs and his subsequent conclusions hold for <u>all</u> cases of impurities in interstellar grains.

Van de Hulst's calculations, for the $\lambda\lambda$443 and 628.3 nm. lines were restricted to grains with refractive index close to unity, and to one particular value for impurity concentration. J.M. Greenberg (1968) has now recalculated '4430' profiles for spherical dirty ice grains of various sizes and distributions of sizes. Greenberg arrives at essentially the same conclusions as Van de Hulst, namely that a symmetric absorption profile

for '4430' requires host grains considerably smaller than those needed to explain the continuous extinction in the visual region.

However, as was noted above (Section 1.2), the profile of '4430' may not be symmetric after all. Indeed, the preliminary Edinburgh image-tube observations (Brück and Nandy, 1968) suggest a violetward emission wing, and this (if substantiated) could allow larger host particles for the hypothetical '4430' impurities. Furthermore, the ice grains considered by Van de Hulst and Greenberg are certainly not the only type of interstellar grain likely to exist in space (see for example Wickramasinghe, 1967). Graphite grains, for example, could be almost an order of magnitude smaller than Van de Hulst's ice grains, so that the theoretical impurity line profile could perhaps then be predominantly an absorption line. Wickramasinghe and Nandy (1969) have performed similar calculations to Greenberg's for single size grains of graphite, silicate and solid hydrogen. They find that for the particular sizes of silicate and solid hydrogen grains that fit the extinction law in the visual region, the apparent emission wing may in fact be <u>smaller</u> than that observed.

1.7 Summary, and Objectives of the Present Investigation

It may be concluded from the above survey that there is still no satisfactory explanation of the DISAFs, nearly forty years after their discovery by Merrill. What is more, the observational profile of even the most carefully studied feature, '4430', is still uncertain.

The object of the present investigation is to consider in detail one of the two rival hypotheses as to the origin of the DISAFs, namely, the grain origin hypothesis. The features are assumed to arise from impurity atoms (of unspecified type) in interstellar dust grains. Profiles are then calculated from classical dispersion theory and scattering theory, following the general method of Van de Hulst (1949) but using exact formulae. The object is to find which - if any - of the likely species of interstellar grains could in fact be hosts to diffuse-line absorbers. The results are quite general in that they are independent both of current opinions as to particular types of grains responsible for continuous extinction, and of the <u>type</u> of impurity atoms needed. In fact no attempt is made to identify the impurities.

New observational profiles of DISAFs are also presented here, and comparisons are made with the theoretical predictions. For the three blue bands at λλ443, 476, 489 nm., the observations were made with an electronographic image tube. The advantages of this method over conventional photography have been pointed out by P.W.J.L. Brand (1967) and by M.T. Brück and K. Nandy (1968). In the present context, the most important advantages are that interpolation of a stellar continuum over a broad DISAF is much safer, the uncertainty associated with the wavelength - dependent photographic emulsion sensitivity having been removed, and that grain noise obscuring the DISAF profile is reduced considerably.

The image tube observations, their method of reduction, and the resulting profiles are described in Chapters 2 and 3. Profiles have also been obtained for some of the red DISAFs as seen in very heavily reddened stars in Cygnus. These observations, which were made photographically, are described in Chapter 4.

The theory of the extinction by interstellar grains with impurities is described in Chapter 5, and the theoretical results are presented and discussed in Chapters 6 and 7.

2. Image Tube Observations:

Observational Details and Reduction Scheme

2.1 Detection and Recording System

The arrangement of apparatus for taking the new observations was very similar to that used by P.W.J.L. Brand (1967). The light collector used was the 36" (f/18) telescope of the Royal Observatory Edinburgh; and the spectrograph, the standard model currently in use at the Cassegrain focus of this telescope. A four-inch grating with 60,000 lines blazed to the blue was used, to give a dispersion in the blue at the focus of an f/3 camera of approximately 4 nm. mm.$^{-1}$ (40 Å/mm.).

Replacing the photographic plateholder was the image tube ensemble. This consisted of a Spectracon Type B image tube with its concentric solenoid (Type IIIb), designed and made by J.D. McGee (McGee et al. 1966, 1969), Imperial College, London, together with ancillary ad hoc fittings designed by Brand (1967) and made at the Royal Observatory Edinburgh.

A Spectracon consists essentially of a highly evacuated tube with a photocathode deposited at one end and a very thin sheet of mica placed parallel to it at the other end. The tube used here (model B134) had an S-11 (SbCs) cathode and a mica window of dimensions 25 mm. x 5 mm. x 4 μm. (For an illustration of the Spectracon Type B and solenoid Type IIIb see McGee et al. (1969).) Photoelectrons complete two full turns of a helical motion in applied parallel electric and magnetic fields,

the distances from the cathode of successive focal planes increasing in approximately geometrical progression. At the second focal plane (at 260 mm.) the photoelectrons encounter the mica window with energies of 40 Kev. About 75% are able to penetrate it, and the electron image is then recorded on electronographic emulsion which is applied directly to the mica surface by a foam-rubber roller, and held there under elastic pressure. A constant potential gradient from -40KV at the cathode to earth at the mica window end is maintained by a bleeder chain of resistors. A constant magnetic field over the tube is maintained by stabilising the current supply and using the specially wound, magnetically shielded solenoid.

In the present investigation, the emulsion used was 15 μm. thick G5 nuclear research emulsion, backed with melinex film about 100 μm. thick. The EHT supply was a Brandenburg generator, model MR 50/R, providing 70 μA at 40 KV. The Brandenburg and an electrostatic voltmeter were enclosed in a dry airtight box and the supply was led into the Spectracon via PTFE plug, socket and tubing (with electrical connections set in Silastomer rubber) to inhibit corona discharge and charge creep. The solenoid current was supplied by either a twin International Electronics stabilised current supply or a Roband-Varex 60-5 supply. The current needed to obtain optimum focussing of the electrons was previously determined in the laboratory, using an optical bench arrangement to project a test pattern image onto the photocathode. It was found to be 1.98 $\pm$ 0.02 A. The cathode end of the image tube

was cooled by running water maintained at about 10°C.

Optical focus and wavelength range in the final arrangement on the 36" telescope were determined with the help of a helium discharge tube positioned in front of the spectrograph slit. The slit width was set at 120 μm. and the wavelength range to λλ395-495 nm., approximately.

2.2. Details of Observations.

Image tube observations were made on the nights of December 12th, 13th, 15th, and 16th 1968, and January 22nd, 24th, 28th, and 29th 1969.

About one third of the spectra obtained had to be discarded, for the following reasons:

(i) underexposure (5 spectra),

(ii) positioning of spectra on a part of the cathode area with a very irregular response (4),

(iii) overlapping of images due to slipping of the film roller (14),

(iv) poor electromagnetic focus (2),

(v) spark discharge from the image tube during exposure (2), and

(vi) scratched or dirty emulsion (4).

Table II summarises the useful spectra obtained. The stars were selected from a short-list of 75 compiled from W.A. Hiltner's catalogue (Hiltner, 1956), together with consideration of Duke's (1951) results for '4430' strength. The four virtually unreddened stars (β Orionis, ε Orionis, 16 Tauri and ρ Leonis) were

Table II

List of Image Tube Spectra Obtained.

HD	Star	l (deg.)	B (mag.)	E_{B-V} (mag.)	Sp.	n	Refs.
12301	53 Cas	131	5.96	0.47	B8 Ib	3	H DB
14322	Per	135	7.09	0.44	B8 Ib	2	H D
20041	Per	142	6.48	0.56	A0 Ia	4	Z DB
21291	2H Cam	141	4.61	0.49	B9 Ia	4	H
21389	Cam	142	5.09	0.56	A0 Ia	4	H DEB
23288	16 Tau	(166)	5.40	0.07	B7 IV	4	Y D
34085	β Ori	(209)	0.05	0.06	B8 Ia+	4	Y D
36371	χ Aur	176	5.18	0.46	B5 Iab	3	Z DEB
37128	ε Ori	(205)	1.52	0.12	B0 Ia	4	Y DE
39970	Tau	185	6.41	0.39	A0 Ia	4	H
40111	139 Tau	184	4.75	0.20	B1 Ib	2	H DE
40589	Gem	183	6.30	0.31	B9 Iab	2	H

(continued)

(Table II continued)

41117	χ^2 Ori	190	4.90	0.51	B2 Ia	2	Y DEB
47240	Mon	207	6.29	0.40	B1 Ib	2	H D
91316	ρ Leo	(235)	3.71	0.12	B1 Ib	4	Y E
199478	Cyg	88	6.13	0.56	B8 Ia	2	H D
202850	σ Cyg	(84)	4.34	0.16	B9 Iab	2	Y D
208501	13 Cep	100	6.53	0.83	B8 Ib	4	H D
223385	6 Cas	116	6.08	0.57	A3 Ia+	1	H D

Key to References:

Sources of stellar details: H Hiltner (1956)

Y Yale Catalogue of Bright Stars (Hoffleit, 1964).

Z Yale catalogue, but with B and E_{B-V} derived from m_v and E_1 .

D Duke (1951), study of '4430' band.

E Edinburgh spectrophotometric survey (Wilson, 1956, 1958b; Butler and Seddon, 1958; Butler and Thompson, 1961) (Seddon, 1967, 1968).

B Brück and Nandy (1968), image tube results for '4430'. See also Brand (1967).

included for comparison purposes.

The eight columns of Table II refer to, respectively, the Henry Draper number of the star, the name of the star (or its constellation name), new galactic longitude (a value in brackets indicating that the star is more than five degrees from the galactic plane), standard stellar magnitude at B on the UBV system, B-V colour excess on the same system, spectral and luminosity types, number of spectra obtained, and references to the sources of the stellar details and other notes. All spectra were widened to 1 mm.

The films were developed for 5 minutes in D19b, with constant gentle rocking of the developing tank. Processing was carried out under an amber safelight.

2.3 Optimum Spectral and Luminosity Types for Accurate Profile Determinations

The wavelength range used here allows investigation of all three interstellar bands in the violet and blue, '4430', '4760' and '4890'.

The reduction technique, described fully in Section 2.4 below, is based on an early automated spectrophotometric method of G.I. Thompson (1966), which in effect automates the usual hand reduction procedure. A spectrum is represented by a model consisting of a continuum and a number of absorption lines. All these lines are assumed to have the same profile, and the positions of all lines are assumed known. After allowance for these lines, the remaining spectral

information (the 'continuum') is fitted by a set of orthogonal polynomials, of maximum degree determined by the noise level. In fact, the continuum constants and the equivalent widths of the lines are calculated simultaneously.

Any features in the spectrum not representable as either 'continuum' or 'lines' in the above sense - such as the broad Balmer lines, or the DISAFs - must be omitted from consideration in the analysis; but the information in such features is not completely lost. For example, the continuum constants permit a more accurate interpolation of continuum level over a DISAF than that obtainable by any conventional method, including Lagrange interpolation. It is precisely this information that we need to establish accurate profiles for the DISAFs. However, the interpolation over such a large region as, say, '4430', is only valid as long as there are no localised variations in detector response nearby. For photographic spectra, variation with wavelength of the emulsion sensitivity makes such interpolation hazardous. The corresponding effect for the Spectracon - a non-uniformity of response of the photocathode and of transmission of the mica window - is less serious in that it is dependent on position on the mica window rather than on wavelength of the incident light. A correction may be applied to allow for it (see Section 2.7).

Thompson's subsequent, more sophisticated automated spectrophotometric methods (Thompson, 1971), aimed exclusively at determining accurate equivalent widths,

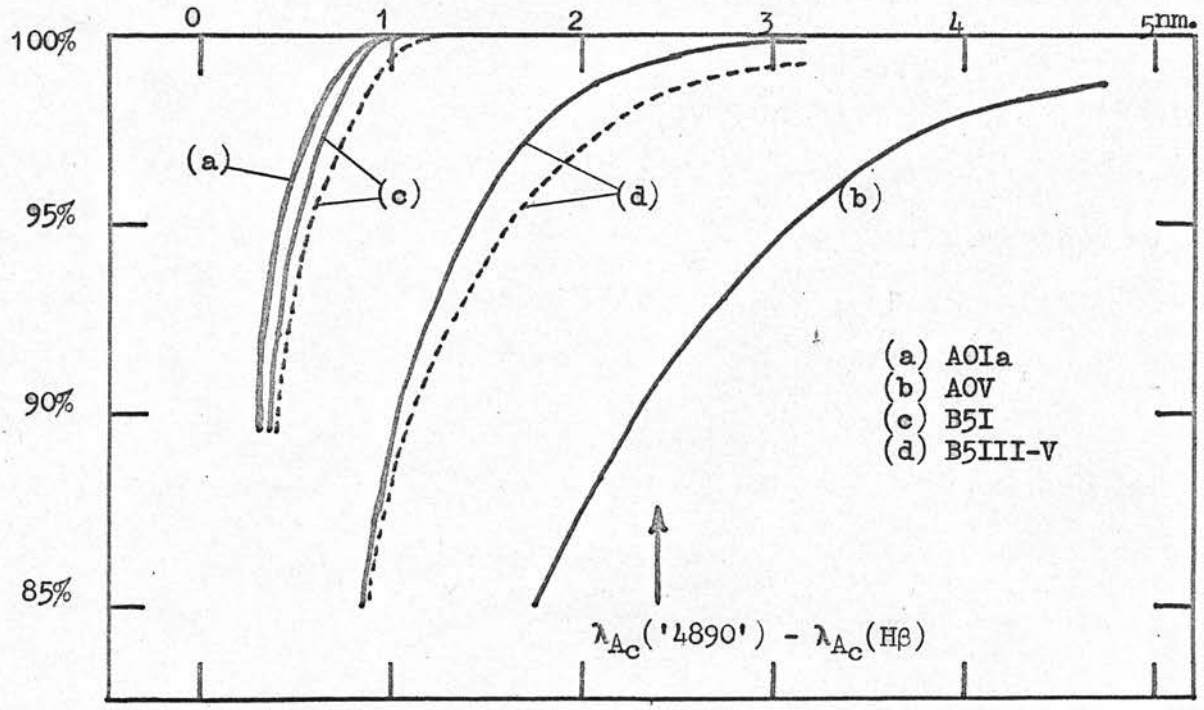

Figure 4(a) (From Figure 2 of Butler and Thompson (1961).)
Profiles of Hγ (——) and Hβ (- - -) wings for B5 and A0 stars.

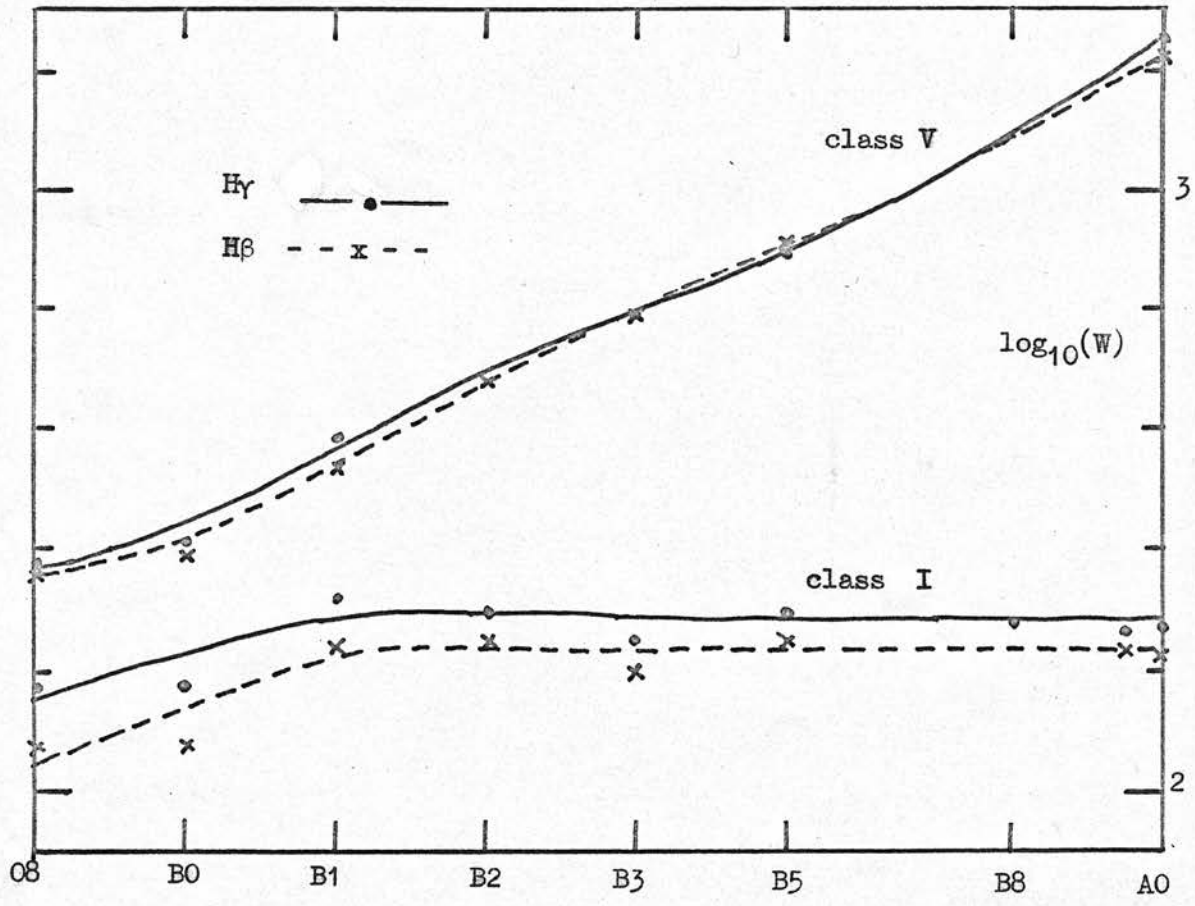

Figure 4(b) Equivalent widths of Hγ and Hβ for dwarfs and supergiants.

cannot be used to derive DISAF profiles because the concept of a continuum is no longer preserved throughout the analysis.

The method of spectrum analysis outlined above immediately indicates preferred types of spectra. All spectrum lines should have the same profile - ideally one that can be easily determined, such as the instrumental profile - and any lines that have to be treated separately (including Balmer lines, and lines in emission) should affect as little of the spectrum as possible. In addition, for optimum use of the automated spectrophotometry, as many spectra as possible should be similar - that is, they should have the same set of absorption lines, with the same line profile.

Now the best stars to look at when we are studying DISAFs are the early-type supergiants. The early-type stars in general have very few detectable stellar lines in their spectra, so that any DISAFs present can be seen relatively easily. And if we look at supergiants we see further into space (and thus see stronger DISAFs, in general) than if we look at dwarfs. Furthermore, the Balmer lines Hγ and Hβ are narrowest for supergiants and so have a minimum effect on the profiles of the broad DISAFs '4430' and (especially) '4890'. Finally, there is a distinct minimum near subtype B8 in the total strength of stellar lines in or near '4430'. These last two points are demonstrated in Figure 4 and Figure 5.

Figure 4(a), taken from a paper by H.E. Butler and

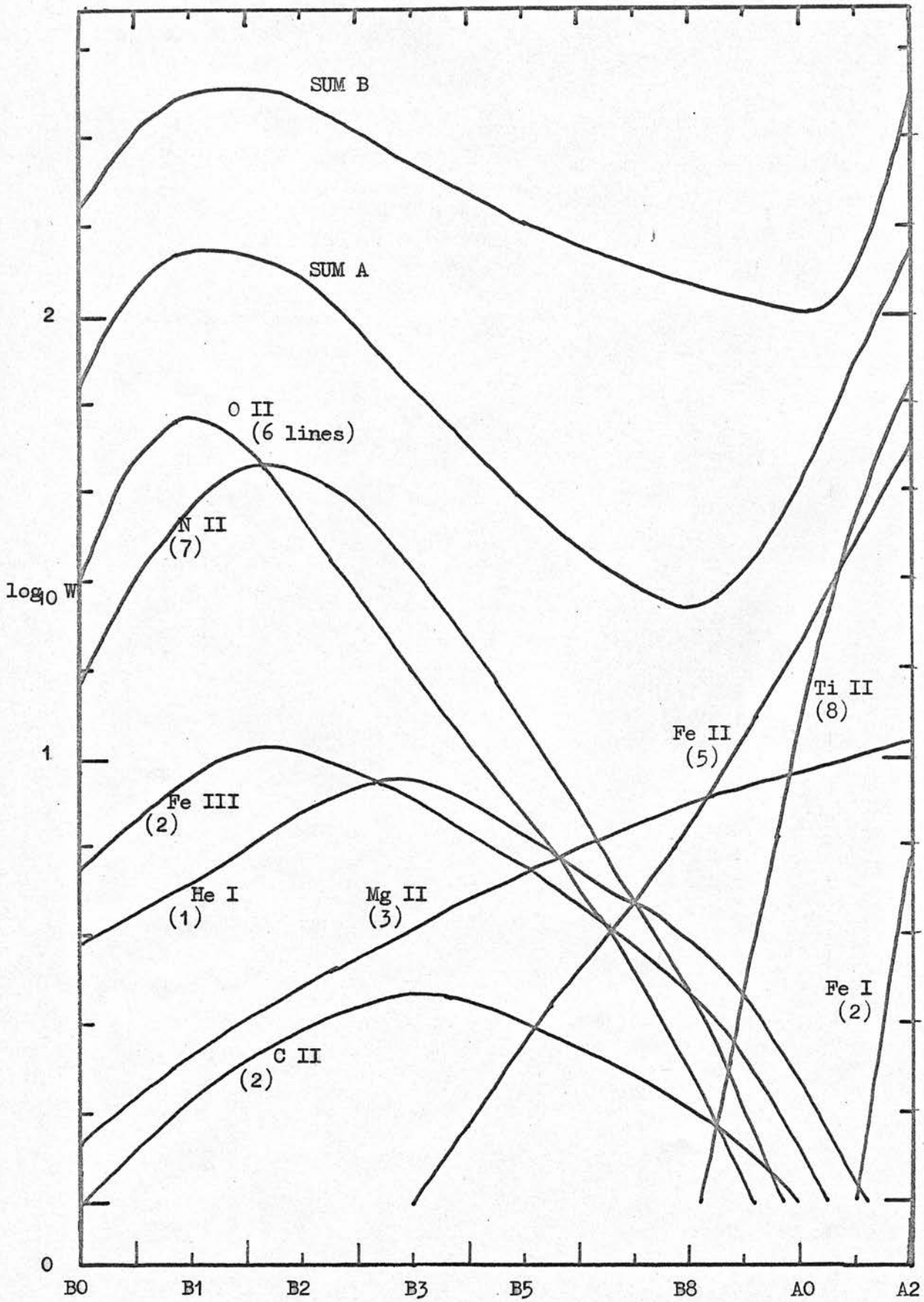

Figure 5 Equivalent widths of stellar lines overlying '4430'. W is in picometres (= 0.01 Å). Range λλ440.5 - 445.5 for individual contributions and SUM A ; λλ438.5 - 447.5 for SUM B.

Thompson (1961), shows Balmer line wing profiles for some B5 and A0 stars. The wavelength separation of the centres of Hβ and '4890' is indicated by an arrow on the abscissa scale. The interference of '4430' and '4890' by Hγ and Hβ respectively is clearly seen to be at a minimum for supergiants. This preference for supergiants is especially well-marked for late-B type stars, as is shown in Figure 4(b), where equivalent widths of Hγ and Hβ are plotted on a logarithmic scale as a function of spectral type, for dwarfs (class V) and for supergiants (class I) separately.

Figure 5 shows the total equivalent widths of stellar lines overlying '4430' for the nine most important atoms and ions, on a logarithmic scale as a function of spectral type for supergiants. The region covered is λλ440.5 - 445.5 nm. The grand total for all lines is plotted as 'SUM A', and this curve shows a sharp minimum at B8, the total there being only one-sixth of its value at B1-B2 or A2. 'SUM B' is the corresponding curve for the larger region λλ438.5 - 447.5 nm. The extra contributions (which are not so important as the contributions to SUM A) come mainly from the He I lines λλ438.8 and 447.1 nm., and from some Ti II lines. The minimum in this curve is at A0 rather than B8.

Combining the criteria for optimum 'visibility' of DISAFs with those for optimum use of the automated spectrophotometric method, we find that the best stars to study are those with luminosity class I and spectral type between B6 and A0.

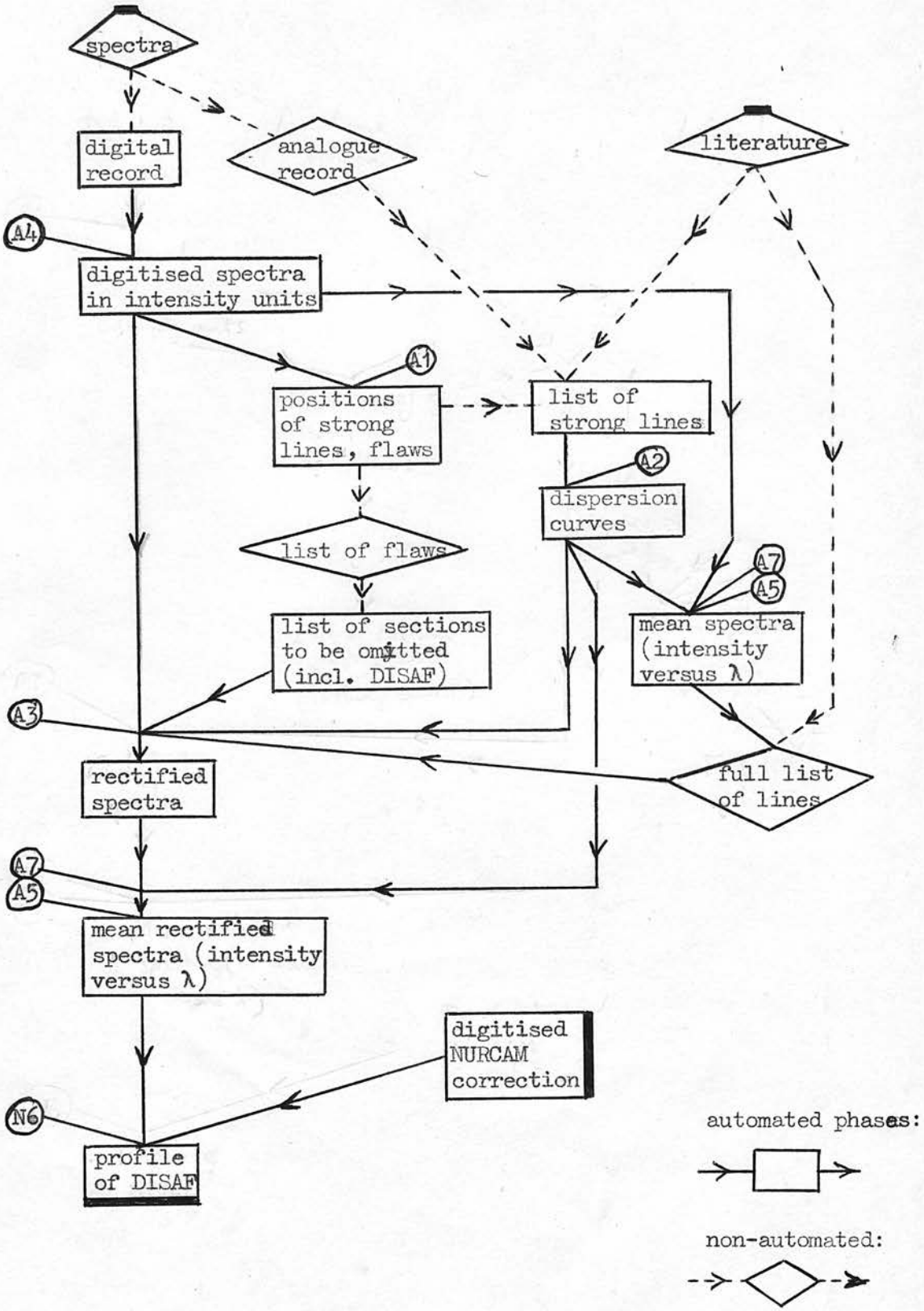

Figure 6. Schematic representation of the overall reduction scheme for image tube spectra. Labels refer to computer programs.

Therefore the 35 image tube spectra of eleven late-B type supergiants (Table II) have been fully reduced by the scheme described below (Section 2.4). The other 22 spectra (of which eight refer to four moderately reddened stars) have only been studied qualitatively.

2.4 Reduction Scheme.

The basic scheme for the reduction of a set of image tube spectra of one star to obtain the profile of an interstellar absorption band is illustrated diagrammatically in Figure 6.

Recordings of the spectra were made with a digitised Joyce Loebl Mark IIICS double-beam microdensitometer. The analysing slit was 20 μm. wide (the same as the projected spectrograph slit width), and the stepping interval for digital output was 12.5 μm. Simultaneous analogue output was obtained with a constant velocity chart recorder. The magnified image of the spectrum was watched during the recording, and positions of any emulsion flaws or other peculiarities were immediately marked on the chart recorder trace for future reference.

The displacement of the optical wedge of the microdensitometer, recorded as a three-digit number on paper tape, is directly proportional to the optical density of the sample studied. Thus, simple subtraction of the background 'fog' level from the spectrum data, followed by multiplication by a predetermined factor (the product of the analogue to digital conversion factor and the 'slope' of the particular optical wedge used) yields the

actual density of the spectrum. Readings of the fog level were taken at 250 μm. intervals. In all cases, the fog was almost constant over the whole length of spectrum to be reduced. A set of polynomials (up to a maximum of fourth degree) was fitted through the fog points, and this smoothed fog level subtracted point by point from the spectrum data.

This conversion of microdensitometer output into units of absolute density is performed by computer (program 'A4': see Figure 6).

The next step in the reduction is to convert the recorded spectrum from these density units to units of relative incident light intensity. For electronographic image tube spectra this is very easy because the relation between density and intensity (corresponding to the 'calibration curve' of photographic emulsions) is to a first approximation a linear one. Brand (1967) has shown that for G5 emulsion the linear law in fact breaks down for densities above about 0.4. With the exception of a few spectra of bright, unreddened stars, all the present spectra have maximum densities less than 0.4, and the linear law was assumed to hold in all cases.

The main spectrum analysis is performed by three programs, A1, A2 and A3 (see Figure 6). These are based upon three procedures written by G.I. Thompson. Programs A1 and A2 set up the dispersion curve for a spectrum.

The digitised spectrum in intensity units (A4 output) is first scanned by computer in order to detect microdensitometer faults and flaws in the spectrum data

(due to emulsion flaws or high spatial-frequency Spectracon response irregularities), and also to find the positions of stellar lines. The latter is effected by convoluting the data with a square function symmetric about both co-ordinate axes in subtended area, which has the effect of emphasising the high spatial-frequency components ('lines') in the data with respect to the low spatial-frequency ones ('continuum'). After discriminating against noise, the positions of remaining maxima (lines) in the convoluted spectrum are determined by parabola fits, and a list of line centres is printed out.

Consideration of the strengths and widths of the maxima in the convoluted spectrum, and comparison with the original analogue microdensitometer record, leads to identification of various stellar lines. For each spectrum, about ten strong unblended lines were chosen for determining the dispersion equation. The lines were chosen from the four Balmer lines, the five strongest He I lines, the Mg II line at λ448.1 nm., and lines of Fe II. The dispersion equation was represented by a set of polynomials of up to fourth degree, the second degree fit usually being of sufficient accuracy. The standard error was typically 30 pm. (0.3 Å) in wavelength, or about half a microdensitometer step.

The main analysis program (A3) takes the spectrum data (A4 output) and solves simultaneously for the continuum polynomial constants and the equivalent widths

for all the stellar lines in the full line list (see Section 2.5), by fitting a given gaussian profile (see Section 2.6) at each line position as calculated from the dispersion curve (A2 output). Sections of the spectrum data that are ignored when finding the solution include regions around flaws, regions surrounding the Balmer lines (which cannot be represented by the given gaussian profile), and a strategic section corresponding to the assumed extent of the DISAF under investigation.

The spectrum, rectified to the model continuum as unity, is output from A3. This rectified spectrum includes the profile of the DISAF as required (although a correction is needed for the NURCAM effect (see Section 2.7) before the true profile is finally obtained).

Averages or weighted means of spectra can be obtained by converting each individually to a spectrum sampled at equal wavelength intervals, using the dispersion curve (A2 output) and the program A7, and then taking point to point means using program A5 (see Figure 6).

2.5 Positions of Stellar Lines

An important prerequisite of the spectrum analysis program is a list of the wavelengths of all stellar lines that are expected to be detectable in the spectrum of the star under consideration.

The 'detectability' of a line is not easy to define, but there must exist a critical line intensity such that the inclusion of any weaker lines begins to show a relative decrease in the total amount of information

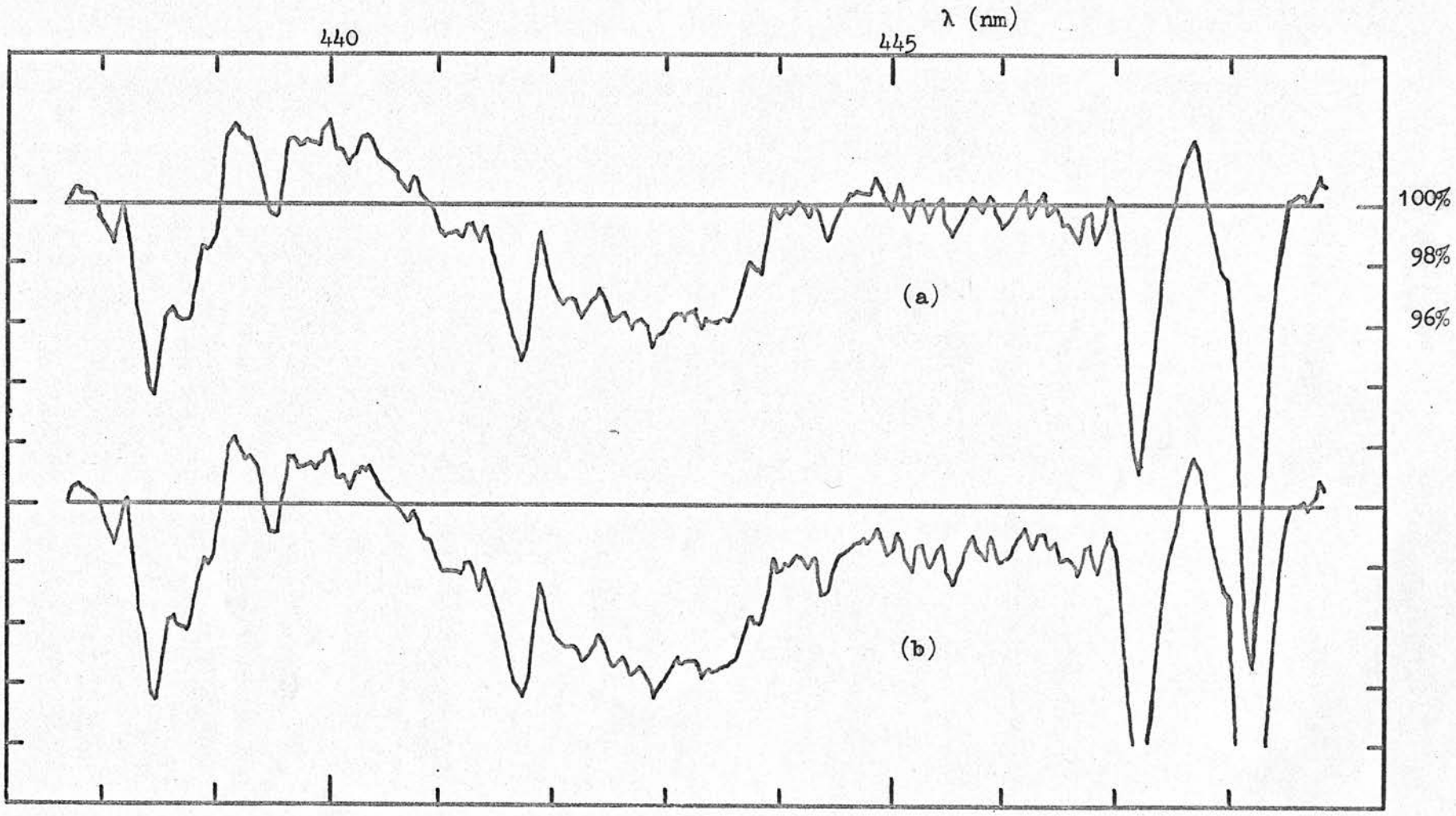

Figure 7 The typical effect on the profile of '4430' of major changes in the line lists.

extracted from the spectrum. Essentially, this happens because the more lines there are to be measured, the less data there is for determining the continuum constants, and because the weaker a line is, the less accurately can its strength be determined.

The compilation of the line list for a star proves to be quite a subtle operation. The importance of obtaining an accurate estimate of the critical intensity in terms of the inclusion or exclusion of actual lines can best be conveyed by a practical example. Figure 7 illustrates two different profiles for '4430'. These were obtained by separate analyses of the same spectra identical but for the line lists.

Figure 7(a) shows a mean profile from three spectra of B8 and A0 supergiants used by Brück and Nandy (1968, see Figure 1 Group A). The line lists used in this case included 30 lines outwith the omitted regions for the B8 star, and 80 lines for the A0 stars. The use of a 'compromise' list for all three spectra of 40 lines (mainly those which could actually be detected by visual inspection of the microdensitometer traces) produced the corresponding mean profile shown in Figure 7(b). Relative to (a), the continuum over the DISAF has been elevated by up to 1½%. The necessity for careful deliberation over the line list compilation is obvious.

The line lists for B8, B9 and A0 supergiants for the present investigation were compiled by comparison of the Hiltner and Williams (1946) atlases of Rigel (B8Ia) and Deneb (A2Ia) spectra, together with the list of Deneb

line strengths given by Grȣth (1961), with three mean spectra for B8, B9 and A0 stars respectively, obtained by computer averaging of the present image tube spectra. Only lines that were expected to be present with a strength of at least 2 pm. (0.02Å) equivalent width were included. This value was arrived at in the following way.

The detectability of a line is mainly determined by the G5 emulsion granularity. This is assumed to be white noise with a standard error in density units given by σ_D where $\sigma_D^2 A = 1.31 \bar{D} + 0.08$ (Brand, 1967). Here, $\bar{D}$ is the mean density and A is the projected area of the microdensitometer scanning slit. In the present case, A was constant at $\simeq 3 \times 10^4$ μm.^{2}, and $\bar{D}$ varied from 0.1 to 0.3. These values give an average standard error of 2% of the mean (or stellar continuum) intensity, assuming a linear relation between density and intensity.

Now one resolved element for these spectra is approximately 300 pm. (see Section 2.6 below), and therefore includes six microdensitometer steps or grain noise samples. The critical equivalent width for detectability was then defined as the area under a rectangle of height equal to the probable error on the mean of six grain noise samples, and of width equal to the resolution, 300 pm. The value of this area is

$$W_c = 0.675 \times \frac{0.02}{\sqrt{6}} \times 300 \text{ pm.} \simeq 2\text{pm.}$$

This definition is somewhat arbitrary, especially in the choice of effective line width and in the fact that blending of lines is not specifically taken into account.

Table III A summary of the multiplets (M) and the total number of lines in each (n) included in regions of the line lists affecting the continuum fitting.

('d' indicates a close doublet)

Ion	I.P. (eV)	B8 list M	B8 list n	B9 list M	B9 list n	A0 list M	A0 list n
He I	24.6	12	1 d	12	1 d	12	1 d
		14	1 d	14	1 d	14	1 d
		16	1 d	16	1 d	16	1 d
		18	1 d	18	1 d	18	1 d
		48	1	48	1	48	1
		51	1	51	1	51	1
		53	1	53	1	53	1
C II	24.4	6	1 d	--		--	
Mg II	15.0	4	1 d	4	1 d	4	1 d
		--		10	1	10	1
Si II	16.3	3	2	3	2	3	2
Si III	33.5	2	3	--		--	
S II	23.4	9	1	--		--	
Sc II	12.8	--		--		7	1
		--		--		14	1
		--		--		15	3

(continued)

(Table III continued)

Ti II	13.6	--		20	1	20	1
		--		31	1	31	1
		--		41	5	41	6
		--		50	2	50	2
		--		82	2	82	2
		--		--		104	1
		--		--		105	2
Cr II	16.5	--		30	2	30	2
		--		31	2	31	3
		--		44	4	44	4
Fe I	7.9	--		--		41	1
		--		--		42	2
		--		--		43	3
Fe II	16.2	27	4	27	4	27	7
		--		28	3	28	5
		--		32	1	32	1
		37	4	37	8	37	10
		38	5	38	6	38	7
		42	1	42	1	42	1
		--		43	2	43	2
		--		126	1	126	2
		--		127	1	127	1
		--		--		172	1
		--		186	2	186	2
		--		--		190	1
		--		--	1	--	1
Ni II	18.2	--		--		11	1
	TOTALS:		29		60		88

However, the results indicate that the minimum standard error on the equivalent width of an isolated line (or on the total equivalent width of a close blend), as measured from different spectra of the same star, is about this value of 2 pm.; and that the above working definition of W_c is also satisfactory in other respects.

Table III lists the multiplets (and the numbers of lines in each) which were assumed to be present. The data were obtained by reference to the Revised Multiplet Table of Miss C.E. Moore (1959). Table III only includes lines in the wavelength regions that influenced the continuum fitting, that is, in the regions $\lambda\lambda$ 400-409, 411-433, 435-439, 447-473.5, 478.5-485, 491-497 nm.

2.6 Profiles of Stellar Lines

The common profile of all the stellar lines in the line list was assumed to be a gaussian curve with full width at half intensity (δ) determined from the instrumental profile. The precise form of the common profile is not particularly important (Thompson, 1966) and the gaussian form is chosen for convenience.

In the pilot study of Brück and Nandy (1968), δ was (somewhat arbitrarily) given the value 200 pm.: this value had been found to be satisfactory by Thompson for photographic spectra of F and G type stars obtained with the same telescope, spectrograph, and slit width. For the present set of spectra, however, the slit width was slightly larger; and in any case it was felt that an independent estimate of δ was needed.

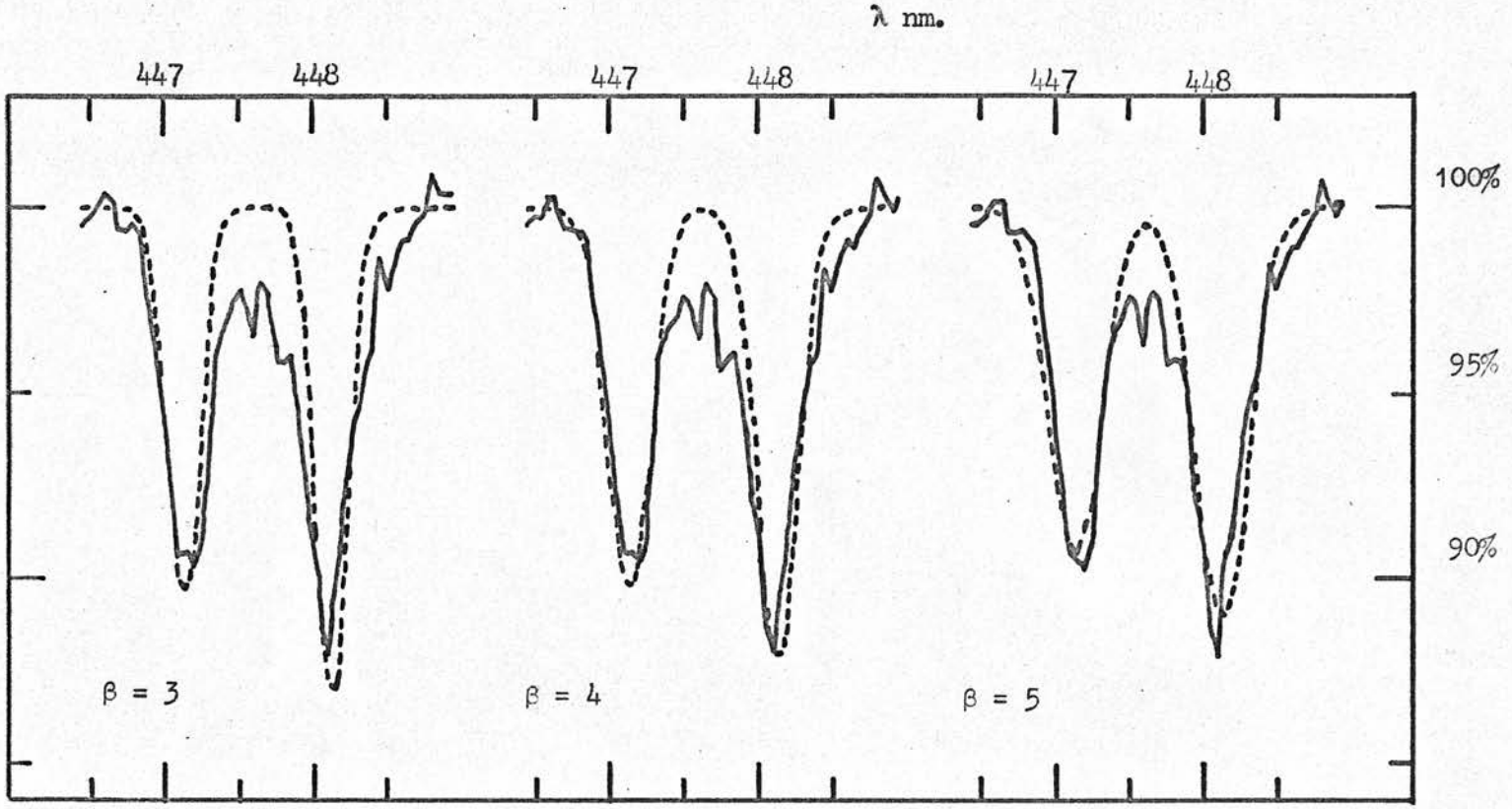

Figure 8(a) The fitting of gaussian profiles with β = 3, 4, and 5 to the two lines λλ 447.1 (He I), 448.1 (Mg II) in one of the Rigel spectra. The fitted profiles are the broken lines.

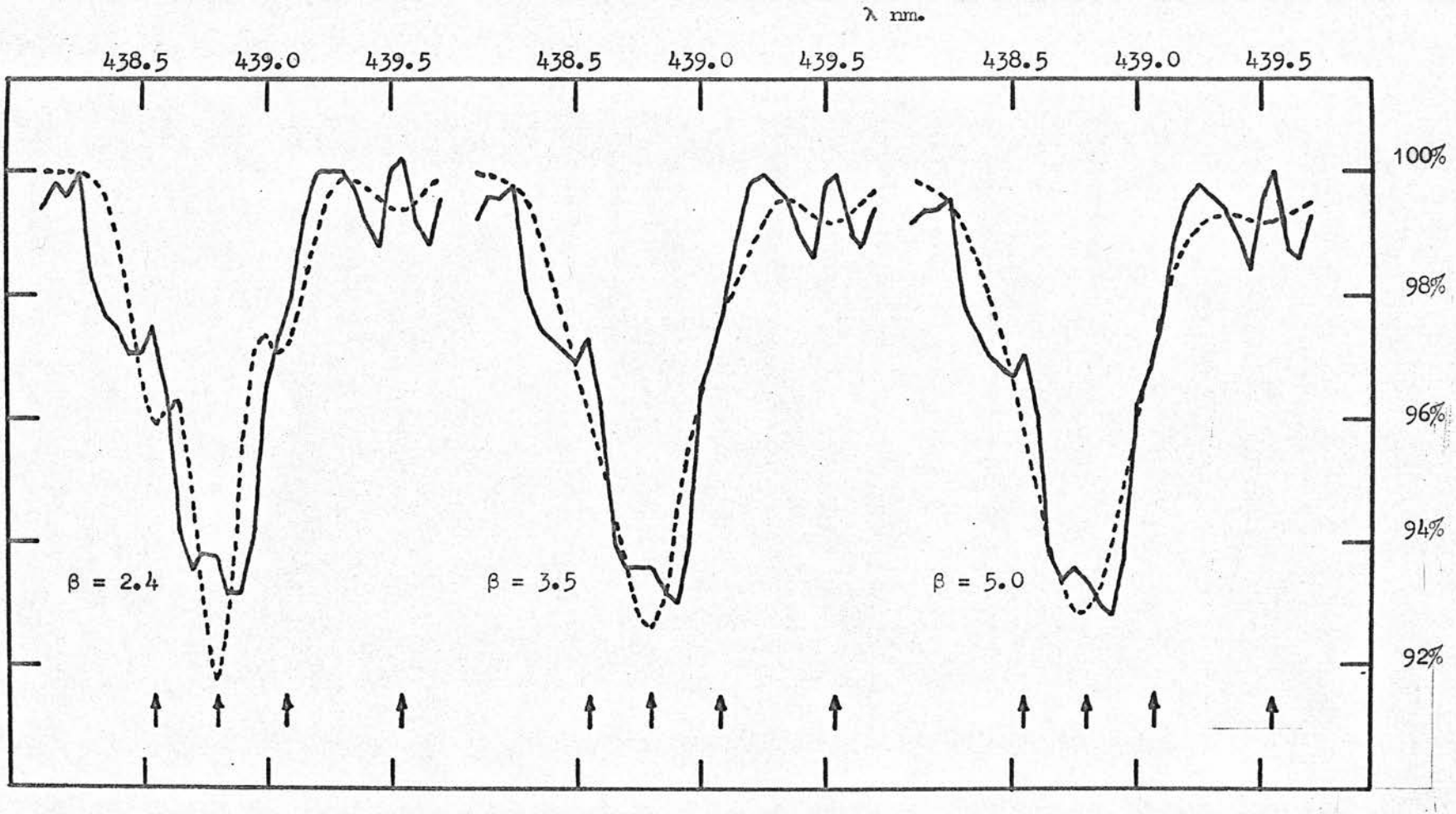

Figure 8(b) The fitting of gaussian profiles with β = 2.4, 3.5, 5.0, to a blend of four lines near λ439 nm. in one of the Rigel spectra.

The fitted profiles are the broken lines.

From microdensitometer tracings across nine lines in two helium arc spectra (obtained with exactly the same instrument settings as the stellar spectra) a mean value for δ of 290 $\pm$ 30 pm. was obtained. Owing to the lack of a fine tilt adjustment on the image tube ensemble, the spectra were not in focus equally for all wavelengths, and lines at the short wavelength end were slightly wider than those at the long wavelength end. For accurate equivalent width determinations, this effect would be significant, but for the present investigation, in which accuracy of the continuum position is of greater importance, it proves to be negligible. Therefore a value of 290 pm. for δ was assumed to hold for all lines in the line lists. The corresponding value of the 'half 1/e width', β, is $0.60\,\delta$ = 174 pm. $\equiv$ 3.5 microdensitometer steps.

The assumption of constant β for all stars is not strictly valid, because of stellar rotational velocity and macroturbulence doppler effects (Thompson, 1971). Indeed, such variations from star to star can be detected even by visual inspection of microdensitometer traces. Of the eleven stars analysed here, Rigel seems to have the broadest lines. Figure 8 illustrates the fitting of a gaussian profile with various values for β to some lines in one of the Rigel spectra. The best value would seem to be about 4, or even higher.

The equivalent widths of strong lines in the four Rigel spectra calculated with β = 3.5 are on average 20% less than those given by Miss A.B. Underhill (1948). Assuming that the photographic results are correct, a

value for β somewhat larger than 3.5 is again indicated. In fact, the equivalent widths do not reach Miss Underhill's values until $\beta \simeq 4.5$ is used. However, at least some of the discrepancy must be due to mismatching of lines as a result of finite errors in the calculation of the dispersion curve. This effect can be seen, for example, in Figure 8(a) where the Mg II λ448.1 nm. line does not seem to be correctly centred. A mismatching of lines always gives a low estimate of equivalent widths. But nevertheless the Rigel line widths seem to require $\beta \simeq 4$. For the ten reddened late B stars, values of β ranging from 3.5 to 4 then seem likely.

Thompson (1971) has recently developed a method for calculating the correct values for β, using only the information contained within the actual spectrum to be studied. Unfortunately, this method was not available at the time of reduction of the present spectra. However, the effect on the resulting continuum position of even quite a substantial change in β is small. For example, consider an increase in β from 3.5 to 4.0 for Rigel. For a dozen lines in each of four spectra the <u>equivalent width</u> estimates increase by about 10% on average, but the corresponding estimate of the <u>continuum position</u> rises by less than 0.1%. This is small compared with errors arising from other sources. Hence, a constant profile with $\beta = 3.5$ was used for all the spectra reduced here.

2.7 Variations in Spectracon Response over the Image Area

In the process of reduction of the present spectra it

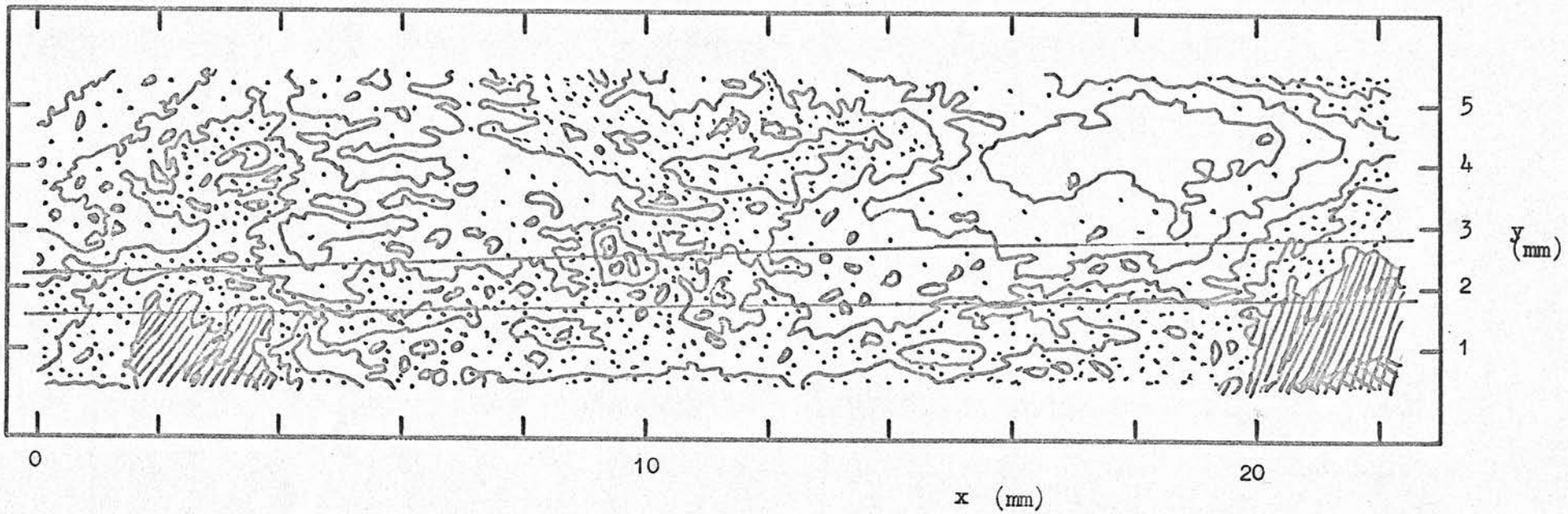

Figure 9 Isodensity map of B134 Spectracon image area, exposed August 4th 1968. Mean density 0.9 ; contour interval 0.08. (Adapted from Figure 1 of Smyth and Brand, 1969).

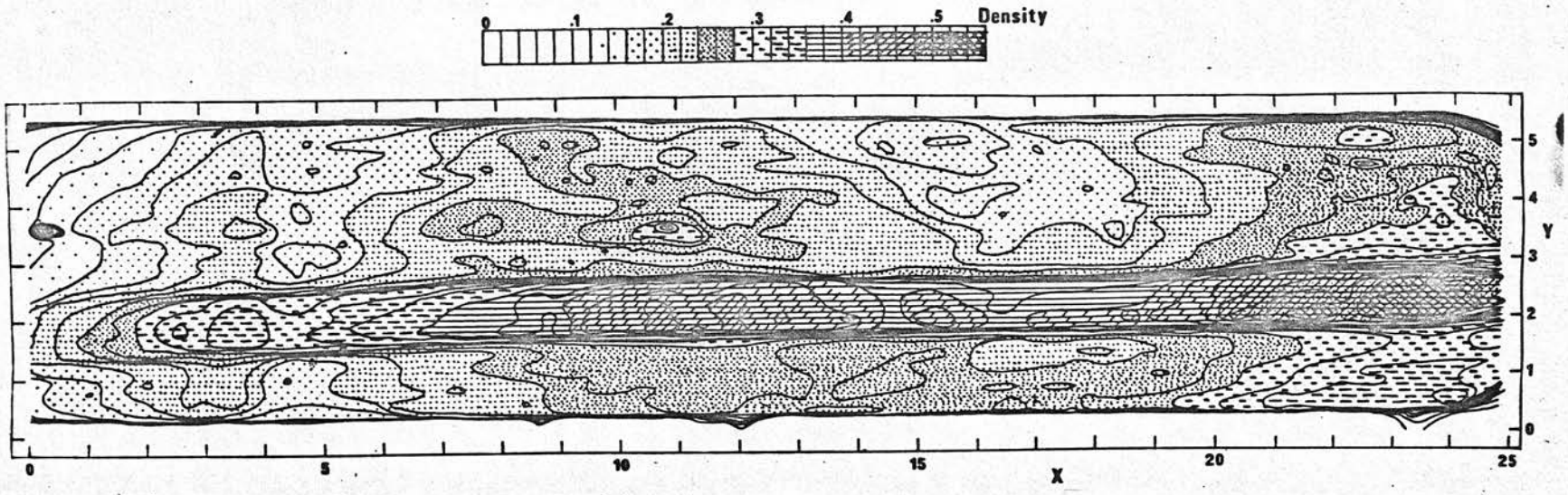

Figure 10 Isodensity map of B134 Spectracon image area, exposed December 16th 1968.

became obvious that the non-uniform response of the cathode and mica-window (NURCAM) of a Spectracon was more serious than had been assumed by earlier workers. This undesirable effect was first emphasised by M.J. Smyth and Brand (1969). Their isodensity map is reproduced in Figure 9 in a form that enables contours to be followed easily.

This map refers to the image tube used in the present investigation, although the electrograph used was taken some 5 months before the time of the present observations. For comparison with the map of Smyth and Brand, therefore, a similar one has been compiled from an electrograph taken during the new observations. This electrograph consists of a stellar spectrum together with a background fog of fairly high density. The map was obtained by scanning the electrograph with the digital Joyce Loebl microdensitometer with a 200 μm. x 200 μm. slit, a steplength of 200 μm. in the x direction and a 200 μm. scanning interval in the y direction. The digital output was transformed by interpolation in x into a list of the co-ordinates of points of equal density, in steps of 0.02.

The resulting countour map is shown in Figure 10. The contour interval is about 8% of the mean background density (a value very similar to that used by Smyth and Brand) and about 5% of the mean density of the spectrum. For comparison purposes, the x and y scales of the two maps have been aligned, and the edges of the spectrum in Figure 10 have been indicated on Figure 9. The original map of Smyth and Brand extended 0.5 mm. further in the

positive y direction and 1.5 mm. further in the negative x direction.

The two maps are similar in many respects. For example, on both maps there are broad bands running in the y direction with a maximum at $x \simeq 3.5$ and a minimum at $x \simeq 5$; and the lower halves ($y < 2.5$) of the images are more dense than the upper halves for almost the whole range of x. The latter effect can be seen clearly even on the spectrum region of Figure 10, from the relative 'crowding' of the contours on the lower edge of the spectrum. On the other hand, there are also some differences in the NURCAM effect as portrayed on these two maps. In particular, the sharp maximum in Figure 10 at (10.8, 3.6) and the associated tail of high density extending to $x = 7$ are completely absent in Figure 9. Also, the whole region $0 < x < 5$, $0 < y < 2$ in Figure 10 is considerably less dense relative to surrounding regions than it is in Figure 9.

These differences could possibly be due to changes in photocathode sensitivity. However, since Smyth and Brand (1969) considered that the major contribution to the NURCAM in their map was due to the cathode, and since most of the features in Figure 9 are preserved in Figure 10, it seems more likely that the few additional features arise from a deterioration in the state of the mica window. They may be evidence of the mica cleaving into separate planes. When such a cleavage occurs, there will be a decrease in the numbers of electrons able to penetrate the

window, leading to a relatively uniform reduction in response of the Spectracon over fairly large sections of the image area. Thus the general depression of sensitivity in the bottom left hand corner of Figure 10 could be explained in this way, whilst the ridge at $7 \lesssim x \lesssim 12.5$, $y \simeq 3.5$, could possibly be a 'cleavage line'.

This general explanation is in accord with the known history of the image tube in question. The tube was received from Professor McGee on March 6th, 1968. The electrograph used by Smyth and Brand was taken on August 4th, 1968; and the one shown in Figure 10 on 16th December, 1968. On April 8th, 1969, the mica window broke during routine loading of film, for no apparent reason other than weakness of the mica. If it was mica cleavage that led to this weakness, then the observed changes in sensitivity could have developed in the period between 8 and $3\frac{1}{2}$ months prior to implosion.

The changes in the NURCAM map from August to December 1968 preclude the use of Figure 9 in setting up a correction curve. In any case, the density resolution in Figure 9 is too low, and the x y correlation with Figure 10 and other spectrum images is too poor, to allow accurate corrections to be made. It is however, interesting to note from Figure 9 that for a region in x from, say, 7 to 14, NURCAM corrections (integrated over the spectrum width of 0.8 mm. in y) amount to less than $\pm$ 5%. Such a region in x would correspond to a stretch of some 30 nm. in wavelength on a spectrum such as that on Figure 10.

Although the full importance of NURCAM was not realised at the time of the present observations, it has been possible to derive, from some electrographs obtained at the time, a reasonably good correction for this undesirable effect, in the manner described below. The correction is accurate to about 0.5% in relative intensity in most places, and to about 100 μm. in position on the mica window.

There is a facility in the form of a 'scanning coil' incorporated in the solenoid assembly (McGee et al., 1969) allowing for displacement of a spectrum across the mica window without change of focus. Experiments were performed with the image tube ensemble on the telescope to establish the shift of a (helium) spectrum for various values of the scanning coil current. The spectrum was found to move 1.2 $\pm$ .2 mm. in y and 400 $\pm$ 40 μm. in x for a current of 400 mA.

Four stellar spectra were obtained with a scanning coil current of 400 mA; whilst for all the other spectra, including the one shown in Figure 10, the current was either 50 mA or zero. With 400 mA current, spectra were displaced from the normal position marked on Figures 9 and 10 a distance corresponding to a little over one spectrum width, towards the 'top' of the window. These four spectra are therefore situated on a section of very irregular NURCAM - including the aforementioned area of high response near x = 11 - and have not been reduced in the present analysis. However, on two of these four

electrographs, the background density was high enough to permit inspection of the NURCAM in the vacated 'normal' spectrum position. Moreover, the presence of the adjacent stellar spectrum allowed an accurate 'wavelength' calibration of the NURCAM spectrum to be effected.

The NURCAM of the area normally occupied by a stellar spectrum was in all ways treated as if it were itself a spectrum: the two quasi-spectra were recorded and reduced in an exactly analogous way to the real stellar spectra, except that no line list was used. The adjacent stellar spectra were also recorded, in order to determine dispersion curves for the quasi-spectra; and a wavelength-independent correction of + 1.4 nm. was applied to allow for the 'red shift' appropriate to a scanning coil current of 400 mA. In this way the quasi-spectra were calibrated in wavelength to an accuracy of 0.2 nm.

Following the practice adopted in the reduction of stellar spectra, the regions containing exceptionally high spatial-frequencies were omitted from the reduction: these regions could almost always be assigned to dirt, scratches or flaws in the emulsion, whilst owing nothing to the NURCAM.

The mean of the two rectified quasi-spectra still showed a noise level of about 2%, and therefore, to obtain a smooth NURCAM correction curve, a running mean of nine points was taken. The disadvantage of this procedure -

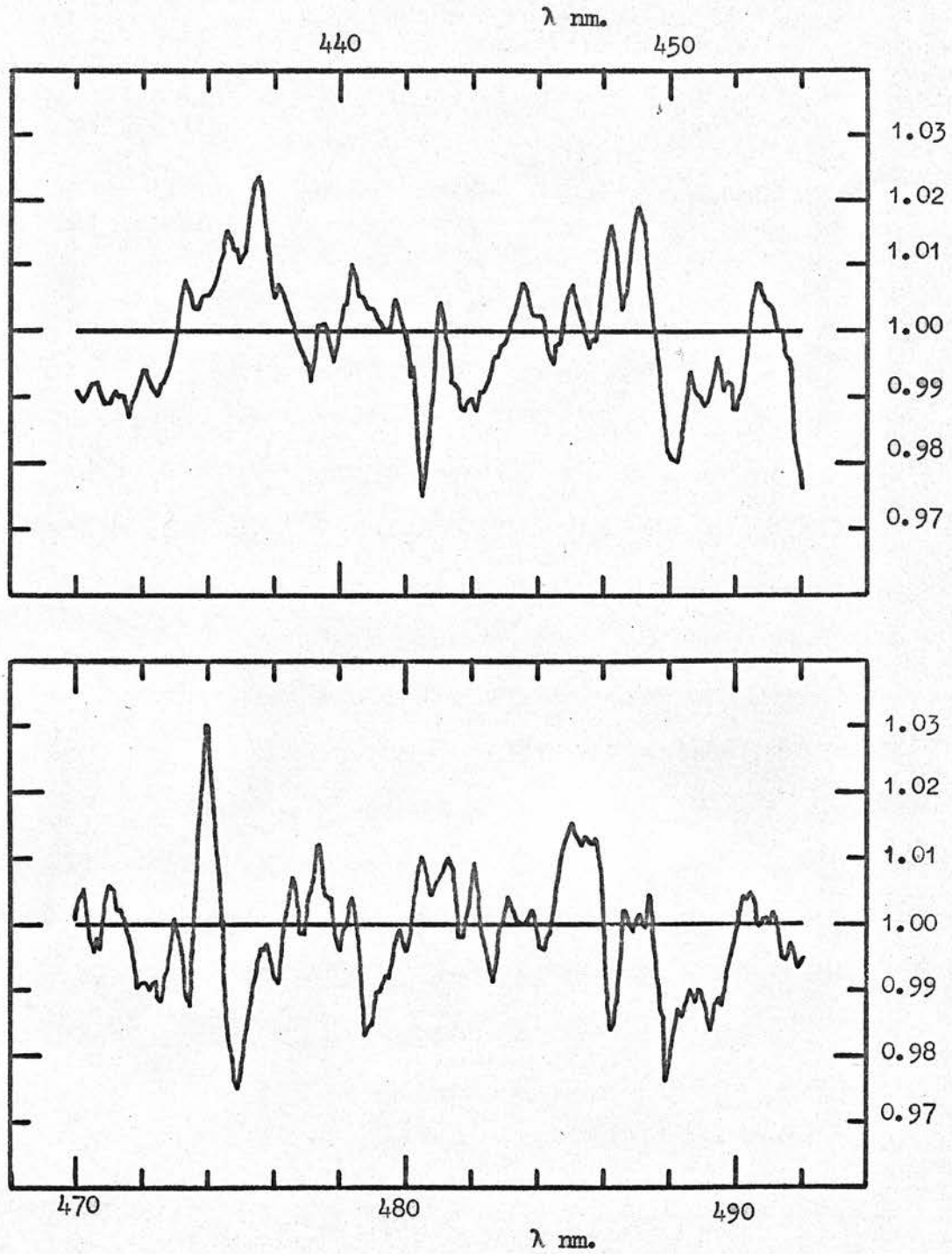

Figure 11 The correction for NURCAM in the vicinity of the three interstellar bands studied.

the loss of resolution of the NURCAM measurement - was considered to be outweighed by the desirability of keeping the random noise to a minimum.

A less noisy, higher resolution NURCAM measurement would require considerably more than two such quasi-spectra. Ideally, at least one NURCAM measurement should be obtained for every two or three stellar spectra, and the corrections should be applied at an earlier stage in the reduction than was done here. In future investigations, therefore, the NURCAM effect should be taken much more seriously. The corrections calculated here, whilst making optimum use of the available data, are nevertheless only accurate to about 0.5%. These NURCAM correction errors are the largest single contributors to the total uncertainty on the final DISAF profiles (see Section 3.4).

The smoothed NURCAM corrections in the vicinity of the three DISAFs under investigation are shown in Figure 11. The rectified stellar spectra were divided point by point by these NURCAM factors to give the final profiles as presented in Chapter 3.

The majority of the spectra listed in Table II were obtained in the same week in December 1968 as the NURCAM quasi-spectra. During this week, the NURCAM seemed to remain constant, and certainly the whole image tube ensemble and spectrograph settings were undisturbed, so that the corrections of Figure 11 apply equally to all these spectra. However, these corrections could not be applied to those few spectra (including the four Rigel

spectra) obtained in late January 1969, because of probable changes with time of the NURCAM, and because the image tube position had been adjusted in the intervening month. Since the importance of the NURCAM effect (and in particular its time-dependent nature) did not become apparent until after all the observations had been made and the reduction was under way, it has not been possible to obtain NURCAM correction curves for the January spectra.

3. Image Tube Observations: The Results

3.1 Results for '4430'

The wavelength region used for determining the '4430' profile was λλ 403-477 nm. This is larger and more symmetrical about λ443 nm. than that used by M.T. Brück and K. Nandy (1968).

The regions omitted in the spectrum analysis were:

(i) 408.6 - 411.6 (Hδ) = 3.0 nm.,

(ii) 432.5 - 435.5 (Hγ) = 3.0 nm.,

(iii) 438.5 - 447.5 (the assumed extent of the DISAF) = 9.0 nm., and

(iv) various small regions around flaws, amounting to 2.4 nm. on average, and varying between 0 and 7 nm. total loss for individual spectra.

The maximum total width of spectrum omitted from the analysis was therefore 30% of the whole wavelength range. Assuming that measurement of each stellar line in the line list uses an equivalent of 0.5 nm. of spectrum, the percentage of the total range left for continuum fitting varied from 50% for B8 stars to less than 20% for A0 stars. Even the latter figure, though, corresponds to about 200 microdensitometer steps (spectrum samples), which is quite adequate for determining the continuum position to the required accuracy. The choice of 2 pm. (≡ 0.02Å) as the critical equivalent width for compilation of the line lists (Section 2.5 above) is thus vindicated.

The length of the strategically omitted section around λ443 nm. used here is the same as in the pilot study

(Brück and Nandy, 1968): the maximum extent of the band is assumed to be ± 4.5 nm. In the literature on '4430', however, one finds estimates of this 'total width' varying from ± 2.5 to ± 7.5 nm. Additional profiles were therefore obtained (for the B8 stars only) with a section only 5 nm. long omitted from the analysis. The apparent absorption maximum, A_c, was on average 0.7% greater than that calculated with an omitted section of 9 nm., and comparison of the two sets of profiles indicated that the feature certainly influences more than 5 nm. of spectrum. In particular, it seems to extend to the violet at least 4.5 nm.

The question of the presence or absence of very extensive wings to '4430' and the other broad DISAFs is an intriguing one. In the limiting case, the wings are so extensive that the DISAF and the continuous extinction become inseparable. This problem is considered again in Chapter 6 in connection with the comparison of predicted and observed profiles. From a practical point of view, it must be remembered that the omitted section cannot be extended very far before intolerable interpolation uncertainties result. The present violet limit, especially, could not be extended far before it effectively merged with the Hγ omitted region. Thus a 9 nm. wide section for '4430' is probably the maximum allowable for the automated spectrophotometric method as used here. This is not a real disadvantage, as long as care is taken when relating such observational results to theoretical predictions.

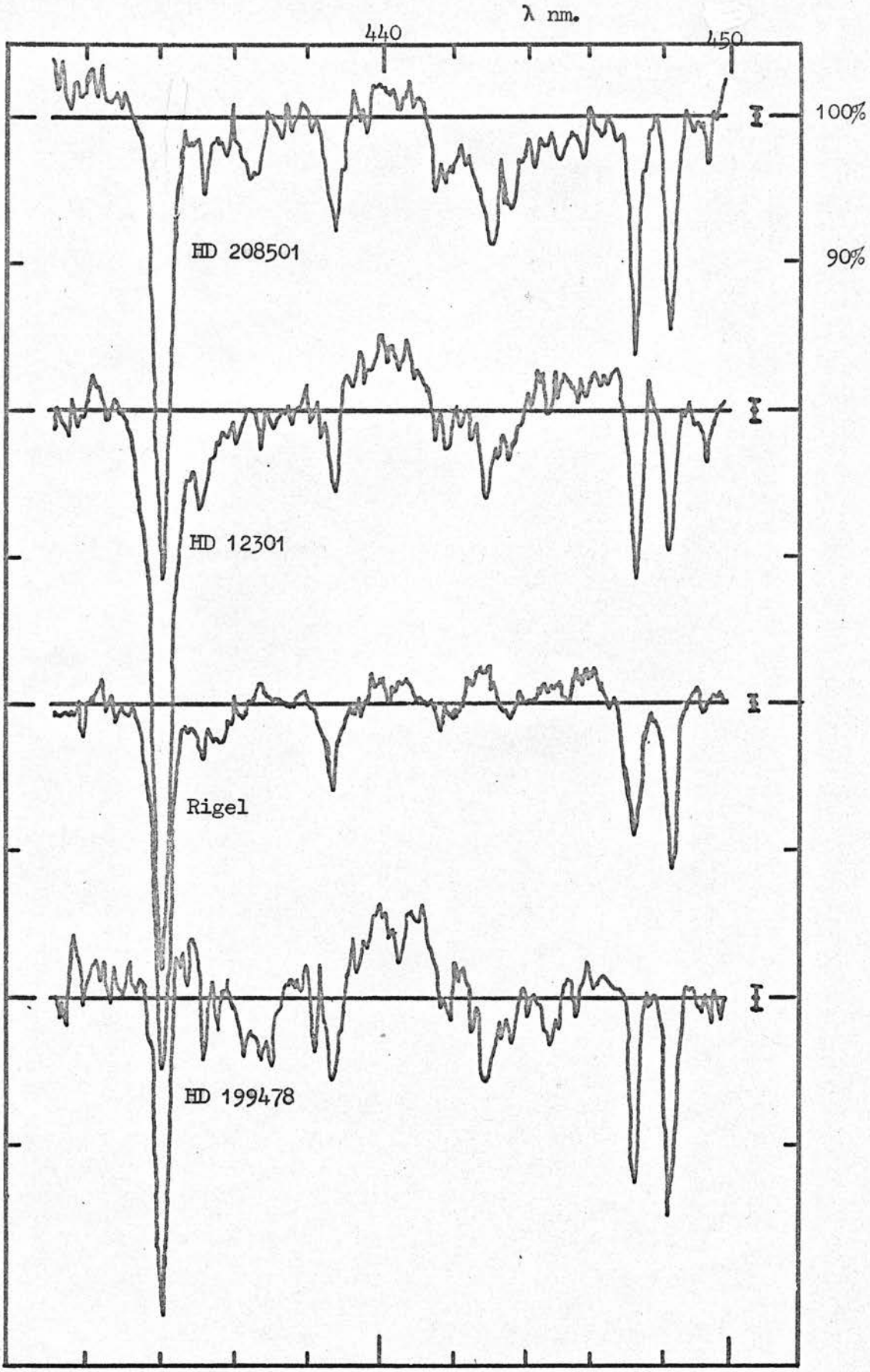

Figure 12 Mean rectified spectra for individual stars, in the region of '4430'. Error bars indicate grain noise level. Stars are in order of spectral type (see Table IV)

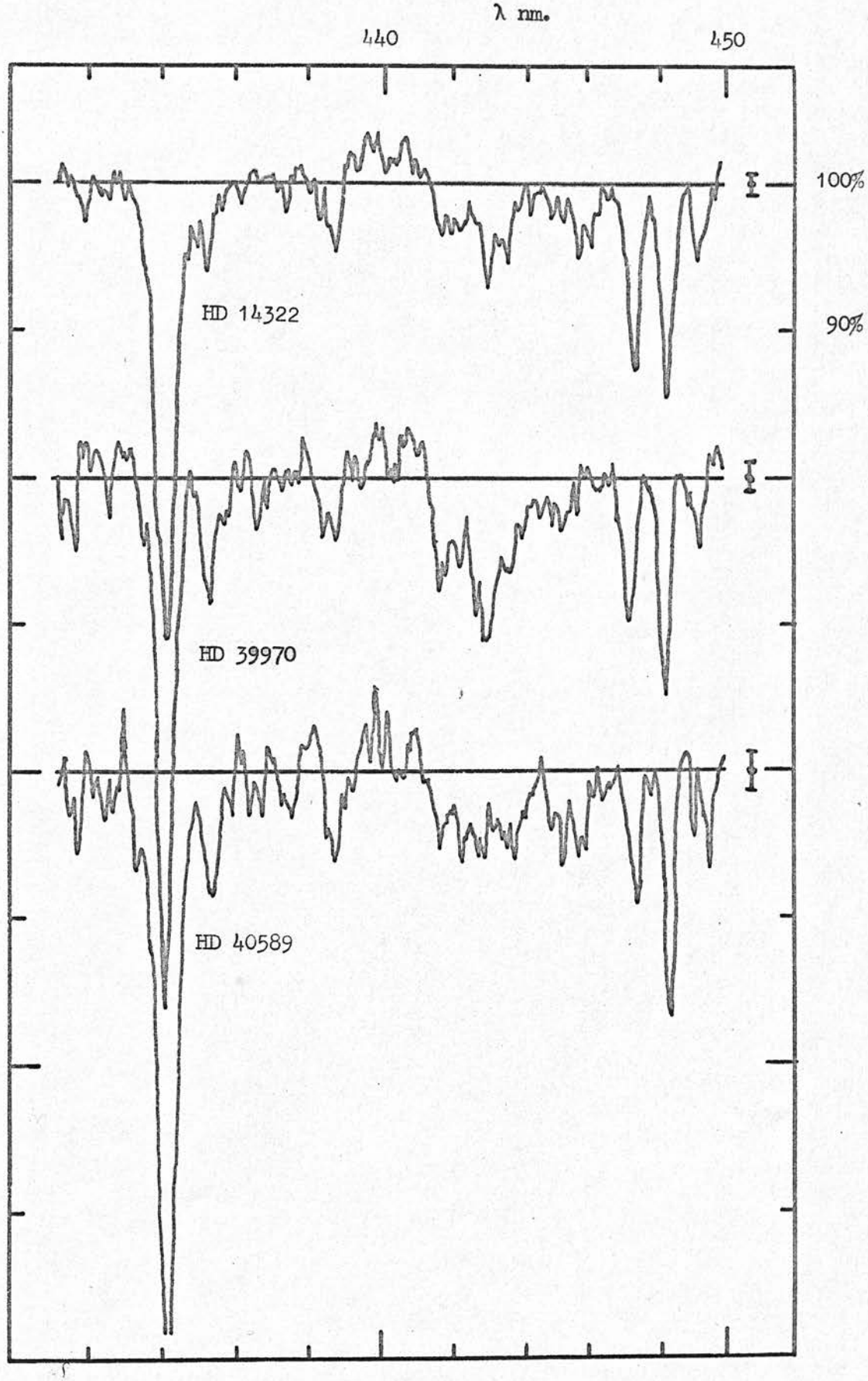

Figure 12 (continued)

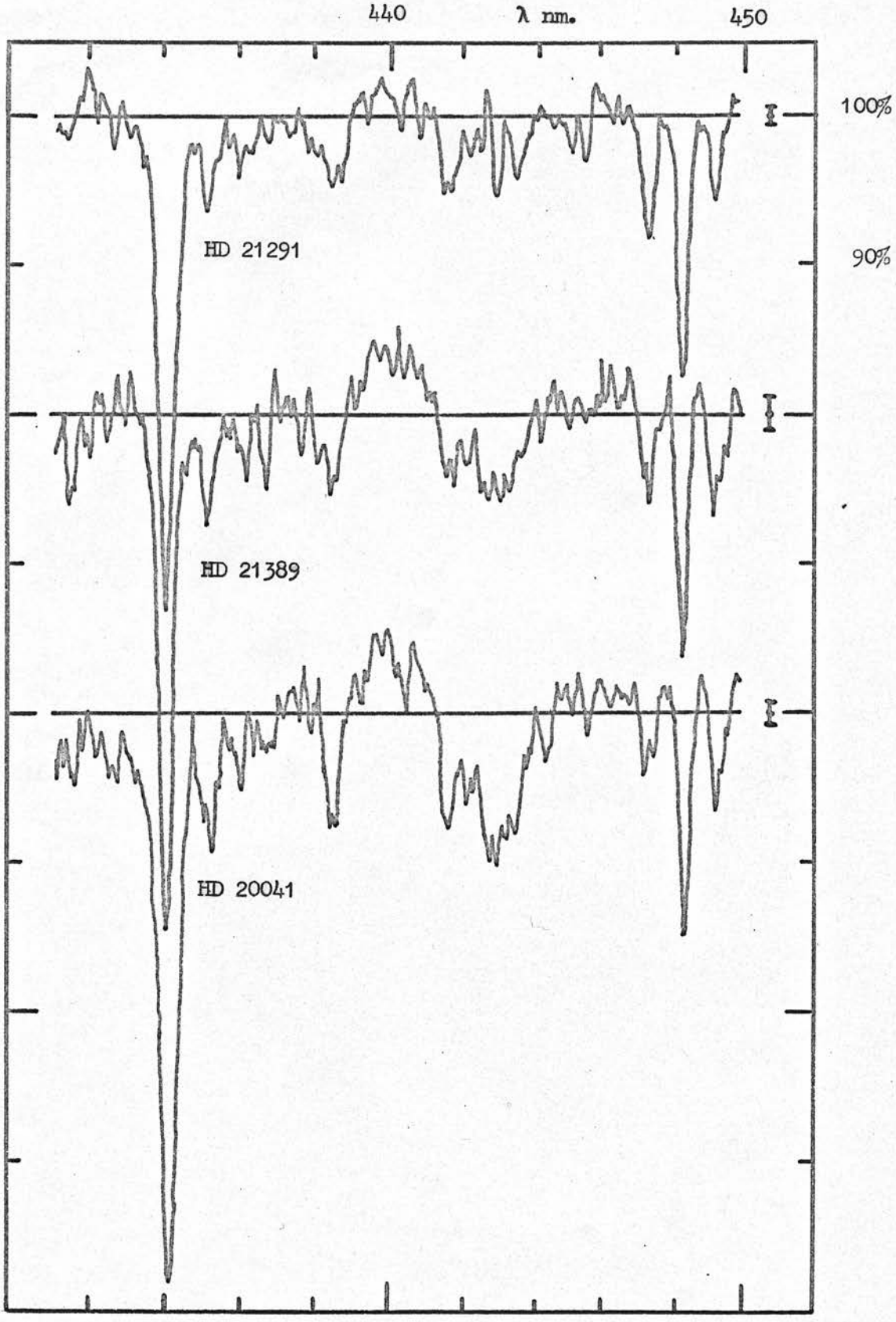

Figure 12 (concluded)

Using the wavelength regions for spectrum analysis listed above, the image tube spectra of the late B supergiants were reduced according to the scheme described in Chapter 2. The results are shown in Figure 12 for nine reddened late B supergiants, and Rigel. For the reasons given in Section 2.7, the Rigel spectra have not been corrected for the non-uniformity of Spectracon response (NURCAM), and hence the Rigel '4430' profile is included here for purposes of qualitative comparison only.

No profile is given for σ Cygni. This is because the two spectra obtained for this star were both overlapped by the 'fog' backgrounds of the succeeding exposures (due to slipping of the film roller), thus rendering NURCAM corrections invalid. This effect was much less serious for the '4890' band, so a profile is given for σ Cygni for this band (see Section 3.3 below).

The profile of '4430' is masked to a certain extent by stellar lines, although their strength is minimal for these late B stars (see Figure 5). The He I λ443.7 nm. line can be seen in the spectra of the B8 stars, but not in the others. The Ti II λ444.3 nm. line does not seem to be present in significant strengths, except for HD 20041, which on this and other evidence given below seems to be of later type than A0. The Fe II line at λ441.7 nm. is present in all the spectra. It is strong at A0 and strongest for HD 20041, where Ti II λ441.8 nm., may be blended with it. At B8 it may be blended with the weak Fe III line at λ441.9 nm., and the even weaker O II doublet $\lambda\lambda$441.5, 441.7 nm. The Mg II pair at

λλ442.8, 443.4 nm. seem to be very weak, even for HD 20041.

The two groups of stellar lines bounding the '4430' band, around λ439 and λ448 nm. are very useful indicators of spectral type (and hence of strengths of weak lines in the band itself). The first group includes Fe II λ438.5, He I λ438.8, and weak MgII lines at λλ438.4 and 439.1 nm. At B8, He I λ438.8 is dominant, but the Fe II line increases rapidly in strength with decreasing stellar temperature, and the He I line correspondingly decreases in intensity. The overall effect is a gradual shift in wavelength of the effective position of maximum absorption from λ438.8 at B8 to λ438.5 at A2 (see for example Apt et al., 1968).

The second group consists of three well-separated strong lines, He I λ447.1 (blended with the relatively weak lines of Ti II λ446.9 and Fe II λ447.3 nm.), MgII λ448.1 nm., and a blend of two Fe II lines, λλ 448.9 and 449.1 nm. At B8, the ratio of the strengths of the three lines is approximately 1:1:0; at A2 it is about 1:4:2, with the major contributions to λ447.1 now coming from the Ti II and Fe II lines there. The ratio of He I λ447.1 to Mg II λ448.1 is particularly useful since both lines are rather insensitive to luminosity variations (see for example Butler and Seddon, 1960, or Butler and Thompson, 1961).

Consideration of both these groups of stellar lines in the spectra of Figure 12 leads to the same conclusions regarding the spectral types of these stars. Taking

Table IV Comparison of MK spectral types with estimated types from three criteria in the region of '4430'.

HD	Effective λ of group of lines near λ 439 nm.	$\frac{A_c \text{ Mg II } \lambda 448.1}{A_c \text{ He I (+ weak blends) } \lambda 447.1}$	$\frac{A_c \text{ Fe II } \lambda 449}{A_c \text{ He I (+ weak blends) } \lambda 447.1}$	Estimated Spectral Type	MK Type
(Mean of 3 B5I stars) (Butler and Thompson)	(438.8)	(0.5)	(0)	--	B5 (I)
183143 (Herbig)	(438.8)	(0.9)	(0)	--	B7 (Ia)
208501	438.7	0.8	0.1	$B7_+$	B8 (Ib)
12301	438.7	0.8	0.1	$B8_-$	B8 (Ib)
34085 (β Orionis)	438.8	1.2	0.1	B8	B8 (Ia+)
199478	438.7	1.1	0.1	B8	B8 (Ia)
14322	438.6	1.1	0.3	$B8_+$	B8 (Ib)
39970	438.6	1.5	0.4	$B9_-$	A0 (Ia)
40589	438.6	1.9	0.4	$B9_-$	B9 (Iab)
21291	438.5	2.1	0.6	B9	B9 (Ia)

(continued)

(Table IV continued)

202850	438.6	2.5	0.7	$B9_+$	B9 (Iab)
21389	438.5	2.5	1.0	A0	A0 (Ia)
20041	438.5	3.0	1.4	$A1_-$	A0 (Ia)
197345 (α Cygni) (Hiltner and Williams)	(438.5)	(4)	(2)	--	A2 (Ia)

standard types to be represented by HD 199478 and Rigel for B8, HD 21291 for B9 and HD 21389 for A0 (see Underhill, 1966), the present stars fall on a continuous sequence as shown in Table IV. The profiles in Figure 12 have been arranged in the same order as the stars in Table IV.

Other indications of variations in stellar line strengths with spectral type in the range B5 to A2 can be discerned from the list of equivalent width estimates given in Appendix I.

Discrepancies between the MK spectral types and those assigned here do not seem to be related to luminosity classes.

The two largest discrepancies in Table IV occur for the stars HD 20041 and HD 39970. Some of the intense '4430' in HD 20041 may be due to unresolved stellar lines, although the central intensity measurement A_c is probably only influenced by the Mg II lines at $\lambda\lambda$ 442.8 and 443.4 nm. (See for example the spectrum of Deneb given by Hiltner and Williams, 1946.) The apparent elevation of the continuum to the red side of the band may well be due to underallowance for stellar lines: there would be an increase in the length of the line list between A0 and A1 greater than the corresponding ones between B8 and B9, or B9 and A0. An estimate of A_c is therefore less accurate for HD 20041 than for the other stars. The assignment of an A0 line list to the 'B9' star HD 39970 is, however, less serious from this point of view.

It can be concluded that for the majority of the stars

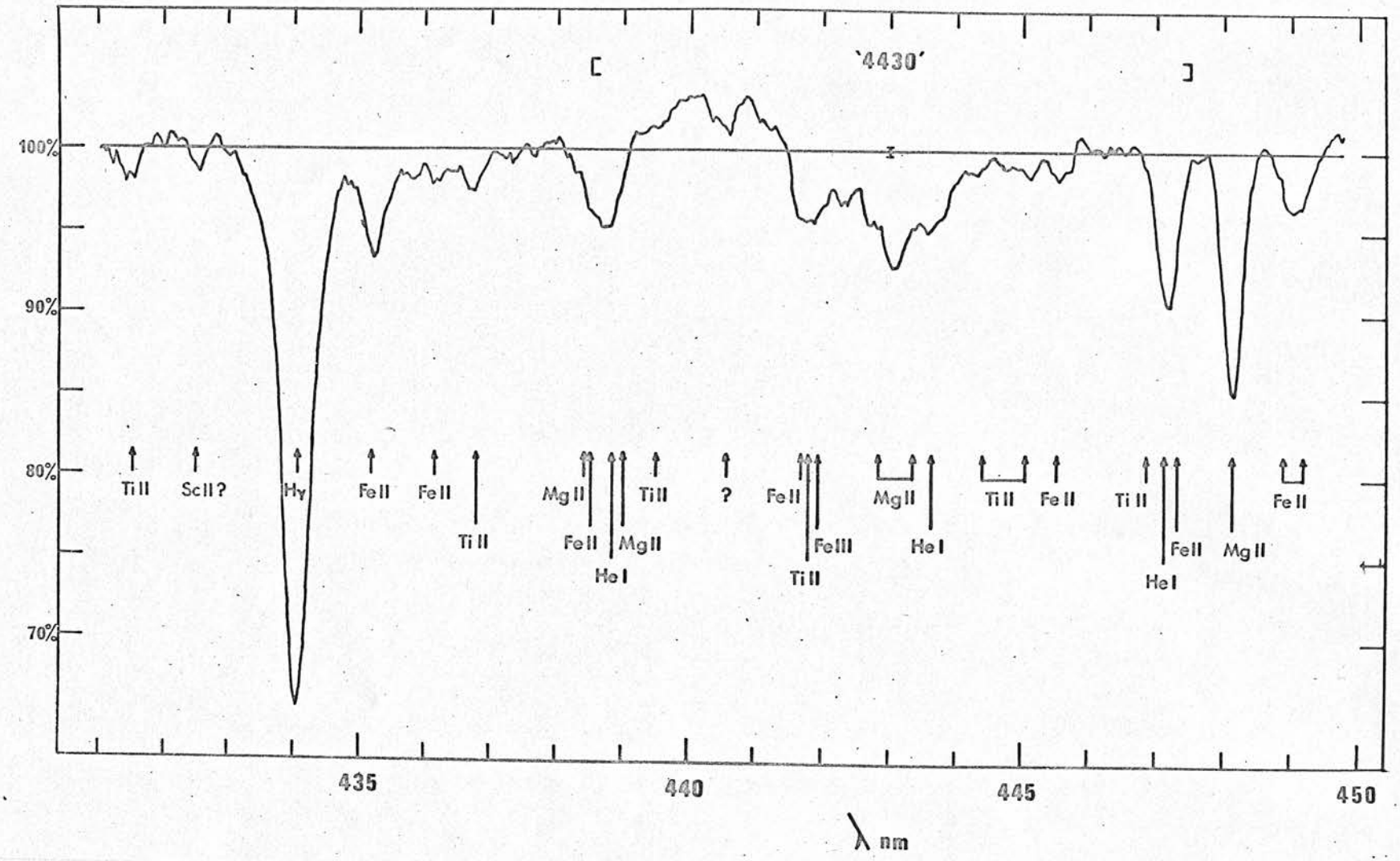

Figure 13 Mean rectified spectrum in the region of '4430'. Mean of 28 spectra of 9 stars.

studied the distortion of the interstellar band profile by stellar lines is only significant near the Fe II line λ441.7 nm. The effects of other lines are only important for HD 20041 and (possibly) HD 21389.

There remain, however, some interesting anomalies in the spectra of Figure 12. There seems to be a stellar line at about λ440.5 nm. in many of the spectra, especially those of HD 199478, 39970, 40589 and 20041. The most likely identification is Fe I (λ440.5), but it is much too strong, even for HD 20041. The line does not behave like an interstellar line, either, and it does not seem to be due to the NURCAM effect. Other peculiar absorptions are seen near λ436.5 in HD 199478 and 208501, and near λλ 437.5 and 445.5 in HD 40589.

The mean of 28 rectified spectra of the 9 reddened supergiants is shown in Figure 13, and the peculiar λ440.5 nm. absorption can be clearly seen. Some of the small scale structure visible in this mean profile may be due to NURCAM correction errors, and only part of the central 'dip' at λ443.0 nm. can be due to the Mg II λλ 442.8 and 443.4 lines. (On this last point, see also Figure 18 and its discussion in Section 3.4 below.)

The most important result here is the appearance in Figures 12 and 13 of a violetward 'apparent emission' wing, centred at about λ440 nm., which confirms the preliminary result of Brück and Nandy (1968). Since the earlier result was obtained from spectra taken with a different image tube from the present one, the emission feature must be taken to be real. It cannot be due to the

Table V — Estimated values of maximum apparent absorption (A_c) and maximum apparent emission in the violet wing (A_E).

HD	E_{B-V}(mag.)	'4430'			'4760'			'4890'	
		n	A_c(%)	A_E(%)	n	A_c(%)	A_E(%)	n	A_c(%)
12301	0.47	3	4	4	3	4	0	--	--
14322	0.44	2	5	2.5	2	3.5	1.5	--	--
20041	0.56	4	9	4.5	4	3	2	1	4
21291	0.49	4	3.5	1.5	3	1	1.5	3	1.5
21389	0.56	3	5	4	4	3.5	1	2	3
39970	0.39	4	9.5	3	4	3.5	1	2	4.5
40589	0.31	2	5	2.5	1	1.5	1	--	--
199478	0.56	2	4	5	2	4	3	2	3
202850	0.16	--	--	--	--	--	--	2	2
208501	0.83	4	7.5	2	4	4	0	--	--

NURCAM effect, since the present spectra have been corrected for this. The absence of such a feature (along with the absence of reddening and of '4430' absorption) in the Rigel spectrum (even though this has not been corrected for NURCAM) also supports its reality.

For one or two of the stars there is also an indication of an emission wing to the red, but it is certainly absent for most of the stars, and it does not appear on the mean profile. There is no obvious asymmetry in the apparent absorption part of the feature, which conflicts with some of the results of other investigations referred to in Table I and Section 1.2.

The mean central absorption is taken to be 6%: this corresponds to a mean A_c/E_{B-V} ratio of 11% per magnitude. The mean equivalent width of absorption in the range $\lambda\lambda$441.5-446 nm., after allowance for stellar lines, is 85 pm. (≡ 0.85Å) so that the mean W/E_{B-V} is about 160 pm. per magnitude; and the mean half-width δ is 1.8 nm. These last results are lower than most previous estimates (see Table I (a)).

The mean value of the maximum apparent emission A_E is almost exactly one half of the mean A_c. The ratio of these two quantities, $\rho = A_E/A_c$, proves to be a valuable tool for comparison with theoretical models (see Chapter 6).

Estimates, from Figure 12, of A_c and A_E for the individual stars are given in Table V, columns 4 and 5. Column 3 gives the number of spectra used to obtain the

separate profiles of Figure 12.

The varying estimates of A_C/E_{B-V} in the past can at least partially be explained by the presence of the violetward emission wing. For example, Duke (1951) seems to have drawn his continuum through the top of the emission wing, because he obtains a mean value for A_C/E_{B-V} of 14% which is approximately equivalent to $(A_C + A_E/2)/E_{B-V}$ in the present results. Other discrepancies can perhaps be attributed to the presence of numerous stellar lines in '4430', since many authors have observed early B type stars, for which the total equivalent width of stellar lines overlying '4430' can easily exceed the equivalent width of the band itself (see Figure 5).

The present results refer to a band at '4430' of assumed total extent $\pm$ 4.5 nm. This fact should always be borne in mind when considering the profiles of Figures 12 and 13, and the estimated A_C and A_E values given in Table V.

A discussion of the experimental errors on the plotted points of Figures 12 and 13 is deferred until Section 3.4 below.

3.2 Results for '4760'

The wavelength range used here was $\lambda\lambda$ 467.5 - 484.5 = 17 nm. and the omitted region was $\lambda\lambda$ 473-479 = 6 nm. Flaws totalled only 0.4 nm. on average and ranged from zero to 1.3 nm. for individual spectra. Allowing for stellar line measurements, the minimum effective number

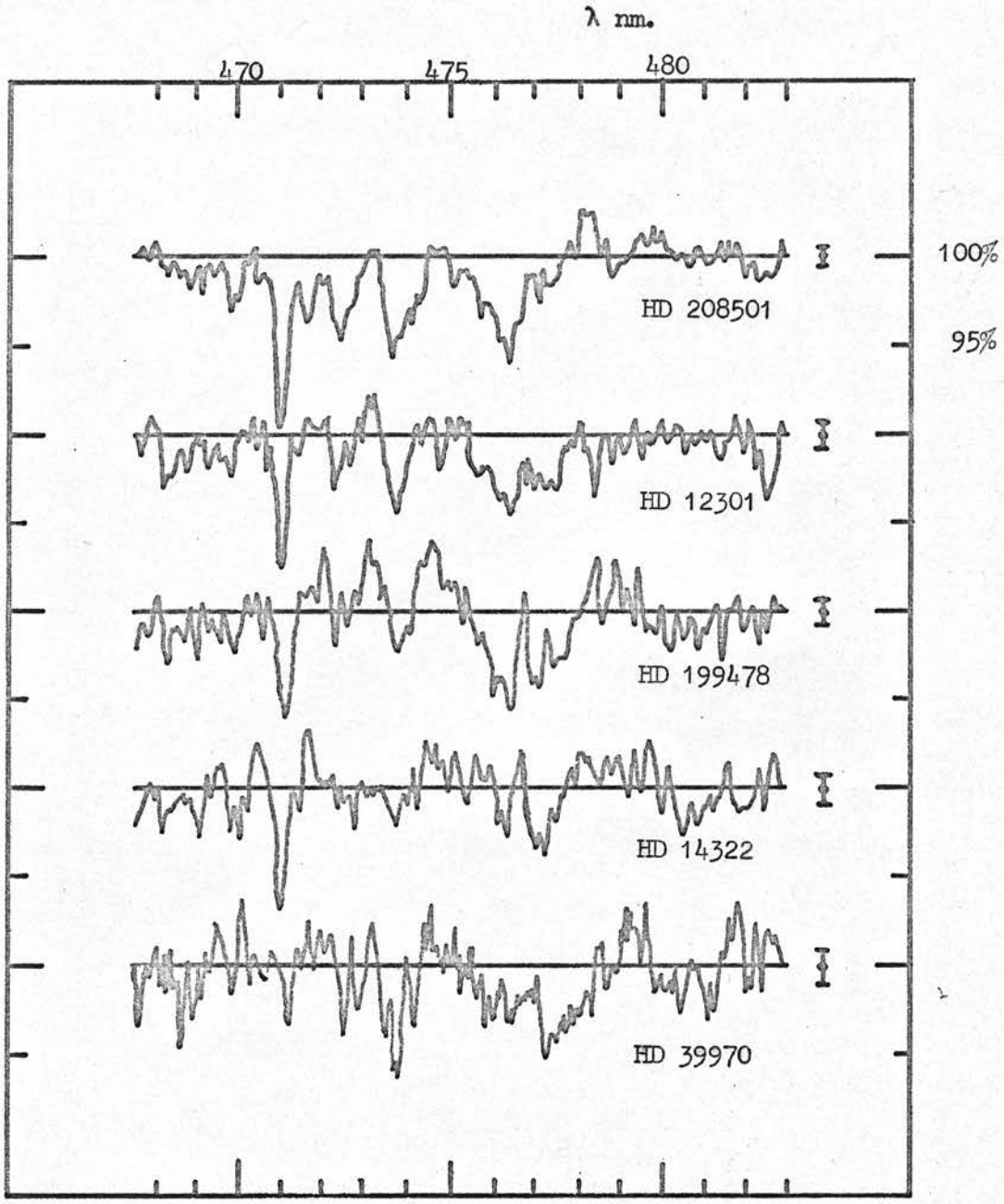

Figure 14 Mean rectified spectra for individual stars, in the region of '4760'.

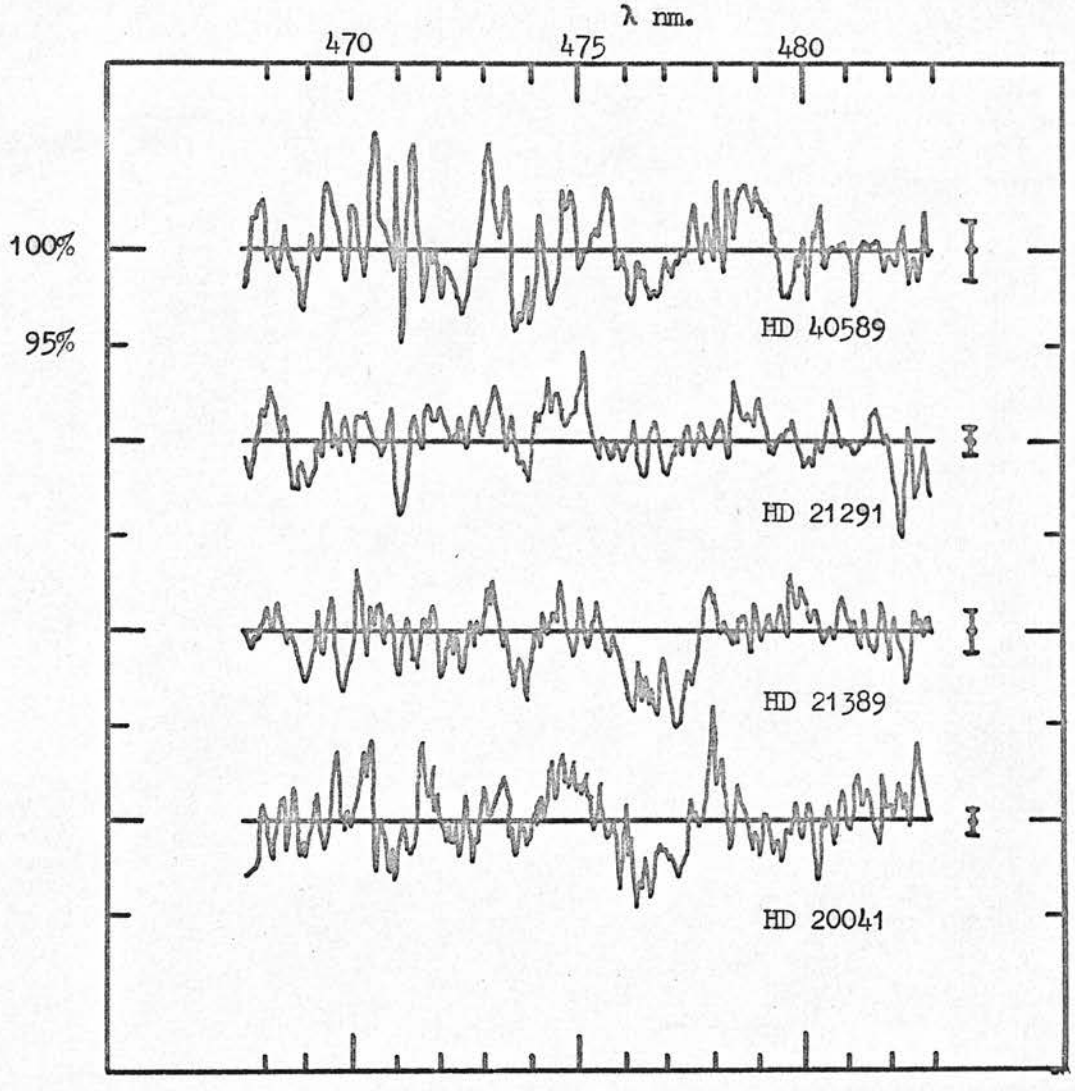

Figure 14 (continued)

Figure 15 Mean rectified spectrum in the region of '4760'.

Mean of 27 spectra of 9 stars.

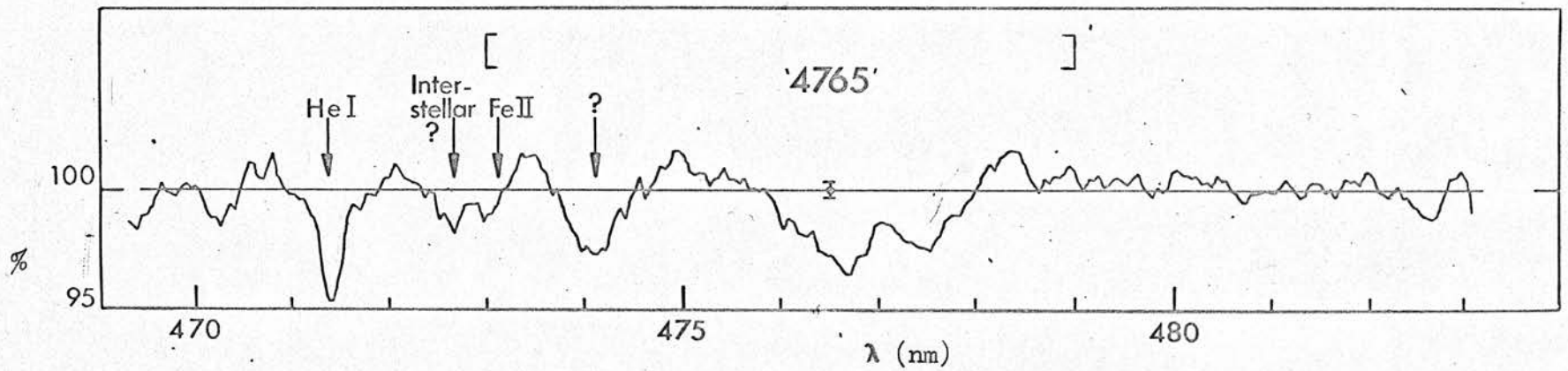

of microdensitometer steps (spectrum samples) left for continuum determination was 170.

The individual profiles are plotted in Figure 14, and the mean of the 27 spectra in Figure 15.

The feature at λ476.6 nm. has a mean central absorption of about 3% and a half-width of 1.2 nm. Although first mentioned in 1942, this band has been seldom seen, and estimates of its half-width have varied from 0.4 nm. (Herbig) to 4.0 nm. (Wilson) <u>for the same star</u>! The value derived here is close to the apparent half-width of the feature as seen in the atlas of Butler and Seddon (1958).

The apparent structure in the band is interesting, but must not be considered definite as it is of the same order as NURCAM correction errors in this region. A slight emission wing to the violet seems to be present for HD 199478 and HD 20041, but not conclusively for the other stars. Estimates of A_C and A_E for this feature are given in Table V, columns 7 and 8.

There are two other unidentified features of interest, at $\lambda\lambda$ 472.6 and 474 nm. The first may be interstellar (see Table I(b)) but it is very weak and is distorted by Fe II λ431.1 nm. in the later type stars. With respect to the computed continuum its central depth is little more than 1%: but since this continuum was fitted up to λ473 nm., it may in fact be slightly stronger. It is certainly less than half the strength of λ476.6 for these 9 stars.

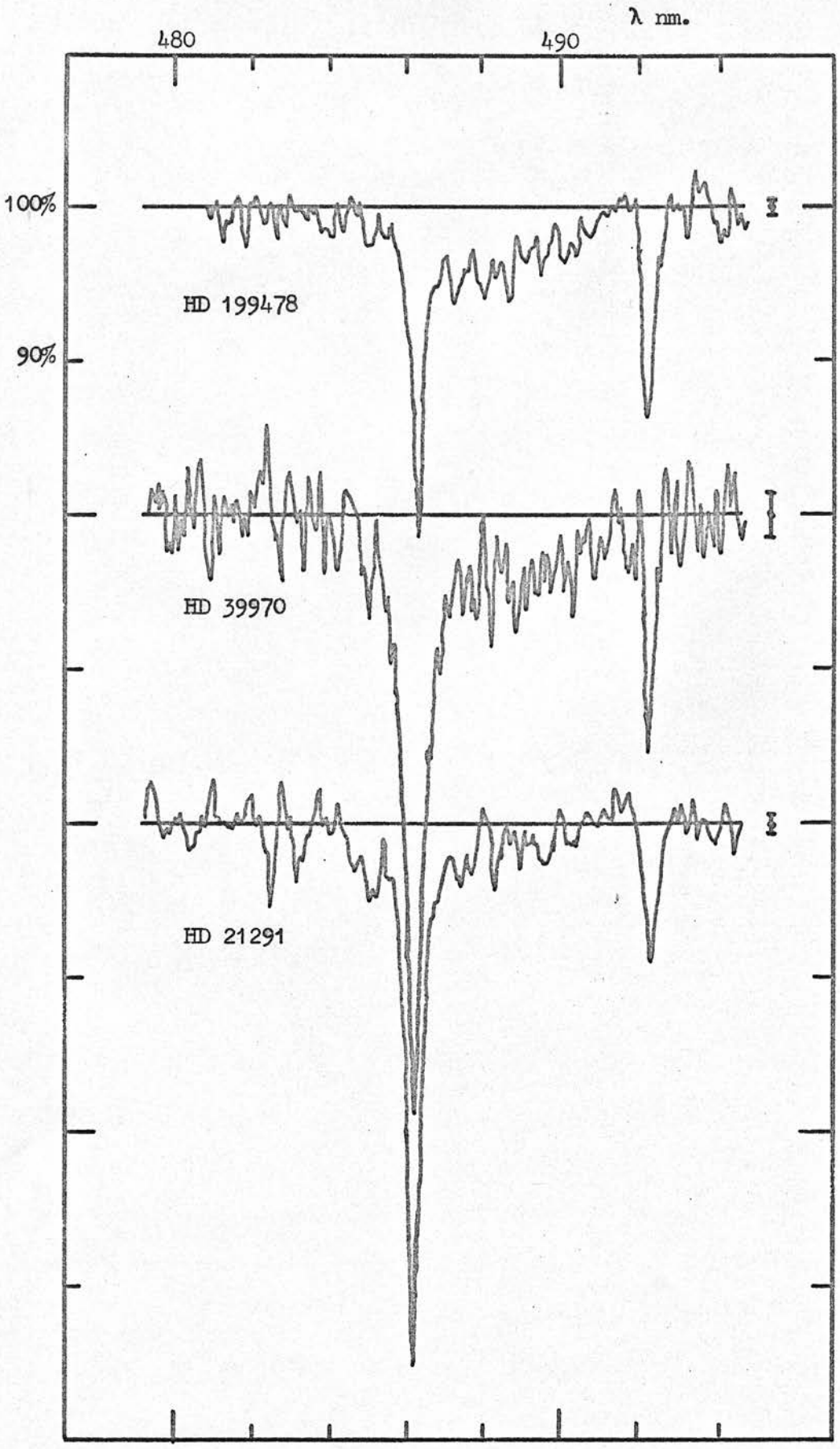

Figure 16 Mean rectified spectra for individual stars, in the region of '4890'.

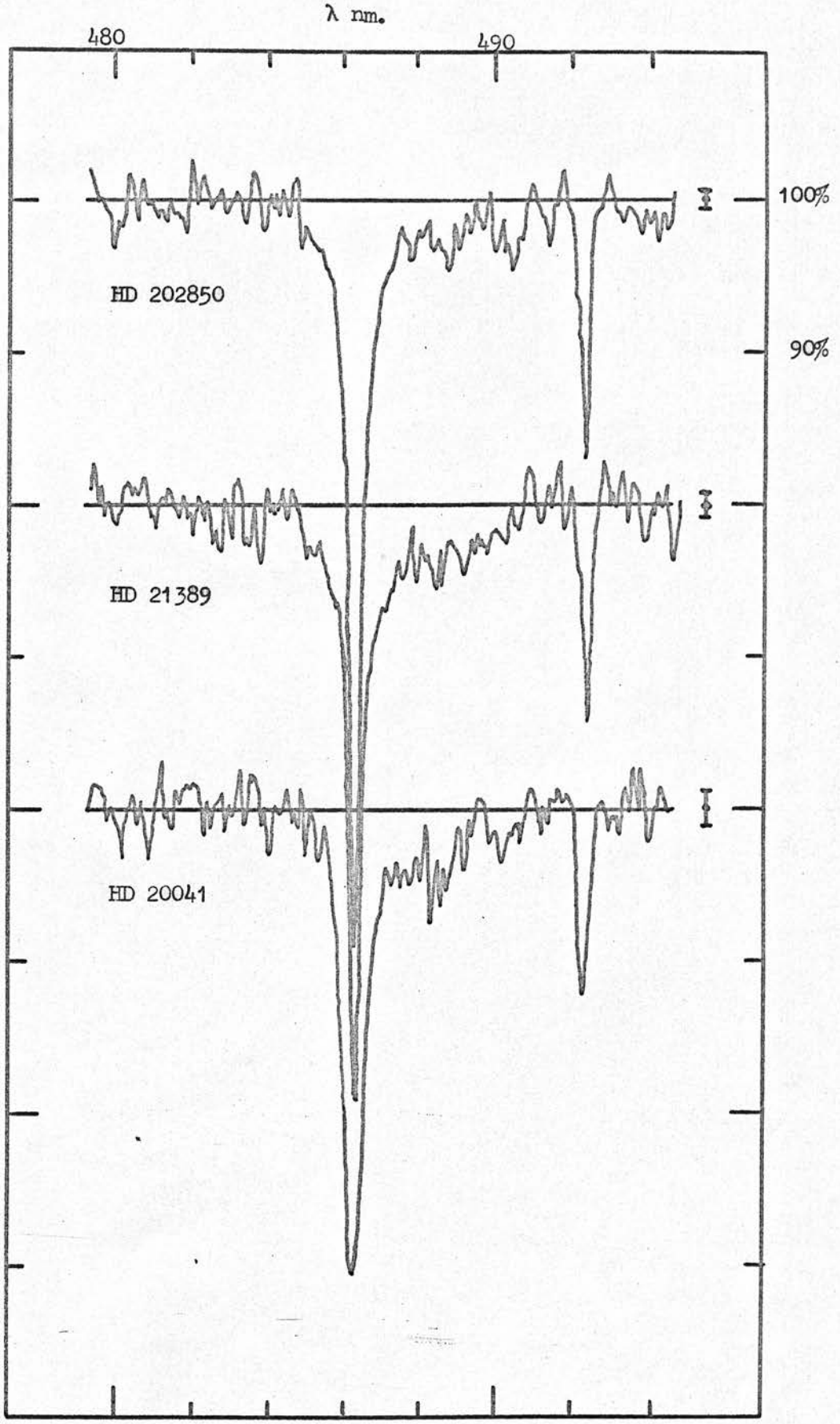

Figure 16 (continued)

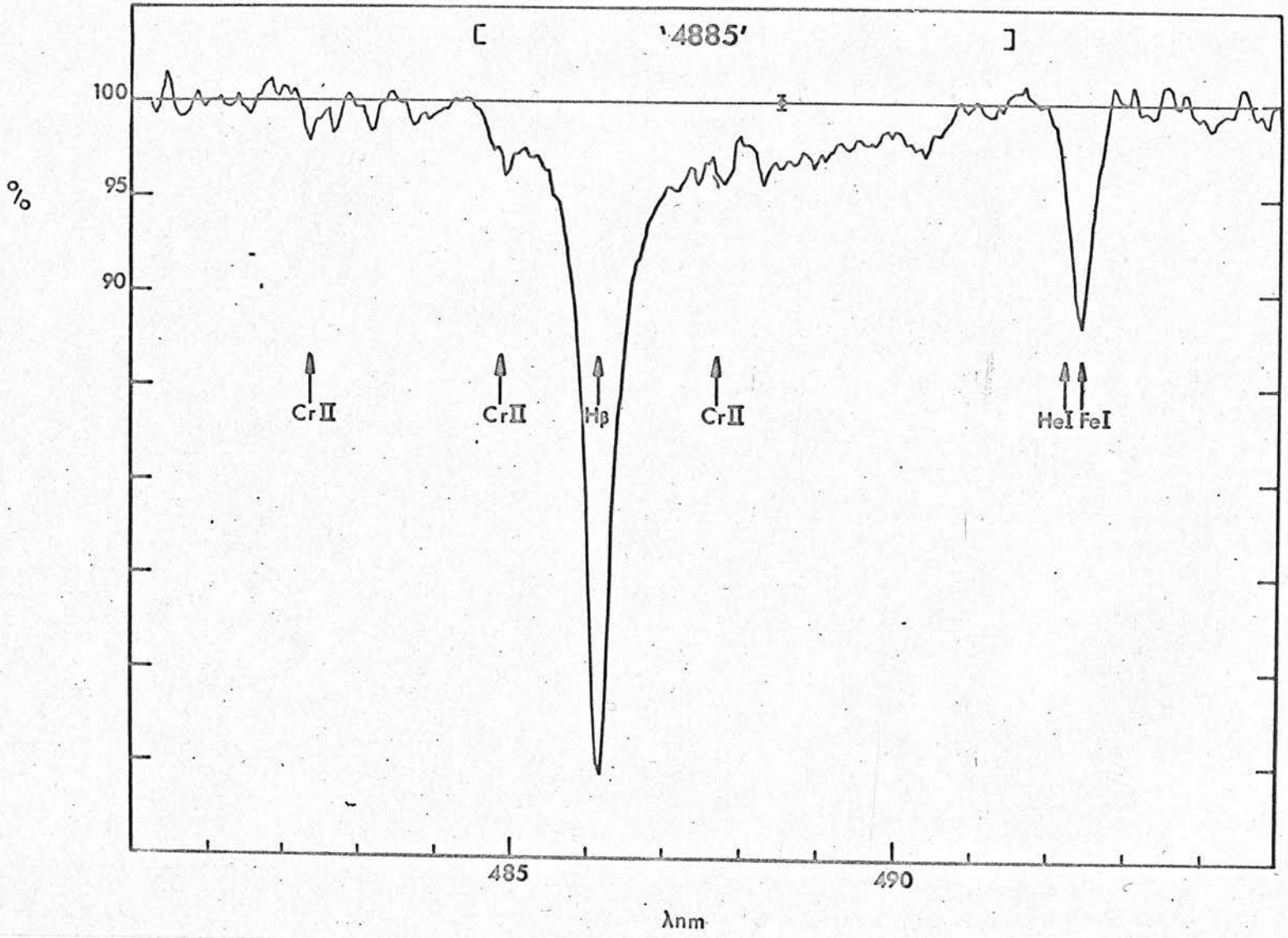

Figure 17

Mean rectified spectrum in the region of '4890'. Mean of 12 spectra of 6 stars.

The second feature, at λ 474 nm., may not be real because it derives most of its strength from the NURCAM correction, which is very irregular in this region, as shown in Figure 11. It may be that an emulsion flaw in one of the NURCAM quasi-spectra escaped detection, and was smoothed out into the observed 'line'. Certainly the strength of the feature in Figures 14 and 15, even if it <u>is</u> real, must not be taken too seriously. The difficulties of correcting for the NURCAM effect are highlighted here.

<u>3.3 Results for '4890'</u>

Only 12 spectra were reduced in the region of this band. The others either did not extend far enough to the red to permit an accurate assessment of the continuum over the band, or else were of a relatively poor quality, the region concerned being at the edge of the spectrum.

The overall wavelength range used was $\lambda\lambda$ 477-497 nm., although the redward limit varied from spectrum to spectrum, in the range $\lambda\lambda$ 495 to 497 nm. The omitted region was $\lambda\lambda$ 484.5 - 491.5 nm. Flaws amounted to only 0.2 nm. on average, and varied between zero and 0.7 for individual spectra. Allowing for stellar line measurements, the minimum number of microdensitometer points left for continuum fitting was 160.

The profiles of '4890' for the 6 stars are shown in Figure 16 and the mean profile of the 12 spectra in Figure 17. The Cr II lines at $\lambda\lambda$ 482.4, 484.8 and

487.6 nm. are visible in the spectra of some of the stars, though not - surprisingly - in the spectrum of HD 20041, the star with the latest spectral type. Apart from Hβ these Cr II lines are the only ones that distort the profile of the interstellar band. But the disturbing presence of Hβ means that accurate measurements of this interstellar band are virtually impossible.

Assuming for the moment that the band extends no further to the violet than λ486.2 nm., then reflection of the violet wing of Hβ onto the red wing separates the two features, because Hβ is almost certainly symmetrical in absorption for these six stars. The result of this procedure applied to Figure 17 indicates that the interstellar band is centred on λ488.5 ± .3 nm., has a central depth A_c of 3% and a half-width of about 2.5 nm., and is slightly asymmetric, being degraded to the red.

The individual profile for HD 199478 in Figure 16, for which both the wings of Hβ and the Cr II lines should be weakest, seems to show the same asymmetry, although the centre of the feature seems to be nearer λ488 nm., and it appears to extend violetward beyond λ486 nm.

Both Seddon (1967) and Herbig (see Johnson, 1970) report that the feature is wider than '4430', which would mean that it does in fact influence spectral regions violetward of the centre of Hβ. If this is indeed true, then the method involving reflection and subtraction of the violet wing of Hβ merely indicates the relative depressions at positions within the band equidistant from Hβ. If there were an emission wing to '4890' hidden in

the Hβ wings, then this would complicate matters still further. However, there seems to be no direct evidence of the existence of such a feature.

Estimates of A_c for the individual stars are given in Table V, column 10. For the purposes of comparison of the mean profile of Figure 17 with theoretical predictions, the absorption band is taken to have a central depth of 3% at λ488.5 nm., and a half-width δ of 2.5 nm. For the mean of the five stars HD 20041, 21291, 21389, 39970 and 199478, the ratio A_c '4890': A_c '4760': A_c '4430' is approximately 0.5 : 0.5 : 1 . The average value for this ratio from other investigations is 0.4 :0.3 : 1, as given in Table I(b).

3.4 Sources of Experimental Error

The true profile of a diffuse interstellar feature (DISAF) for a particular star or set of stars can be defined as the wavelength distribution of the intensity ratio of starlight <u>including</u> the DISAF extinction to the same starlight but <u>excluding</u> the DISAF. The observed profiles described in Sections 2.1 to 2.3 above are estimates of the true profiles, rendered uncertain by the following factors:

(1) The practical approximation to the condition of 'starlight excluding only the DISAF extinction'.

(2) Factors rendering uncertain the translation of this experimental definition of profile into a derived profile such as those given in Figures 12 to 17 here.

(3) The separation of DISAF from stellar lines and other effects in the derived profiles.

This section is concerned with the various sources of experimental error that fall into categories (1) and (2). Category (3) errors arise in the conversion of Figures 12 to 17, for example, to the estimates of A_C and A_E of Table V, and have been discussed qualitatively in the preceding Sections in this connection.

Category (1) errors could be called 'errors inherent in the choice of method of observation and reduction'. Some of the variations in the profiles of '4430' to be found in the literature, and listed in Table I(a), must be due to inaccuracies that fall into this category.

For example, in one common method, the DISAF-free spectrum is represented by the spectrum of a <u>different</u> star. This second star is chosen to be of the same spectral type as the first star, but unreddened by interstellar dust so that it (presumably) has no DISAF. Direct comparison of the spectral energy distribution for the two stars has the advantage of eliminating most of the instrumental distortions. It yields a profile for a DISAF superimposed upon a continuous extinction curve. The separation of the DISAF from the continuous extinction, if considered worthwhile or meaningful, is then considerably easier than its separation from a complicated stellar intensity spectrum, whilst category (3) errors are small.

The category (1) errors inherent in this method are fairly obvious. No two stars are alike, even if they have

the same MK spectral type; and unreddened early type supergiants are very rare indeed. In the range B6-A1 only Rigel qualifies as an unreddened supergiant, and even Rigel is not ideal because it has high luminosity and is in fact reddened by a small amount. (E_{B-V} is about 0.06, a value that could mean an A_c '4430' of perhaps 1%). The profile of a DISAF from this 'subtraction' method is therefore inevitably a relative profile, between spectra of two different stars, and thus can be expected to show differences from estimates of absolute profiles.

The errors inherent in the present automated spectrophotometric method for estimating absolute profiles arise from the following assumptions:

(a) The stellar spectrum can be represented by a model consisting basically of a continuum and a set of line absorptions which are all capable of being detected.

(b) A DISAF is localised in wavelength, that is to say, its total extent can be defined.

(c) The hypothetical DISAF-free continuum can be represented by an interpolation of the surrounding stellar continuum.

These three assumptions, which are in fact linked inseparably, are to be found in almost all spectrophotometry, especially in the measurement of atomic line strengths and profiles. That they represent an approximation to reality is understood, but the approximation is certainly a very good one. In practice, these assumptions virtually

define the feature under consideration.

From this standpoint, the uncertainties in the profiles of Figures 12 to 17 are all category (2) errors. These consist of:

(i) errors in the correction for the NURCAM effect,

(ii) recording and photometric calibration errors,

(iii) underallowance or overallowance for stellar lines outwith the 'omitted' regions, due to errors in the line list and in the choice of the 'given' profile for the lines,

(iv) electronographic emulsion granularity, and

(v) continuum polynomial interpolation errors.

(i) The NURCAM effect has been discussed at length in Section 2.7. The errors incurred in neglecting the effect during a profile determination by automated spectrophotometry can be 3% or more, even if the spectra have been positioned on the least irregular sections of the image area. Indeed, cursory studies of NURCAM for Spectracons other than the present one indicate that the effect can be considerably worse than that encountered here.

The final profiles of DISAFs presented in Sections 3.1 to 3.3 have been corrected for NURCAM, but the correction applied was not free from error. The wavelength calibration of the NURCAM correction was only accurate to 0.2 nm., mainly because of inaccuracies in the dispersion curves for the NURCAM quasi-spectra. In addition, even though the rectified quasi-spectra were smoothed, emulsion granularity still made the correction curves a little noisy. Finally, there were errors in the

reduction of the quasi-spectra: the peculiar feature at λ474 nm. in Figure 15, for example, may represent an error in the separation of NURCAM from emulsion flaws.

The errors on the NURCAM correction are thus neither randomly distributed nor dependent in any regular way on the wavelength to which the correction refers. From the above considerations, the error is estimated to be about 0.5% on average, for all three DISAF profiles.

(ii) Recording and photometric calibration errors are small compared with NURCAM errors and with the emulsion grain noise - especially for the measurement of shallow features such as the broad interstellar bands. The most serious uncertainty in this category is in the assumption of a linear relationship between density and intensity: the linear law has been assumed for all the image tube spectra reduced here. In fact, for the densities ($D < 0.4$) used here, the rate of change with density of percentage deviation from linearity is probably less than unity (see Brand, 1967). Therefore, the error on a typical A_C or A_E value of 5% is at most about 0.4% of 5%, that is, only 0.02%. This is small compared with NURCAM errors. It is, however, systematic in that all estimates of A_C or A_E are very slightly on the low side.

(iii) As pointed out in Sections 2.5 and 2.6, uncertainties in the choice of the given profile for stellar lines, and in the extent of the line list, lead to corresponding uncertainties in the estimate of the continuum position. The chosen value for the 'full 1/e width' of the given profile was seven microdensitometer steps, with an

uncertainty of about ± 0.5 step. From computations made with various values of the full 1/e width for Rigel spectra, an uncertainty of ± 0.5 step was found to correspond to an error of only 0.05% in the continuum position near lines, and even less in line-free regions.

The errors arising from uncertainties in the compilation of the line list are a little more difficult to assess. Certainly the line lists are believed to be accurate in content to within about 5 lines, assuming that the chosen value of 2 pm. for the critical equivalent width for inclusion is the correct one. In fact, with the possible exception of HD 20041, very few extra lines would have to be included in any of the lists if the critical level were to be lowered to, say, 1 pm. Thompson (1971) found that in a fairly even distribution of lines along a spectrum, an addition of 32 lines to a list of 57 raised the continuum level by 0.5%, whilst a further addition of 32 lines raised it another 0.3%. It seems reasonable to assume that the change in continuum level over an interpolation region will be of the same order as this average change for an even distribution of additional lines. Thus, for the uncertainty of ± 10 lines in the line lists assumed here, the error in the continuum level is estimated to be 0.1%. This value is therefore assumed to be the appropriate contribution to the error on the '4430' profile. For '4760' and '4890' however, the uncertainty is only ± 2 or 3 lines, so that the errors from this source are small for these two bands.

(iv) and (v) Brand (1967) measured G5 emulsion granularity

as a function of mean density, and found it to be representable by the equation:

$$A\,\sigma_D^2 = 1.31\,\bar{D} + 0.08 \qquad (\pm 5\%)$$

where A is the projected area of the microdensitometer slit.

An estimate of the grain noise on the mean '4430' profile is then $1/\sqrt{28}$ times the expectation value of σ_D calculated from the appropriate $\bar{D}$ values for the 28 spectra. With the σ_D values expressed as percentages of $\bar{D}$ in each case, the result is $\tilde{\sigma} = 0.37\%$.

Now this value has to be adjusted a little because, in order that averages of several spectra might be obtained, the rectified spectra (which were derived from spectra sampled at equal intervals in position on the film) have each been resampled at equal intervals in <u>wavelength</u>. This reduces the apparent noise somewhat. It also reduces the maxima of sharp stellar lines, although since there are six microdensitometer steps in each resolved element, this effect is not too serious. In fact, very little information was lost in this resampling process because one microdensitometer step only varied from 47 to 49 pm. in length across the whole spectrum, whilst the new samples were taken at 50 pm. intervals.

For independent random samples, and for a <u>constant</u> discrepancy C between the positions of the two sets of sampling points, it can be shown that the reduction in apparent variance is given by

$$\sigma'^2/\sigma^2 = 1 - 2\,C/S + 2(C/S)^2.$$

S is the common step length, and $0 \leq C \leq S/2$. In the

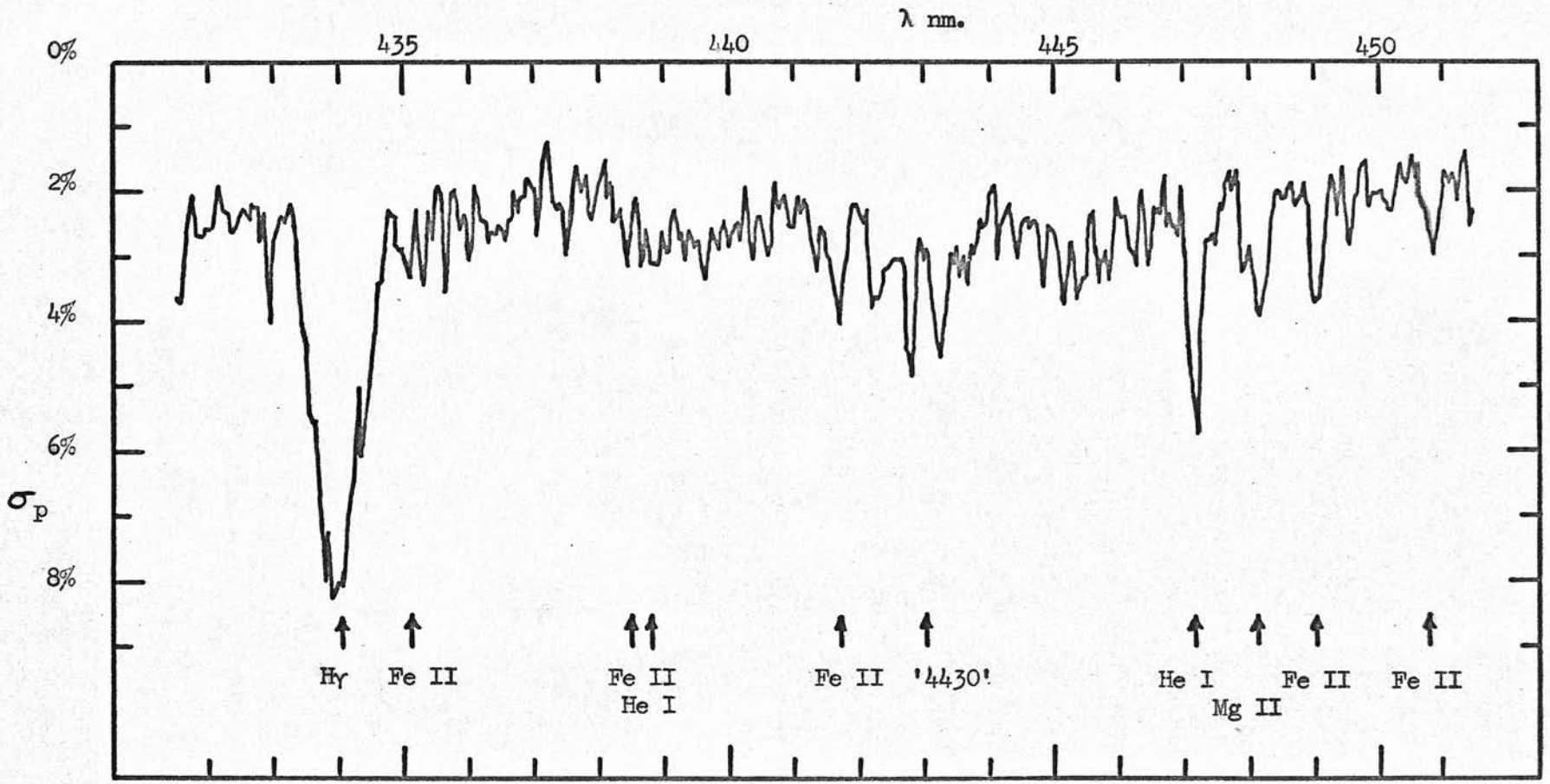

Figure 18 Standard deviations about the mean (Figure 13) of 28 rectified spectra near '4430', as percentages of the mean values.

present case, the dispersion curves are very nearly linear, so that C/S varies slowly and regularly with wavelength, whilst the number of samples concerned is many times the length of one cycle of variations in C/S. The reduction in the variance is therefore:

$$\sigma'^2/\sigma^2 = 1/(S/2) \int_0^{S/2} (1 - 2C/S + 2C^2/S^2)\, dC = 2/3.$$

Hence, the predicted value of σ for the mean '4430' profile is 0.30%.

The corresponding results for the mean '4760' and '4890' profiles are 0.33% and 0.38% respectively. Values for the individual profiles have been indicated by error bars on Figures 12, 14, and 16. It should be emphasised that these error bars do not represent the overall errors, but only the emulsion grain noise estimates.

An independent estimate of the actual grain noise can be obtained by statistical analysis of the rectified spectra themselves. At the same time, this method indicates the size of the continuum polynomial interpolation errors. In Figure 18 are plotted the percentage standard deviations (σ_p) about the mean of the 28 rectified spectra near '4430'. (The mean itself is plotted in Figure 13). An important advantage of using Figure 18 rather than Figure 13 to assess random errors is that the σ_p are independent of NURCAM errors and NURCAM correction errors, because the same NURCAM function applies to all the 28 spectra.

The variations in spectral type (and hence in stellar atmospheric conditions) amongst the nine stars appear as exceptionally large σ_p values over strong spectrum lines.

The ratio of excess σ_p to mean A_c for a line indicates the rate of change of line strength with spectral type. For example, values for this ratio from Figure 18 and corresponding results for other regions, together with Figures 13, 15 and 17 are as follows:

Hγ:	0.17	He I λ447.1 :	0.38	Mg II λ448.1 :	0.13
Hβ:	0.15	He I λ471.3 :	0.25	Fe II (blend) λ449.0 :	0.50

These results show, for example, that the Fe II lines are increasing in strength much faster at B8-A0 than Mg II λ448.1, and that the He I lines are decreasing in strength faster than Mg II λ448.1 is increasing.

Of 206 points in Figure 18 in the region $\lambda\lambda$ 431.5 - 451.5 nm. outwith stellar lines, 114 are inside the strategically omitted 9 nm. around λ443, and 92 are outside it. The expectation value of σ_p for the first group is 2.89% and for the second group it is 2.19%. In the approximation of equal densities for all 28 spectra, it can be shown that the corresponding σ for the mean '4430' profile is given by the expression

$$\left(\frac{N(M-1)}{M(N-1)} \cdot \frac{1}{M} \right)^{\frac{1}{2}} \cdot \tilde{\sigma}_p$$

where M(= 28) is the number of spectra and N(= 114 or 92) is the number of spectrum points used to calculate $\tilde{\sigma}_p$. Thus the calculated values of σ are 0.41% for the region outwith the '4430' band, and 0.54% for the region within it, with a sampling error of about 0.03% in each case.

The difference between the calculated value of 0.41% and the predicted one of 0.30% can only partly be due to the equal density approximation, and cannot be accounted

for by sampling errors. There must therefore be a significant polynomial fitting error. The increase in the calculated σ over the '4430' region, however, does not necessarily indicate increased polynomial fitting errors, because there must be an intrinsic variation in '4430' strength. Indeed, the excess σ_p at 443 nm. (Figure 18) for a mean A_c of 6% roughly corresponds to the root-mean-square deviation of 0.15 magnitudes on the mean E_{B-V} of 0.53. The calculated value for σ of 0.41% is therefore taken to represent the combined grain noise and polynomial fitting error for the mean '4430' profile. The corresponding values for '4760' and 4890' are 0.43% and 0.58% respectively.

The rather rapid variations in σ_p near the very centre of the '4430' DISAF (Figure 18) are interesting. They are very unlikely to be due to the weak Mg II lines there, and could therefore possibly be an indication of variations in the detailed structure of the band centre from star to star. Such variations would not be so easily detectable in the profiles of Figure 12 and 13 because those profiles are subject to NURCAM correction errors.

To summarise the main results of this Section, the NURCAM correction error is estimated to be 0.5% for all three DISAFs, whilst combined grain noise and polynomial fitting errors for the mean profiles amount to 0.4% for '4430' and '4760' and 0.6% for '4890'. Errors from other sources are small, except that the '4430' profile is subject to about 0.1% error from uncertainties in the

allowance for stellar lines in the line list.

The total experimental errors on plotted points of the mean profiles of '4430' (Figure 13), '4760' (Figure 15) and '4890' (Figure 17) are thus estimated to be 1.0%, 0.9% and 1.1%, respectively.

Photographic spectra at similar densities would have been much noisier than these electronographic ones, whilst to have obtained comparable signal-to-noise ratios, IIaO exposures would have had to have been about five times longer, under the same observing conditions. And even then, the uncertainties involved in interpolating over a broad DISAF in spectra obtained by the photographic process would have made electronographic ones preferable by far.

Thus, whereas photographic spectra could only have been used safely to derive <u>relative</u> profiles of broad DISAFs (in the manner described briefly at the beginning of this section), the present image tube spectra have been used to obtain absolute profiles within acceptable limits of uncertainty.

4. Photographic Observations of Diffuse Features in the Red.

A program of image tube observations of the interstellar features in the red was planned, but had to be abandoned when the mica window of an S20 Spectracon broke during final focus tests on the 36" telescope, there being no satisfactory replacement tube available. Photographic observations in the red were therefore made, to supplement the image tube observations described in Chapters 2 and 3. Since the 36" telescope in the photographic mode is not a powerful enough detector to enable spectra of sufficiently reddened stars to be obtained, the 98" Isaac Newton Telescope of the Royal Greenwich Observatory, Herstmonceux, was used.

4.1 Observational Details

Nine spectra, on unbaked IIaF emulsion, of heavily reddened stars with $E_{B-V} > 0.9$ magnitudes, were obtained on the nights of October 16th and December 4th and 6th, 1970. In addition, some spectra of moderately reddened and 'unreddened' stars, and one spectrum each of the two stars HD 15497 and 50064 in the blue (on unbaked IIaO emulsion) were obtained, for comparison purposes.

Microdensitometer traces of two sections of the spectrum of HD 50064 are shown in Figure 2, Chapter 1.

The standard I.N.T. Cassegrain spectrograph was used, with Schmidt camera number 2(f/1.4), and a grating of 1200 lines per mm. blazed to the first order red, giving a

Table VI — IIaF Spectra Reduced: General Data.

Star	V (mag.)	E_{B-V} (mag.)	Spectral Type	Projected Slitwidth (units of λ, in nm.)	Width of Spectrum (mm)
BD +41°3804 (Cygnus OB2 No. 10)	9.84	1.77	09.5 Ia	0.2	(a) 0.3 (b) 0.1
Cygnus OB2 No. 12	11.2	3.7:	B5 0	0.2	(unwidened)
HD 2905 (κ Cas.)	4.16	0.40	B1 Ia	0.1	0.5

dispersion of 6.1 nm. $mm.^{-1}$. The wavelength range used was approximately $\lambda\lambda$ 560 - 680 nm. A copper-argon arc comparison spectrum was photographed alongside each stellar spectrum for wavelength calibration.

With the spectrograph used, only one stellar spectrum can be photographed on each plate (the plate size is 26 x 16 mm.), but to permit photometric accuracy and consistency, up to 17 of these small plates, together with sufficient plates for photometric calibration spectra, can be cut from the one large plate as supplied by the manufacturers. As many of the exposed plates as possible were developed together (along with the calibration plates) in a special tank, connected to a nitrogen bubbler to ensure even development.

4.2 The Cygnus OB2 Spectra.

Particular attention has been paid to the spectra obtained of two stars in the Cygnus OB2 (= Cygnus II = VI Cygni) stellar association. Stellar details are given in Table VI. Data on the star κ Cassiopeiae is included: this star is only slightly reddened (compared with the Cygnus OB2 stars) and has been used as a comparison star in the present reduction.

The Cygnus OB2 association, situated some 2 kiloparsecs away along the local spiral arm, was discovered in 1953 by L. Münch and W.W. Morgan. It contains a large number of exceptionally young, heavily reddened early type stars (see for example, Reddish et al., 1966). About a dozen have been classified spectroscopically: of these,

the latest spectral type is B5 (Sharpless, 1957), for star number 12 on D.H. Schulte's (1958) list. Of the other stars classified with reasonable certainty, number 10 is the next latest at O9.5.

The spectra obtained here are believed to be some of the first calibrated spectra of Cygnus OB2 stars to have been taken at moderate dispersion. Certainly, no quantitative analysis of any other such spectra has appeared in the literature.

Star number 12 is the most heavily reddened early type star known. V.C. Reddich, L.C. Lawrence and N.M. Pratt (1966) place its B-V colour excess at 3.7 magnitudes. Twice as red as Mars or Betelgeuse, and a deep crimson hue to the light-adapted eye, this star is very beautiful indeed.

H.L. Johnson (1965) has performed multicolour photoelectric photometry for both No. 12 and No. 10, out to passband L (3.5 μm. effective wavelength). No. 12 is brighter than magnitude +2 at L. Johnson also found that these stars are reddened according to the 'normal' law in the visible and infrared. He estimates a value of 3.6 for the ratio of total to selective absorption, A_V/E_{B-V}. Combined with the apparent V magnitude of 11.2 and the E_{B-V} of 3.7, this result leads to the remarkable value of -13.6 for the absolute visual magnitude of No. 12, which implies that this star is 10^7 times as luminous as the Sun. Furthermore, if all interstellar grains were to be removed from the line of sight to this star, it would look rather

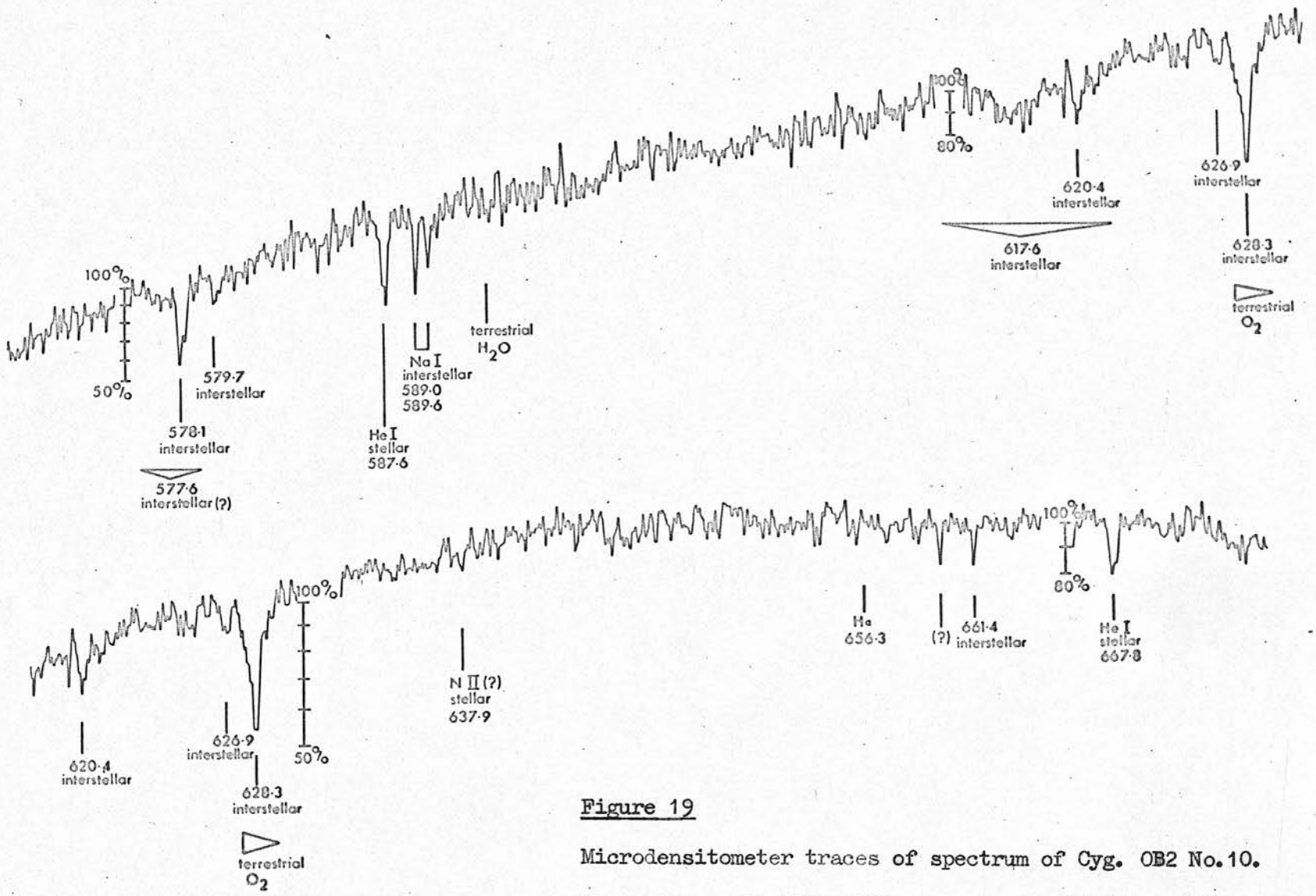

Figure 19

Microdensitometer traces of spectrum of Cyg. OB2 No.10.

Upper trace: λλ 570 - 631 nm. ; lower: λλ 618 - 675 nm.

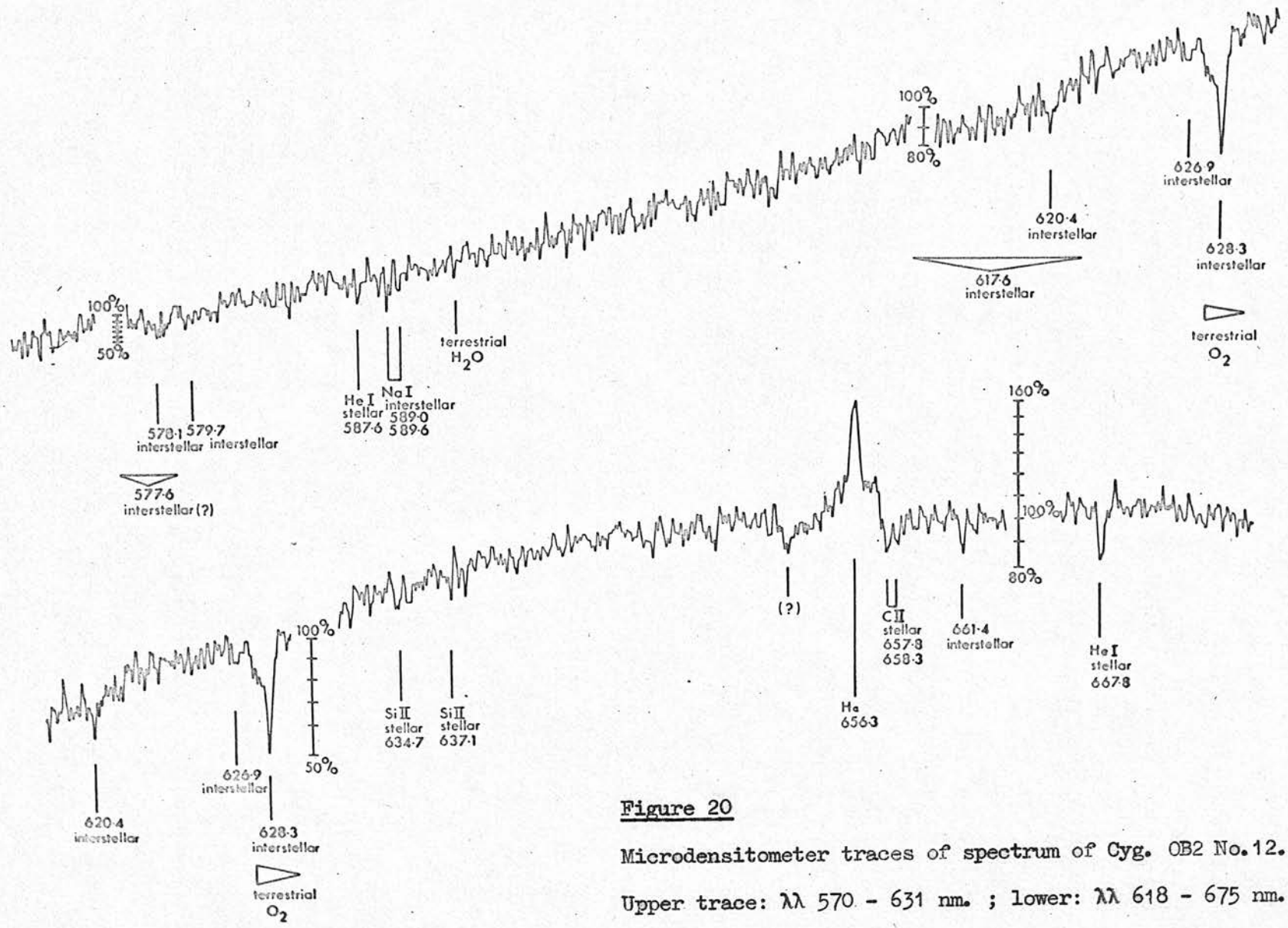

Figure 20

Microdensitometer traces of spectrum of Cyg. OB2 No.12.

Upper trace: λλ 570 - 631 nm. ; lower: λλ 618 - 675 nm.

like Sirius - just as bright and just as blue - even though it is two kiloparsecs away.

Though only half as reddened as No. 12, No. 10 still has a larger colour excess than any known star brighter than V = 10, with the exception of the emission-line (Of) variable star OB2 No. 5.

Because the strengths of the DISAFs are correlated fairly well with E_{B-V} (Merrill and Wilson, 1938; Duke, 1951; Kellmann, 1970) up to about E_{B-V} = 1.6 magnitudes, the spectra of No. 10 and No. 12 would be expected to show exceptionally strong interstellar features. Microdensitometer tracings of two of the three spectra obtained for these stars are reproduced in Figures 19 and 20, and these do in fact show the strongest diffuse interstellar features in the red so far reported in any stellar spectra.

Relative intensity scales, calculated from the photometric calibration curves described below, have been inserted at representative points along the tracings of Figures 19 and 20.

The strengths of the helium lines in these spectra are consistent with the assigned spectral types of O9.5 for No. 10 (Johnson and Morgan, 1954) and B5 or B8 for No. 12 (Sharpless, 1957; H.L. Johnson, 1965). In fact, the calculated equivalent widths (Section 4.4) for the two He I lines in No. 10, compared with results for standard stars (Wilson, 1958b, see his Figure 2), indicate a spectral type between O9 and B0 for this star.

The Si II lines at λλ 634.7, 637.1 nm. in No. 12 seem rather weak, even for a B5 supergiant (compare, for

example, these lines in the spectrum of the B6 supergiant shown in Figure 2, Chapter 1), but this may be a luminosity effect. The C II lines at $\lambda\lambda$ 657.8, 658.3 nm. are the only other stellar lines visible, and these, unfortunately, are known to be poor indicators of spectral type (Butler and Seddon, 1958, 1960; Butler and Thompson, 1961), although their strength certainly seems to rule out the possibility of No. 12 being a B8 star.

The strong Hα emission in No. 12 seems to be closely stellar in origin. As noted in Table VI, this spectrum was not trailed, but an extended object slit was used, so that any circumstellar Hα emission could be detected. As it turned out, the spectrum showed no significant extension of Hα beyond the stellar image. Taking the distance to the star as 2.1 kpc. (Reddish et al., 1966), this result shows that there is no region of Hα emission of greater intensity than the threshold of detection (which was 3% of the stellar continuum intensity) outwith a sphere of radius 0.03 pc. (= 6000 A.U.) around the star.

There is, in fact, a conspicuous lack of hydrogen recombination regions in the Cygnus OB2 association as a whole (Reddish, 1967). Theories involving solid hydrogen grains (Wickramasinghe and Reddish, 1968) or partial separation of gas and dust by diffusion (Reddish, 1971) have been proposed, to try to explain this anomaly.

The interstellar sodium D lines (Figures 19 and 20) are not particularly strong. In fact, they are only as strong as would be expected for a colour excess of half a magnitude or so, which corresponds to the interstellar

extinction between the association and us (Reddish et al., 1966).

The weakness of the sodium D lines is thus a further indication of a very low ratio of gas to dust in the regions surrounding these stars. There seems to be additional evidence here to support the hypothesis that the origin of the DISAFs is very close to the dust grains, because all the DISAFs are very strong indeed in these spectra.

4.3 Reduction Method

Of the four IIaF spectra that have been reduced in this study of Cygnus OB2 stars, one of OB2 No. 10 and one of the comparison star 16 Cassiopeiae were obtained on October 16th, 1970. The other two - one each of No. 10 and No. 12 - were taken on December 6th. In each case, the two stellar spectra and two sets of photometric calibration spectra were exposed on plates cut from the same large IIaF plate, and were all processed together.

Development was for 10 minutes in 'Microphen', with a nitrogen gas burst of 0.4 seconds duration every 8 seconds. After a one minute rinse in glacial acetic acid solution, the plates were fixed for 15 minutes in 'Hypam' or 'Unifix', washed in tap water for 30 minutes, wiped with a wetting agent on cotton wool, and left to dry by evaporation in a warm clean atmosphere, emulsion side uppermost.

Both stellar spectra and calibration spectra were recorded with the Joyce Loebl microdensitometer (analogue

mode), and density measurements were taken manually from these records. Calibration curves were plotted of Baker density $\Delta = \log_{10}(\text{antilog}_{10}D - 1)$ versus given values of the logarithms of exposure ratios, for wavelengths from 550 to 670 nm. at intervals of 20 nm. For the range of densities needed, these curves appeared to be linear, so best straight line fits were calculated through the relevant experimental points. The slope of the calibration line was found to remain constant with wavelength to within experimental error.

Full use was made of the presence of the copper-argon arc comparison spectra for aligning the microdensitometer slit perpendicular to the dispersion of the stellar spectra, and hence for accurately calibrating the latter in wavelength. An accuracy of $\pm$ 20 pm. in wavelength was achieved.

Measurements have been made on the DISAFs, the interstellar sodium D lines, the He I stellar lines and Hα in these four spectra. In all cases, the stellar continuum interpolation was drawn in manually as a straight line linking two line-free regions just outside the assumed extent of the feature under consideration. Such a procedure is fairly easy for spectra of early type stars in the red at moderate dispersion, because stellar lines are rare.

This interpolation is safe for the narrow features, but more uncertain for '5780' and '6180' DISAFs. It was evident from the microdensitometer traces of these and other spectra that the feature at '5780', considered by

earlier workers to be a fairly narrow 'diffuse line', actually consists of a line superimposed upon a broader feature, the latter centred on λ577.6 nm. approximately. This broad feature, which can be seen clearly on Figure 19, has also been reported recently by Herbig (in private correspondence with F.M. Johnson, 1970) for the star HD 183143.

For '5780', then, and certainly for the very broad DISAF called '6180', continuum interpolation on photographic spectra is rather uncertain, owing to the unpredictable wavelength-dependent plate sensitivity variations. The results presented here for these two features are therefore preliminary, but if (as seems likely) the DISAFs seen here are the strongest visible in any stellar spectra, then the proportional interpolation error is at a minimum here, and more accurate absolute profiles will only be possible when good image tube spectra in the red can be obtained.

The other interstellar features in the red are narrow enough to be free from such interpolation troubles.

The density measurements (from the analogue records) of both spectrum and interpolated continuum were punched onto paper tape, and were then converted to intensity units and rectified to the interpolated continuum as unity, using a computer program.

4.4 Results for Cygnus OB2 No. 10 and No. 12, and a Comparison Star.

Equivalent width measurements are presented in

Table VII Measured Equivalent Widths for Cygnus OB2 Nos.10 and 12, and χ Cas.

Feature	Integration Region (nm)	Measured E.W.s in pm.(= 0.01 Å) OB2 No.10	OB2 No.12	χ Cas.	χ Cas. (Other Workers)
'5780' DISAF (blend of 2)	576.8 - 579.1	269	280:	52	30 (M+) (577.7-8.3)
'5797' DISAF	579.1 - 580.3	58	50:	18	7 (M+) (579.5-9)
He I 'D_3'	586.0 - 588.4	140	40:	85	88 (Ws) (586.6-8.0)
Na I 'D_2' (interstellar)	588.4 - 589.3	76	70:	62	54 (M+) (588.8-9.2)
Na I 'D_1' (interstellar)	589.3 - 590.4	85	50:	65	51 (M+) (589.4-8)
'6180' DISAF (blend of 2)	(i)613.8 - 622.0	421	432	109	--
	(ii)619.8 - 621.0	101	104	18	--
'6270' DISAF	626.5 - 627.6	35	37	13	--
O_2 'a' band (terrestrial)	627.6 - 628.1	318	330	42	--
'6283' DISAF	628.1 - 629.6			45	49 (M+) (627.9-8.8)

(continued)

(Table VII continued)

Hα + C II (2)	(i) 654.1 - 658.6	+16	-434	--	--
	(ii) 654.1 - 656.3	--	-237		
	(iii) 657.6 - 658.6	--	+43		
'6614' DISAF	660.6 - 662.3	29	25	--	--
He I λ667.8 nm.	667.0 - 668.8	91	76	--	--

References

M+ Merrill et al. (1937) ; Merrill and O.C.Wilson (1938).

Ws R.Wilson (1956).

(Integration regions are given in brackets in the last column.)

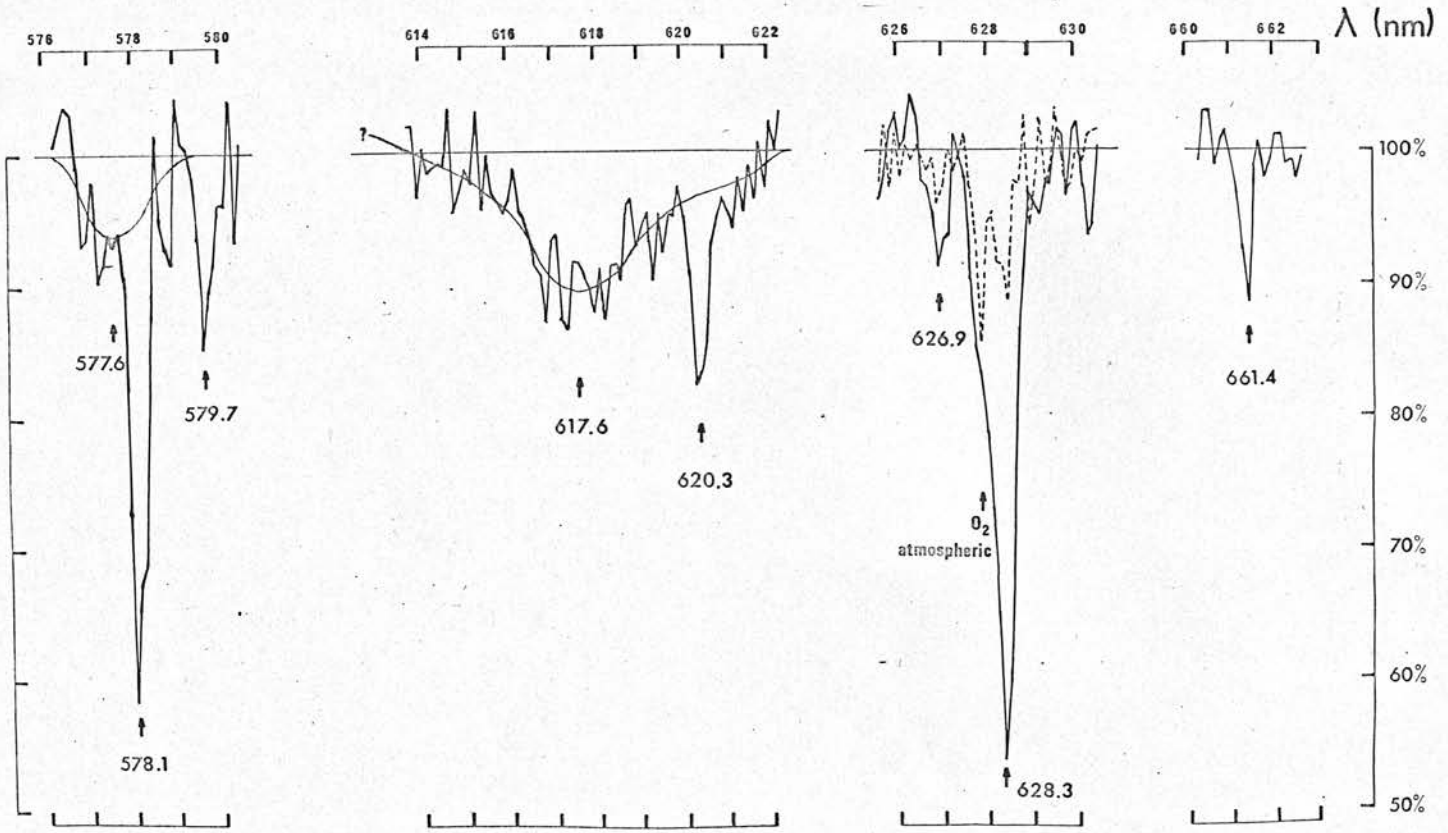

Figure 21 Mean profiles of diffuse interstellar features in the red, for Cyg. OB2 Nos. 10 & 12. The broken line refers to 16 Cas., a less reddened star.

Table VII. The integration regions used are listed in column 3: consideration of these limits is of the utmost importance when comparing results from different investigations, such as those given in Table I, Chapter 1. In the final two columns are listed (for comparison) some results for κ Cassiopeiae given by Merrill et al. (1937) and by R. Wilson (1956), together with the integration regions used by these authors.

The relatively large photometric errors quoted in Table VII for measurements of No. 12 shortward of 600 nm. stem from the low density of the spectrum in this region: it is a consequence of the extreme reddening of this star that only one short section of its visible spectrum can be correctly exposed at a time.

Mean profiles of the DISAFs in the Cygnus OB2 spectra are shown in Figure 21. The profile of the group of three lines near λ578 nm. in fact refers to one spectrum of No. 10 only. The other two spectra were so noisy in this region that there was no advantage in incorporating them into a mean profile. For the other lines, the profiles are the mean for the three rectified spectra.

In the region of the strong λ628.3 nm. line, the rectified spectrum of κ Cassiopeiae has also been drawn in, as a broken line. The higher resolution of this spectrum, together with the relative weakness of the interstellar line, permits adequate separation of the latter from the terrestrial oxygen bandhead nearby. For the κ Cas. spectrum, the equivalent width of the terrestrial feature was estimated to be 42 pm. The other measures of λ628.3nm.

Table VIII Strengths and Widths of Features in the Spectra of Cyg. OB2 Nos. 10 and 12.

Feature	Mean Wavelength (nm)	Equivalent Width No. 10 (pm)	Equivalent Width No. 12 (pm)	Central Depth (A_c) No. 10 (%)	Central Depth (A_c) No. 12 (%)	Mean Half-width (δ) (pm)
'5780'	577.6 ± .2	(100:)269 ± 5	280 ± 30	6)41	30:	1600 ± 300
	578.08 ± .06	(170:)		36)		360 ± 50
'5797'	579.66 ± .08	58 ± 3	50 ± 20	14	10:	300 ± 50
'6180'	617.6 ± .2	360:)421 ± 10	(370:)432 ±15	(12	11	2500 ± 300
'6203'	620.35 ± .03	60:)	(60:)	(14	13	290 ± 50
'6270'	626.90 ± .03	35 ± 3	37 ± 5	9	7	280 ± 50
'6283'	628.33 ± .03	272 ± 10	278 ± 15	45	48	370 ± 50
'6614'	661.35 ± .04	29 ± 2	25 ± 3	12	10	200
λ 589.59 Na I 'D_1' (interstellar)		85 ± 10	50 ± 20			
λ 589.00 Na I 'D_2' (interstellar)		76 ± 8	70 ± 20			
λ 656.28 Hα		+16 ± 5	-503 ± 20	0:	-60	
λ 587.56 He I 'D_3'		140 ± 3	40 ± 20			
λ 667.82 He I		91 ± 3	76 ± 3			

have then been corrected for the terrestrial absorption by assuming direct proportionality of total absorption with the mean air mass at the time of observation. Corrections for other terrestrial absorptions were smaller than the photometric error for these spectra.

Estimates have been made, from Figure 21 and the individual rectified spectra of the OB2 stars, of the contributions to the equivalent widths of '5780' and '6180' from the separate features at λλ 577.6, 578.1, 617.6, and 620.3 nm. These are given in Table VIII, together with the corrected values for '6284', and central depths, mean central wavelengths and mean half-widths for all the diffuse features.

The mean half-widths have been taken from the profiles of Figure 21, and some allowance has been made for instrumental broadening by applying a first order correction, assuming gaussian profiles for all lines. The mean central wavelengths are relative to the stellar He I lines: individual central wavelengths were determined by 'bisecting areas' in the rectified spectra.

The equivalence of the strengths of all the DISAFs for the two OB2 stars (Table VIII) is an extreme example of a deviation from the general correlation with reddening. No. 12 is twice as reddened as No. 10, but the DISAFs in their spectra are equally strong. Extrapolation of the 'normal' relations for moderately reddened stars shows that the DISAFs are probably deficient in No. 12, rather than overabundant in No. 10. Wampler (1966) found a similar,

but less pronounced, change, in the slope of the " '4430' core strength versus colour excess" curve, for Cygnus OB2 stars.

Reddish, Lawrence and Pratt (1966) find that interstellar extinction on the way to the OB2 association amounts to only 0.6 magnitudes in E_{B-V}, whilst the obscuration within the association is mostly due to circumstellar clouds less than one parsec in radius. If this is indeed the case, then the ratio of DISAF to continuous extinction must be many times larger in the circumstellar cloud around No. 10 than in that around No. 12. One explanation of this could be that the 'diffuse line carriers' are associated preferentially with one species in the dust population, and that this particular species is, for some unknown reason, present in reduced numbers, relative to the other species, in the cloud around No. 12.

4.5 Relative Profiles for '6180'.

In addition to the profiles presented above, relative profiles of '6180' have been determined by the 'subtraction' method (which has been described briefly in Section 3.4 above), for

(a) Cygnus OB2 No. 10 with respect to κ Cassiopeiae, and

(b) Cygnus OB2 No. 12 with respect to No. 10.

Since in each case the relevant spectra were exposed on parts of the same original plate, and were processed together, the relative profiles obtained are free from emulsion sensitivity uncertainties.

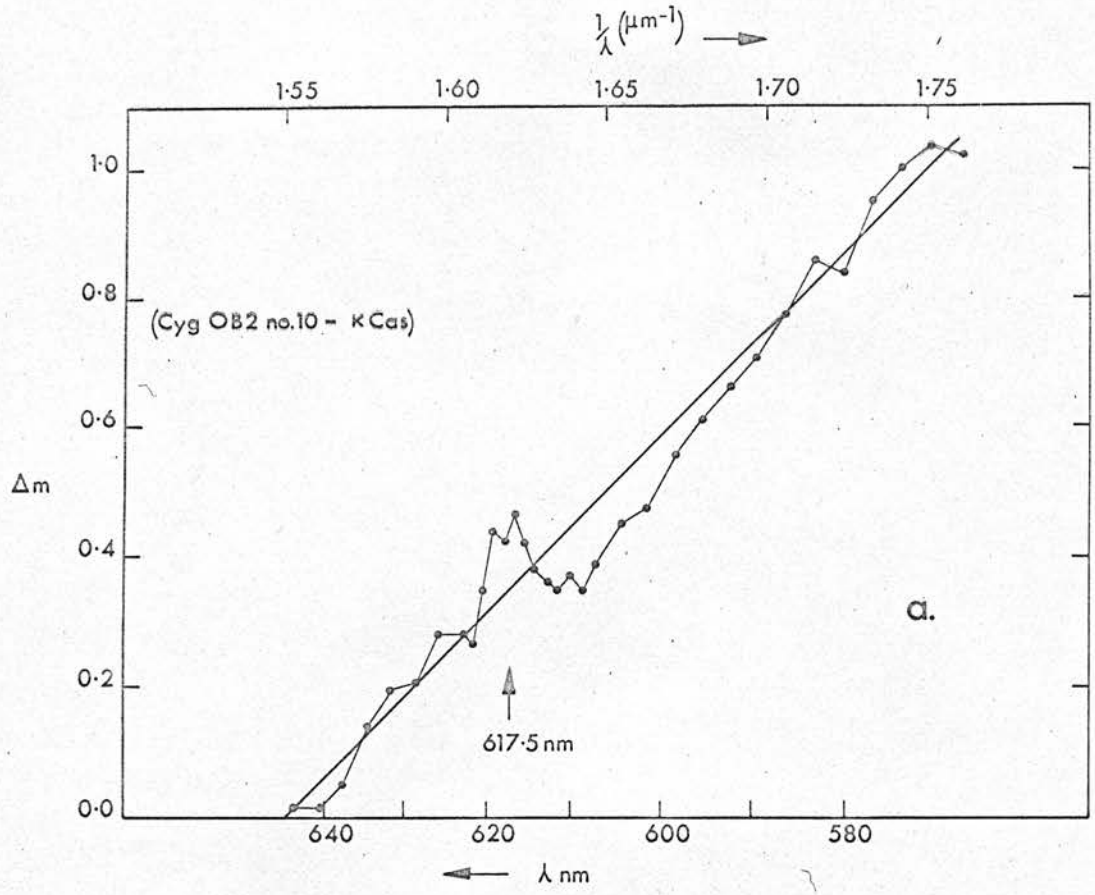

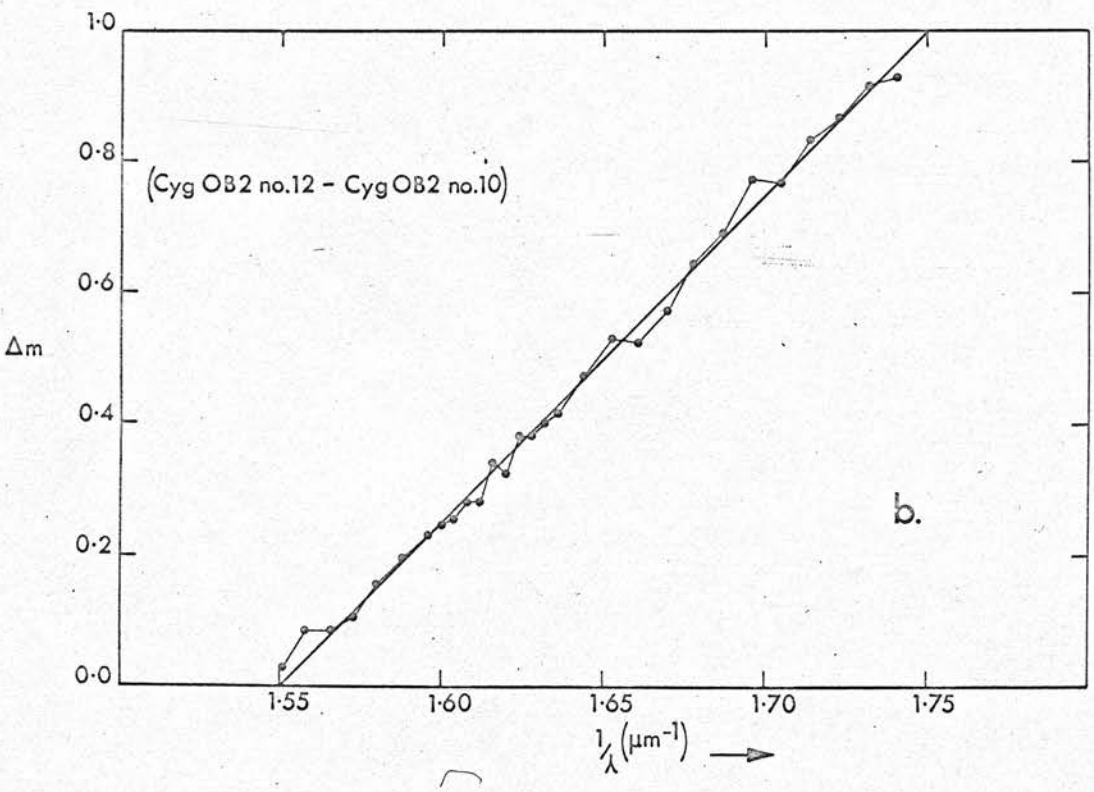

Figure 22 Reddening curve near '6180' for Cyg. OB2 Nos. 10 & 12.

Densities at continuum points and points within '6180' were read off the microdensitometer traces at intervals of 3 and 1.5 nm. respectively, and monochromatic magnitude differences for each pair of stars were computed. These are plotted as a function of wavenumber in Figure 22. The ordinates have been normalised to zero at 1.55 μm^{-1} and unity at 1.75 μm^{-1}. The form of these curves is determined by the law of continuous extinction by interstellar dust grains (the reddening law), together with the extinction caused by the '6180' absorbers.

The reddening law is expected to be linear over this short wavelength range (Nandy, 1964; H.L. Johnson, 1965), whilst other contributions to the magnitude differences - differential terrestrial atmospheric absorption and stellar temperature effects - are small compared with the interstellar extinction, and so do not appreciably affect the shape of the curve. For pair (a) the differential colour excess ΔE_{B-V} is 1.4 magnitudes, and for (b) it is 1.9, whereas the intrinsic colour indices differ by only 0.07 magnitudes for pair (a) and 0.20 for pair (b), and the air mass difference was only 0.04 for (a) and 0.17 for (b).

The reddening curve of Figure 22 (b) is indeed linear, to within the accuracy of the experimental points. The '6180' band has been cancelled out: the equivalent width measurements for this band (Table VIII) showed that its strength was the same for the two stars No. 10 and No. 12, and now Figure 22(b) shows that its profile is also the same for the two stars.

For pair (a), however, a non-trivial relative profile for '6180' emerges. Although there is a little uncertainty as to where to draw the continuous reddening line, it seems certain that the relative '6180' for this pair of stars shows an apparent emission wing (that is, a decrease in Δ m below the continuous reddening line) to the short wavelength side of the main absorption. This 'emission' wing is exactly analogous to the ones found on absolute '4430' profiles (Section 3.1).

Pending confirmation from corresponding profiles for other pairs of stars, this result must be considered preliminary, although the 'discontinuity' at '6180' found by G.A.H. Walker, J.B. Hutchings and P.F. Younger (1970) in low resolution reddening curves may well be evidence of the same phenomenon. The observation of an 'emission' wing on an interstellar band other than '4430' further supports the theory that the DISAFs arise from impurity atoms in interstellar grains, as is shown in Chapter 6.

5. The Extinction of Light by Interstellar Grains Containing Impurities.

5.1 Extinction by Pure Grains

The continuous interstellar extinction of visible starlight is observed to vary inversely with the wavelength, to a good approximation. The only particles that can reproduce such a law of extinction are those that are comparable in size with the wavelength of the light itself. Smaller particles scatter according to the Rayleigh λ^{-4} law, whilst larger objects do not affect the colour of the incident light appreciably.

Interstellar dust grains of the intermediate size were first suggested by H.N. Russell in 1922, and the first detailed comparisons of theoretical and observational curves were made by C. Schalén in 1939, for metallic grains. Subsequent calculations and hypotheses have led to many different kinds of dust grains being proposed, but they are all of approximately the same size, namely, between about 50 and 500 nm. in radius. The various types of grains that have been proposed over the years in explanation of the continuous extinction are listed in Table IX (Section 6.1).

The extinction problem for particles of about the same size as the wavelength cannot be formulated in any simple way, unlike the corresponding problems for smaller or larger types of particle. Instead, recourse has to be made to exact solutions of Maxwell's equations with the appropriate boundary conditions.

If the shape of the particle under consideration is closely related to some simple co-ordinate system (such as spherical or cylindrical polars for spheres or infinitely long circular cylinders, respectively), then the boundary conditions can be written down explicitly, and the problem can be solved in a relatively straightforward way. Thus G. Mie (1908) and, independently, P. Debye (1909) solved the equations for homogeneous spheres many years ago. But the corresponding problems for ellipsoids and irregularly shaped particles are of a different order of complexity. F. Möglich (1927) got as far as writing down the boundary conditions for ellipsoidal particles (using ellipsoidal co-ordinates), but an explicit solution has still not been obtained.

For this reason, virtually all theoretical interstellar extinction curves have been computed using Mie's solution, assuming interstellar grains to be spherical in shape. The phenomenon of polarisation by interstellar dust grains probably requires the real grains to be somewhat elongated, but it seems likely that the orientation of such grains is only slightly non-random, in which case the Mie solution would be expected to apply once more. Discrepancies from the Mie values may well occur in the far ultraviolet for spheres with irregular surfaces or for non-spherical objects in general (Greenberg, 1968; Shah and Vardya, 1971). However, the overall effect at wavelengths relevant to this investigation will be small.

Furthermore, the use of the Mie solution is necessary

here because direct comparison is to be made between optimum sizes and types of grains for fitting DISAF profiles, on the one hand, and optima for fitting continuous extinction curves, on the other - and the latter have always been derived from Mie computations.

The majority of the present calculations therefore refer to spherical interstellar grains, and the exact Mie equations have been employed. These results are presented in Chapter 6. In addition, a few calculations have also been performed for spheroids, by making optimum use of Lord Rayleigh's first order approximate solution. Since these calculations are not so accurate as those of Chapter 6 for spheres, the object is merely to estimate the degree of influence that changes in grain shape have on theoretical DISAF profiles. Polarisation profiles for the diffuse features have also been obtained from these calculations for spheroids, which are described in Chapter 7.

For comparison with observations, the basic quantity to be abstracted from the solution to the theoretical problem is the cross section for extinction, C_{ext}. This represents the fractional reduction in intensity of the radiation incident upon the particle. C_{ext} as a function of wavenumber is directly comparable with the observational extinction curves, provided that both are normalised at the same two wavenumbers.

In the exact Mie solution, C_{ext} is expressed in terms of a set of 'Mie coefficients', a_n and b_n ($n = 1,2,3, \ldots \infty$).

The oscillating charges and currents in the scattering particle can be represented by an infinite series of electric and magnetic multipoles, with multipole moments a_n and b_n. These, in turn, can be expressed in terms of Riccati-Bessel functions. In Mie's solution, the equations for a_n and b_n may be written as 2 x 2 determinants.

Extinction is caused by interference of the forward scattered wave with the incident wave. There are two, and only two, parameters determining the amount of extinction for spheres. These are the 'size parameter', that is, the radius expressed as a difference in phase of the incoming wave, $2\pi a/\lambda = x$, and the (complex) refractive index of the grain material, m. The arguments of the Riccati-Bessel functions are x and mx.

Rapid changes in the refractive index occur, for example, at localised regions in wavelength corresponding to natural frequencies of electrons in matter. These give rise to rapid changes in C_{ext}, which are seen as 'absorption lines'. It is this process that has been considered by many authors in attempts to explain the DISAFs. It has been proposed that they are 'absorption lines' of impurity atoms or molecules embedded in the interstellar grains (see Section 1.6).

Two basic computer programs have been written for the present investigation. One refers to simple homogeneous spheres. C_{ext} in this case is calculated from the equations of Mie as given by M. Kerker (1969) (see also Van de Hulst, 1957; and Wickramasinghe, 1967). The other refers to coated spheres, consisting of a spherical

core and a concentric spherical 'mantle'. The extension of the Mie solution to this type of particle is due to A.L. Aden and Kerker (1951). A Güttler solved the same problem (independently) in 1952, and the equations of Güttler have been used here.

The solution for coated spheres is rather more complicated than Mie's solution, because there are now two sets of boundary conditions to be fulfilled, two different complex refractive indices, and two size parameters. The expressions for the multipole moments a_n and b_n are now 4 x 4 determinants, and all the intermediate computations become correspondingly more tedious.

The present Güttler programs have been written for the general case of complex refractive index for both core and mantle. This has seldom been done before, and for 'pure' interstellar grains it is not usually necessary because the mantle is most commonly supposed to be a dielectric (with real m) that has condensed out of the interstellar gas surrounding the grains. In the present study, however, it <u>is</u> necessary to allow for complex m in both core and mantle, in order that cases of impurity absorptions in either region may be considered.

The programs, written mainly in Algol, were run on the ICL 4130 computer of the Royal Observatory Edinburgh. For the most part, single precision arithmetic (48 bits) was used, but various assessments of the accuracy of the programs were carried out via a duplicate program written partly in an assembly language, using double precision arithmetic. Forward recurrence relations were used to

generate the Riccati-Bessel functions as required for the Mie coefficients, and the C_{ext} values were calculated to five significant figures.

Expressions involving complex arguments were expanded manually, and real and imaginary parts of variables were carried through as separate ones. This procedure was preferred to the alternative one of working with variables declared and stored as 'complex', for the following reasons. Firstly, there was no satisfactory Fortran compiler available, so that sections involving complex variables would have had to have been written in assembly language (which is very tedious). Secondly, the method chosen was slightly more economical on central processor time, many superfluous calculations being omitted in the manual expansion. Thirdly, and probably of most importance, the method chosen enabled assessments to be made of the accuracy of the Mie calculations, by the use of double precision arithmetic, as mentioned above.

Identical results were obtained using single or double precision arithmetic over the whole range of size parameters and refractive indices of interest, and beyond, to cases where even the sixtieth term in the Mie multipole-moment series was needed. (For the real data, it was never necessary to exceed the tenth term).

Cross sections were also checked by comparison with tables in fourteen literature references - mainly references quoted by Kerker (1969) and Wickramasinghe (1967). There was slight disagreement in two cases. Firstly, three of the earlier references (notably Chromey (1960) gave

discrepancies of up to 0.5% for absorbing spheres (but not for dielectrics). Data from two of these have been questioned elsewhere in the literature and it seems that Chromey's results also must be slightly in error. Secondly, there were discrepancies with the results of Kerker et al. (1962) for coated spheres when the size parameter $x = 2\pi a/\lambda$ exceeded 25 - especially when the coating was very thick. Fortunately, such cases lie far outside the range of parameters used in the main program, but the discrepancies have not been resolved. For all the other literature, no discrepancies were found. In particular, there was agreement with Fenn and Oser (1965) (the only available tabulation for coated spheres with both core and mantle absorbing), and with Giese (1961) for metallic spheres. Calculations for the latter extended to the 49th. term in the Mie series.

On this evidence, it was concluded that, for the present purposes at least, the forward-recurrence generation of Riccati-Bessel functions was numerically stable to accumulation of rounding errors, and that more elegant computational schemes (see, for example, Kattawar and Plass (1967)) were not required.

5.2 Introduction of Impurities

A determination of the theoretical profile for an absorption line due to impurities in interstellar grains requires calculations of the extinction cross section C_{ext} for such grains with and without impurities. The variation of C_{ext} over a line depends on the phase

difference between the incident and scattered electromagnetic waves - which in turn depends on the refractive index of the grain.

The refractivity F and the refractive index m_o ($=n_o-ik_o$) of a homogeneous dielectric medium are given as a function of circular frequency ω from classical dispersion theory by the Lorentz-Lorenz-Clausius-Mossotti equation (see for example, Ditchburn, 1963, p. 565; Van de Hulst, 1949, p. 30):

$$\frac{F(\omega)}{3} = \frac{m_o^2(\omega) - 1}{m_o^2(\omega) + 2} = \frac{4\pi}{3} N_o \frac{e^2}{m_e} \sum_{s=1}^{j} \frac{f_s}{\omega_s^2 - \omega^2 + i\gamma_s\omega} \qquad (1)$$

where N_o is the number density of atoms; e and m_e are the electronic charge and mass; γ_s and ω_s, for each of j types of oscillator, are the damping constant and resonant frequency for the free motion of the electron oscillator; and f_s is the relative number of oscillators of the s^{th} type.

Consider the same substance to contain impurity atoms dispersed at random throughout its volume. If these atoms have k types of oscillator then the new index m is given by:

$$\frac{m^2-1}{m^2+2} = \frac{m_o^2-1}{m_o^2+2} + A \sum_{s=1}^{k} \frac{Nf_s}{\omega_s^2 - \omega^2 + i\gamma_s\omega} \qquad (2)$$

where N is the number concentration of <u>impurity</u> atoms, and

$$A = \frac{4\pi e^2}{3 m_e}$$

From the work of Burkhardt (1950) it can be shown that equation (2) is equally valid for metallic grains as for dielectric ones provided that the appropriate (complex) value for m_o is used. It is moreover the only one that leads to the correct profile of an impurity absorption line as the host particle size tends to zero.

Equation (2) has been used by Greenberg and Stoeckly (1971) and by Kelly (1971) in studies of impurity line profiles for cylindrical grains.

Wickramasinghe and Nandy (1970a, 1971b) have used the alternative (Sellmeyer-Drude) form of (1) (see, for example, Hertzfeld and Wolf, 1925; Ditchburn, 1963, p. 567; Aller, 1963 p. 161). This leads to an <u>approximate</u> form of (2):

$$m^2 = m_o^2 + 3A \sum_{s=1}^{k} \frac{Nf'_s}{\omega_s'^2 - \omega^2 + i\gamma_s'\omega} \qquad (3)$$

In general, the form of the function m^2/m^2_{max} derived from (2) and that derived from (3) are dissimilar, and this leads to dissimilar profiles for impurity lines. However, if m_o is real, $k=1$, and $Nf_1A \ll \gamma_1\omega$, (2) and (3) are equally valid, and then

$$\omega_1' \simeq \sqrt{\omega_1^2 - N_o f_1 A} \simeq \omega_1 \; ; \; \gamma_1' \simeq \gamma_1 \; ; \; f_1' \simeq \left(\frac{m_o^2 + 2}{3}\right)^2 f_1 \qquad (4)$$

In the present investigation it was found that virtually identical profiles were obtained for all cases when m_o was real, provided that (4) were satisfied. But (2) is to be preferred to (3) in general, because the unprimed parameters

are physically more meaningful than the primed ones.

Substituting in (2) values for the physical constants, we obtain, finally:

$$\frac{m^2-1}{m^2+2} = \frac{m_o^2-1}{m_o^2+2} + \sum_{S=1}^{k} \frac{2.98984 \times 10^{-10} \; (Nf_s)}{\lambda_s^{-2} - \lambda^{-2} + i\gamma_s \lambda^{-1}} \qquad (5)$$

where the Nf_s are in units of μm^{-3}, the γ_s in wavenumber units (μm^{-1}), and λ and the λ_s are wavelengths in μm. For a restricted frequency range near an <u>isolated</u> impurity line such as '4430' (but <u>not</u> some of the red diffuse lines) we can simply put k = 1.

In the present investigation, various values were used for m_o, corresponding to the various materials that have been proposed over the years for the composition of interstellar grains.

The extinction cross-section C_{ext} was then calculated as a function of wavenumber, for particular values of Nf_s, γ_s, λ_s and m_o, using the Mie and Güttler programs described in Section 5.1.

The function C_{ext} $(1/\lambda)$ is directly comparable with the observational reddening curve when both are normalised at the same two wavenumbers $(1/\lambda)_{N1}$ and $(1/\lambda)_{N2}$ (Wickramasinghe, 1967). Therefore normalised C_{ext} values were output from the computer for each model, firstly for 'pure' grains and secondly for 'impure' grains. Finally, the profile of the impurity line under consideration was output, in units of the 'pure' continuum as a function of wavelength . To calculate this profile, values have to

be assumed for the normalisation constant, $\eta = C_{ext}(1/\lambda)_{N1} - C_{ext}(1/\lambda)_{N2}$. Since the reddening law is linear for wavenumbers less than about $2.3\mu m^{-1}$ (Nandy, 1968; Harris, 1969), we have

$$\eta = E_{B-V} \cdot \frac{(1/\lambda)_{N1} - (1/\lambda)_{N2}}{(1/\lambda)_B - (1/\lambda)_V} = \frac{E_{B-V}}{0.45} \cdot ((1/\lambda)_{N1} - (1/\lambda)_{N2}) \quad (6)$$

(Allen, 1963).

Table IX Types of Grains Considered.

Type	References	m_o (λ 443 nm.)	References
Iron	(Lindblad (1935))	1.25 - 1.40 i *	(Schalén (1939,1965)
	(Schalén (1939,1965))		(Greenberg (1968)
	(Hoyle and Wickramasinghe(1970))		
		2.8 - 2.8 i	Lenham and Treherne (1968)**
Water Ice	(Eddington (1937))	1.33	(HCP[a]
	(Van de Hulst (1948,1949))		(Allen (1963)
	(Knacke et al. (1969b))		
Dirty Ice	(Isobe (1970))	1.33 - 0.10 i	Van de Hulst (1949)
Graphite	(Cayrel and Schatzman (1954))	2.46 - 1.42 i	Taft and Phillip(1966)
	(Hoyle and Wickramasinghe(1962))	2.65 - 1.25 i	Greenaway et al.(1969)
	(Cernuschi et al. (1967))		
Impure Graphite	(Wolstencroft et al. (1969))	1.8 - 0.8 i	Gilbert (1962)
Silicates (Olivine, Enstatite)	(Gaustad (1963))	1.66	(HCP[a]
	(Dorschner (1968))		(Huffmann & Stapp(1971)
	(Knacke et al. (1969a))		
Impure Silicate	(Wolff and Ney (1969))	1.66 - 0.10 i	
	(Hoyle and Wickramasinghe(1970))		
Crystal Quartz	(Cudaback et al. (1971))	1.56 *	(AIPH[b]
			(Allen (1963)

(continued)

(Table IX continued)

Solid Hydrogen	(Wickramasinghe & Reddish(1968)) (Reddish (1970))	1.05 - 0.10 i	(Wickramasinghe and (Nandy (1968) (Wickramasinghe and (Krishna Swamy (1969)
Silicon Carbide	(Friedemann (1969)) (Gilman (1969))	2.75	Choyke & Patrick(1968)

Notes

a Handbook of Chemistry and Physics.

b American Institute of Physics Handbook.

* In these cases, wavelength-dependent m_o values were used. In all other cases, m_o was assumed to be constant over the range $\lambda\lambda$ 430 - 460 nm.

** See Wickramasinghe and Nandy (1971a). Lenham and Treherne (1966) also disagree markedly with Greenaway et al. and with Taft and Phillip over refractive indices of graphite.

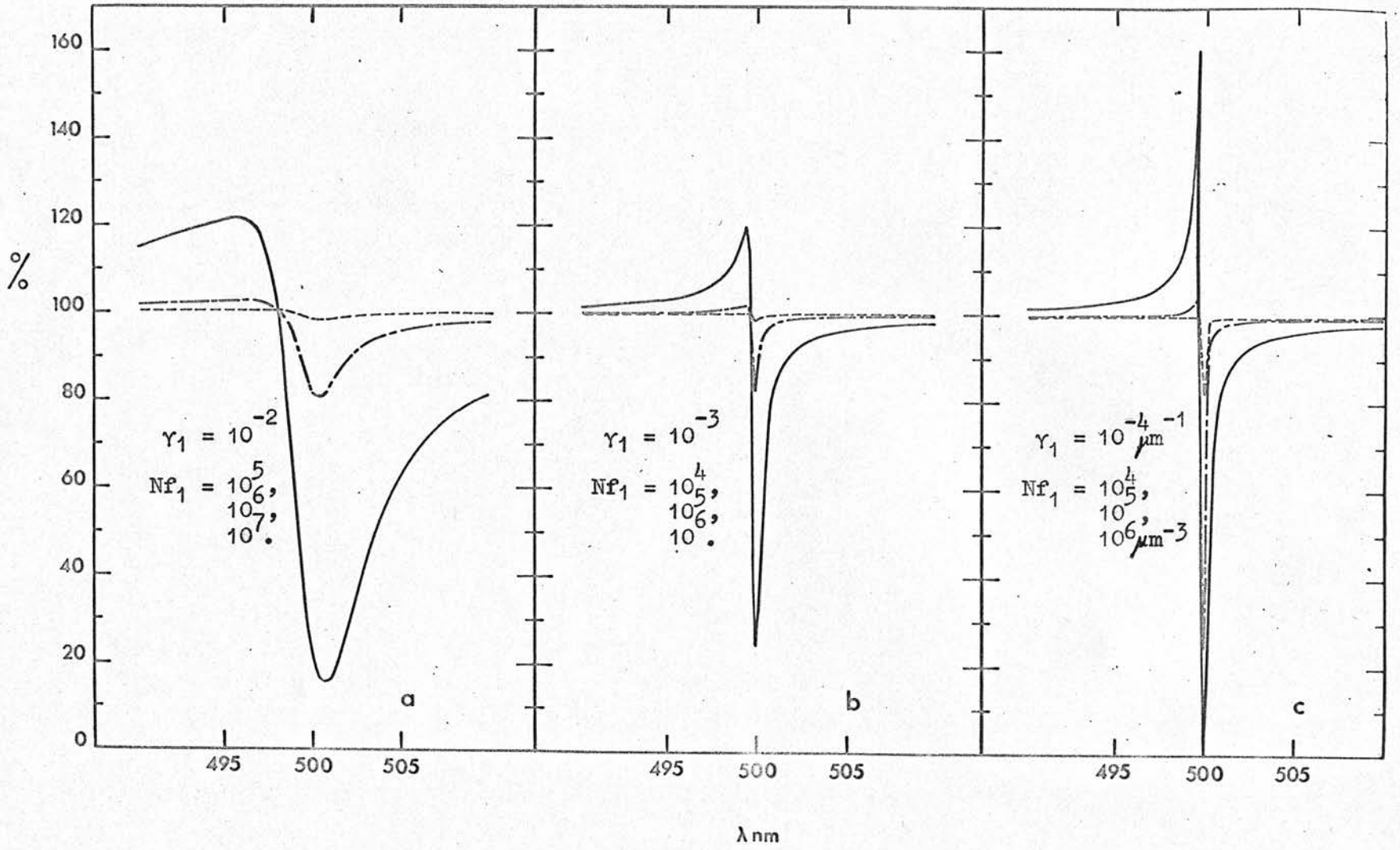

Figure 23 Profiles of an isolated line at λ_1 = 500 nm., for 100 nm. radius silicate spheres.

6. Theoretical Profiles for Spheres and Coated Spheres

6.1 Types of Grains Considered

The various types of grains considered here are listed in Table IX, column 1. Column 2 gives selected references to the literature concerning the possible roles of each type of grain in interstellar space. The adopted values of m_o at λ443 nm. are given in column 3, with references to sources in column 4.

6.2 Profiles of '4430' for Spheres

Profiles of an isolated line at λ_1 = 500 nm. for one typical model, namely, silicate spheres (m_o = 1.66) of radius 100 nm. are shown in Figure 23 for various combinations of Nf_1 and γ_1. The colour excess E_{B-V} was set equal to one magnitude. All the profiles have roughly the same ratio of peak apparent emission to peak absorption A_E/A_c except when the line approaches saturation. Changing the size or composition of the particles, however, produces a substantial change in this ratio, as is demonstrated below.

To compare the theoretical profiles directly with observations, the three input parameters for each model, Nf_1, γ_1, λ_1, were varied by iterative procedures until the three output quantities - central depth, half-width, and central wavelength of the absorption profile - were matched with observations. Figure 24 illustrates the chosen '4430' profile, together with the corresponding refractive indices and normalised extinction curves, for

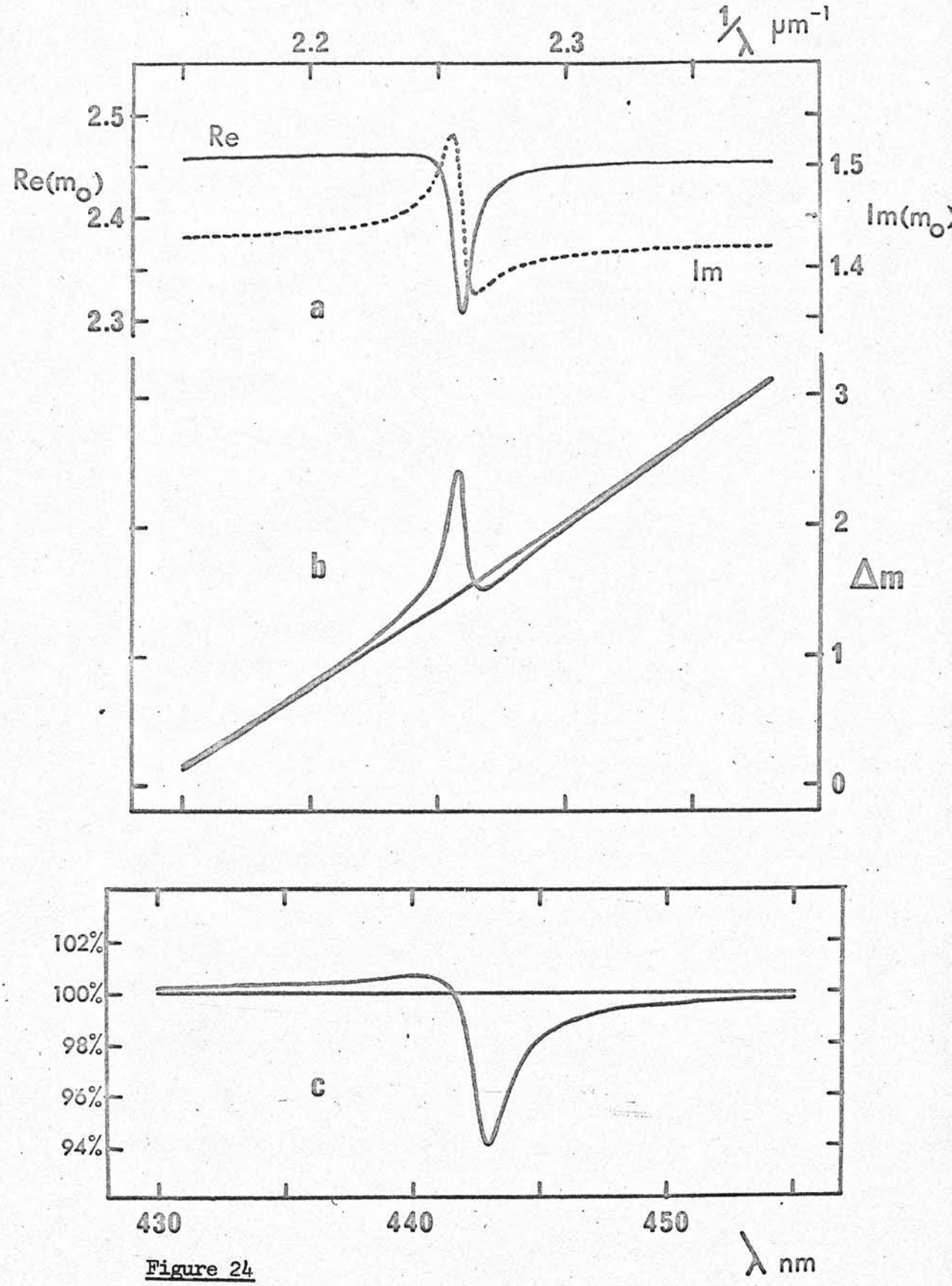

Figure 24

(a) Change in refractive index over impurity line, and (b) corr-esponding extinction curves and (c) line profile, for 40 nm. graphite spheres.

graphite spheres of radius 40 nm. Nf_1, γ_1, and λ_1 were varied to give the observed <u>absorption</u> as in Figure 13, that is,

central depth = A_c = 6%; central wavelength = λ_{A_c} = 443.0 nm; full half-width = δ = 1.8 nm.; and colour excess = E_{B-V} = 0.53 magnitudes. The resulting violetward '<u>emission</u>' wing is only one-fourth as strong as that observed, so that this particular model does not agree with the observations.

The corresponding results for a wide variety of models are summarised in Table X.

Columns 4 to 6 give the chosen values of Nf_1, γ_1 and λ_1; and columns 7 and 8 give the size A_E and position λ_{A_E} of the violetward apparent emission wing. A_E is seen to be strongly dependent on the type and size of host particle.

<u>The ratio of peak apparent emission to peak apparent absorption $\rho = A_E/A_C$ increases with size and with both real and imaginary parts of the refractive index of the particle</u>.

This is a generalisation of the result of Van de Hulst (1949, 1957) for $m_o \simeq 1$. It is particularly interesting that exactly the same trends in ρ have been reported by Greenberg and Stoeckly (1971, see figure 1) for the case of infinite cylinders as host particles.

Figure 25 illustrates the change in profile for silicate grains as the radius is increased from 60 to 120 nm.

For all cases when m_o is real, very similar profiles

Table X Models for '4430' for Homogeneous Spheres.

Fixed parameters: $A_c = 6\ \%$; $\lambda_{A_c} = 443.0$ nm. ; $\delta = 1.8$ nm. ; $E_{B-V} = 0.53$ mag.

Grain Type	m_o	a (nm)	Nf_1 (x $10^5\ \mu m^{-3}$)	γ_1 (x $10^{-3}\ \mu m^{-1}$)	$(\lambda_{A_c}-\lambda_1)$ (nm)	A_E (%)	$(\lambda_{A_c}-\lambda_{A_E})$ (nm)
Iron	(1.25 - 1.40i)	30	27.5	8.8	0.1	0.1	8:
		40	22.0	8.4	0.2	0.5	3.2
		50	12.0	7.8	0.3	1.1	2.2
Iron	(2.8 - 2.8 i)	30	23.0	9.6	0.1	0.0	--
Water Ice	(1.33)	100	2.17	8.7	0.2	0.3	5:
		150	3.80	7.4	0.3	1.3	1.9
		180	3.59	6.8	0.4	2.2	1.5
		200	4.56	6.4	0.4	2.8	1.4
Dirty Ice	(1.33 - 0.10i)	200	4.25	5.8	0.5	3.6	1.2

(continued)

(Table X continued)

Graphite	(2.46 - 1.42i)	30	14.0	9.0	0.1	0.2	6:
		40	20.0	8.0	0.4	0.7	2.8
		50	27.5	6.8	0.4	2.1	1.7
		60	30.0	5.0	0.5	6.4	1.1
Graphite	(2.65 - 1.25i)	60	30.0	3.8	0.4	9.6	0.9
Anthracite	(1.8 - 0.8 i)	60	14.0	7.4	0.4	1.3	2.1
Silicates	(1.66)	60	3.50	8.8	0.1	0.1	8:
		100	7.24	7.8	0.3	1.0	2.4
		110	8.70	6.7	0.5	2.1	1.7
		120	7.80	4.9	0.5	5.3	1.1
Dirty Silicate	(1.66 - 0.10i)	120	6.80	4.8	0.5	6.3	1.1

(continued)

(Table X continued)

Grain Type m_o	a	Nf_1	γ_1	$(\lambda_{A_C}-\lambda_1)$	A_E	$(\lambda_{A_C}-\lambda_{AE})$
Crystal Quartz (1.56)	40	1.04	9.0	0.0	0.0	--
	60	2.76	9.0	0.1	0.1	8:
	80	4.26	8.5	0.2	0.3	5:
	100	5.34	8.0	0.3	0.7	2.9
	120	7.83	6.6	0.4	2.2	1.6
	140	5.18	4.7	0.6	6.6	1.1
Solid Hydrogen (1.05 - 0.10i)	200	1.45	8.7	0.1	0.2	6:
	350	1.40	8.3	0.2	0.4	3.5
Silicon Carbide (2.75)	40	3.94	9.0	0.1	0.0	--
	60	8.05	8.5	0.2	0.3	5:
	80	6.70	6.5	0.2	0.8	2.3
	90	13.0	8.8	0.3	1.7	1.8

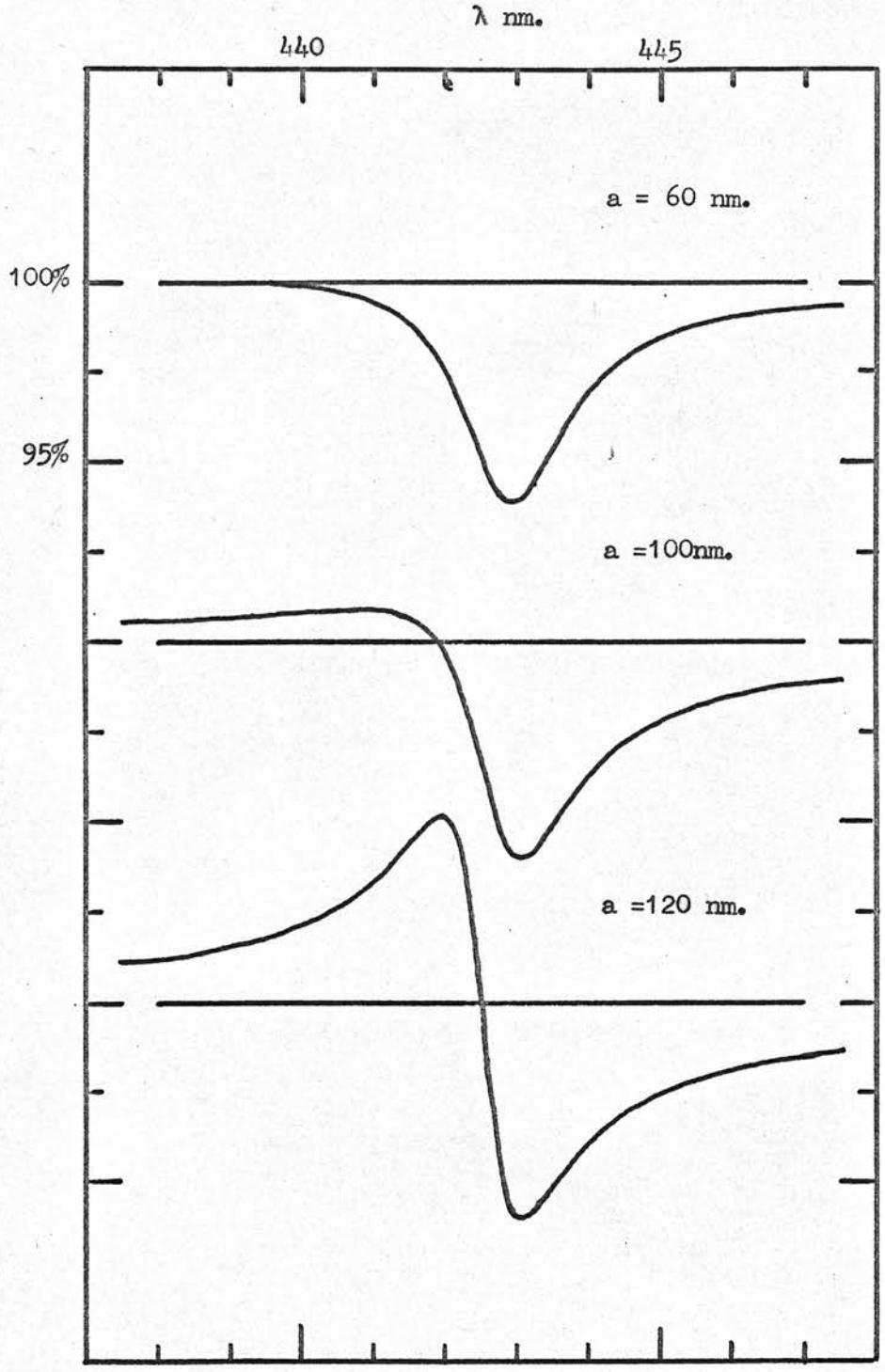

Figure 25

Profile of '4430' for silicate grains of radii a.

Table XI Dependence of $\rho = A_E/A_c$ on Observational Parameters A_c, δ, and A_c/E_{B-V}.

Fixed parameters: $m_o = 1.66$ (silicates) ; a = 120 nm. ; $\lambda_{A_c} = 443.0$ nm.

A_c (%)	δ (nm)	A_c/E_{B-V} (% per magnitude)	Nf_1 (x $10^5 \mu m^{-3}$)	γ_1 (x $10^{-3} \mu m^{-1}$)	$(\lambda_{A_c}-\lambda_1)$ (nm)	ρ	$(\lambda_{A_c}-\lambda_{A_E})$ (nm)
2	1.8	11	7.6	5.0	0.5	0.85	1.1
6	1.8	11	7.8	4.9	0.5	0.88	1.1
12	1.8	11	8.0	4.8	0.5	0.93	1.1
20	1.8	11	8.0	4.6	0.5	1.02	1.1
6	1.6	11	7.0	4.4	0.5	0.87	1.0
6	1.8	11	7.8	4.9	0.5	0.88	1.1
6	2.0	11	8.6	5.5	0.6	0.87	1.2
6	2.2	11	9.4	6.0	0.6	0.87	1.4
6	1.8	7	5.3	5.1	0.5	0.88	1.1
6	1.8	11	7.8	4.9	0.5	0.88	1.1
6	1.8	15	10.5	4.7	0.5	0.89	1.1

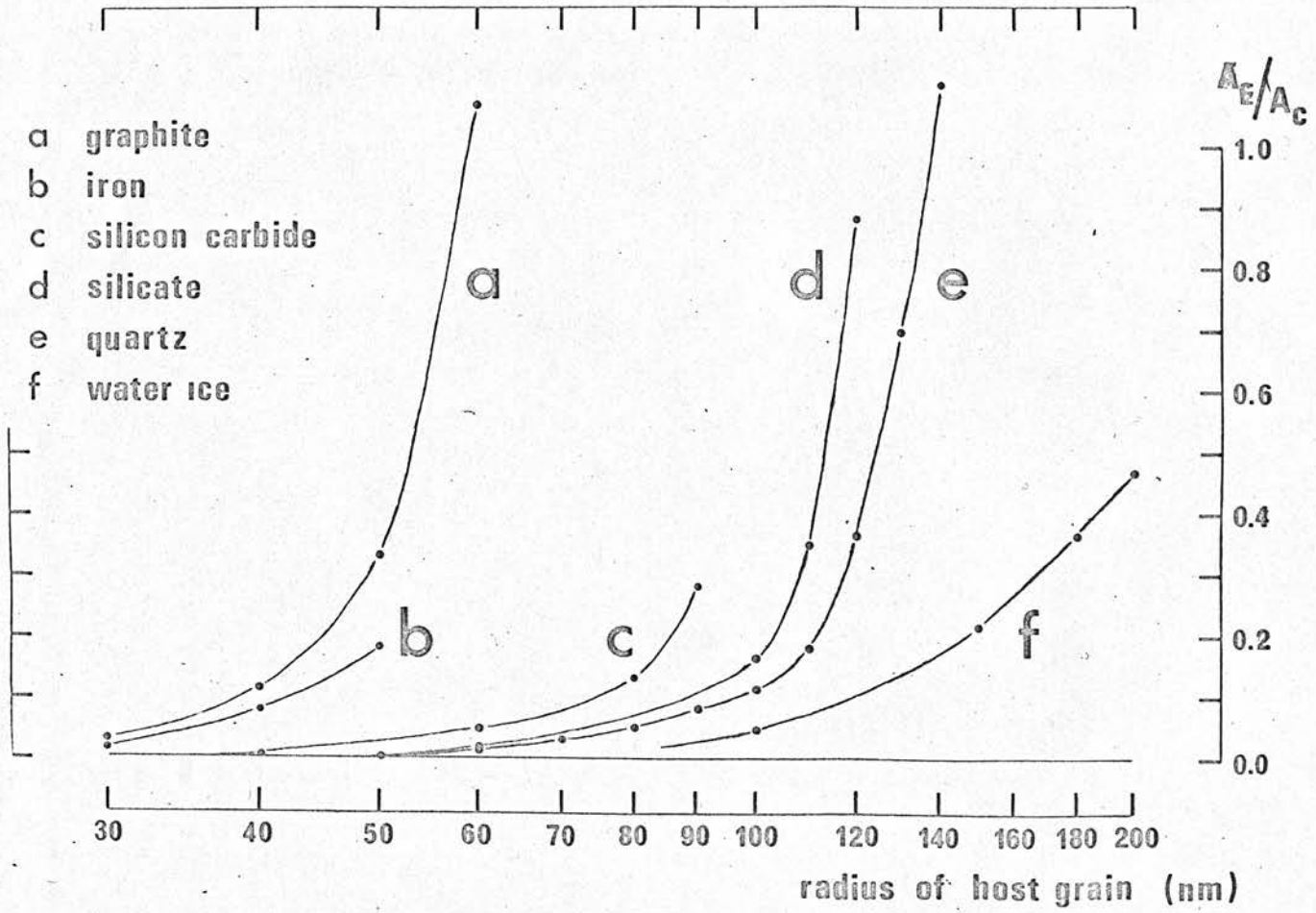

Figure 26 $\rho = A_E/A_c$ as a function of host particle size and type.

are obtained if the approximate dispersion formula (3) (Section 5.2) is used instead of (2). However, for graphite and iron, profiles using (3) have 'emission' wings redward of the main absorption when the particle radius a is less than about 50 nm. This redward 'emission' becomes very strong (that is, the theoretical interstellar medium becomes very transparent near λ443 nm.) for $a \rightarrow o$. For example, for 10 nm. radius iron spheres $\rho = 4.9$. Such use of (3) thus leads to obvious inaccuracies.

6.2.1 Variation in ρ with Observational Parameters

The trends in ρ as the observational parameters A_c, δ, and A_c/E_{B-V} (the ratio of discrete to continuous extinction) are varied are shown in Table XI for the typical case of silicate grains of radius 120 nm. Virtually the whole range of observed variations has been covered here. (Compare Table I(a), Chapter 1).

It is evident that ρ is almost invariant: even the slight increase with A_c disappears if δ is allowed to increase very slowly with A_c. Values of ρ from Table X therefore apply equally well to the whole range of observed absorption profiles of '4430'. These values are plotted in Figure 26 as a function of host particle size and type.

There is agreement with the value of ρ derived by Wickramasinghe and Nandy (1970a) for silicate grains of radius 70 nm. Van de Hulst's curves (1949) seem to be accurate for ice grains, but not for the substances

Table XII Models for '4430' for Size Distributions of Grains.

Fixed parameters: as for Table X.

For explanation of symbols see text and Figure 27.

Grain Type (and m_o)	Type of distribution	a_o (nm)	a_{pc} (nm)	W (nm)	Nf_1 ($\times 10^5 \mu m^{-3}$)	γ_1 ($\times 10^{-3} \mu m^{-1}$)	$(\lambda_{A_c} - \lambda_1)$ (nm)	A_E (%)	$(\lambda_{A_c} - \lambda_{A_E})$ (nm)
Graphite	A	100	61	36	27.0	6.5	0.5	3.4	1.4
(2.46 - 1.42 i)	B	40	57	29	27.0	6.5	0.4	2.8	1.4
	single size	--	50	--	27.5	6.8	0.4	2.1	1.7
	single size	--	60	--	30.0	5.0	0.5	6.4	1.1
Silicates	A	150	108	59	6.75	7.5	0.3	1.2	2.1
(1.66)	B	80	121	51	7.50	6.5	0.5	2.6	1.5
	C	80	119	62	7.50	6.7	0.5	2.2	1.6
	D	80	122	63	7.75	6.5	0.5	2.6	1.5
	single size	--	110	--	8.70	6.7	0.5	2.1	1.7
	single size	--	120	--	7.80	4.9	0.5	5.3	1.1

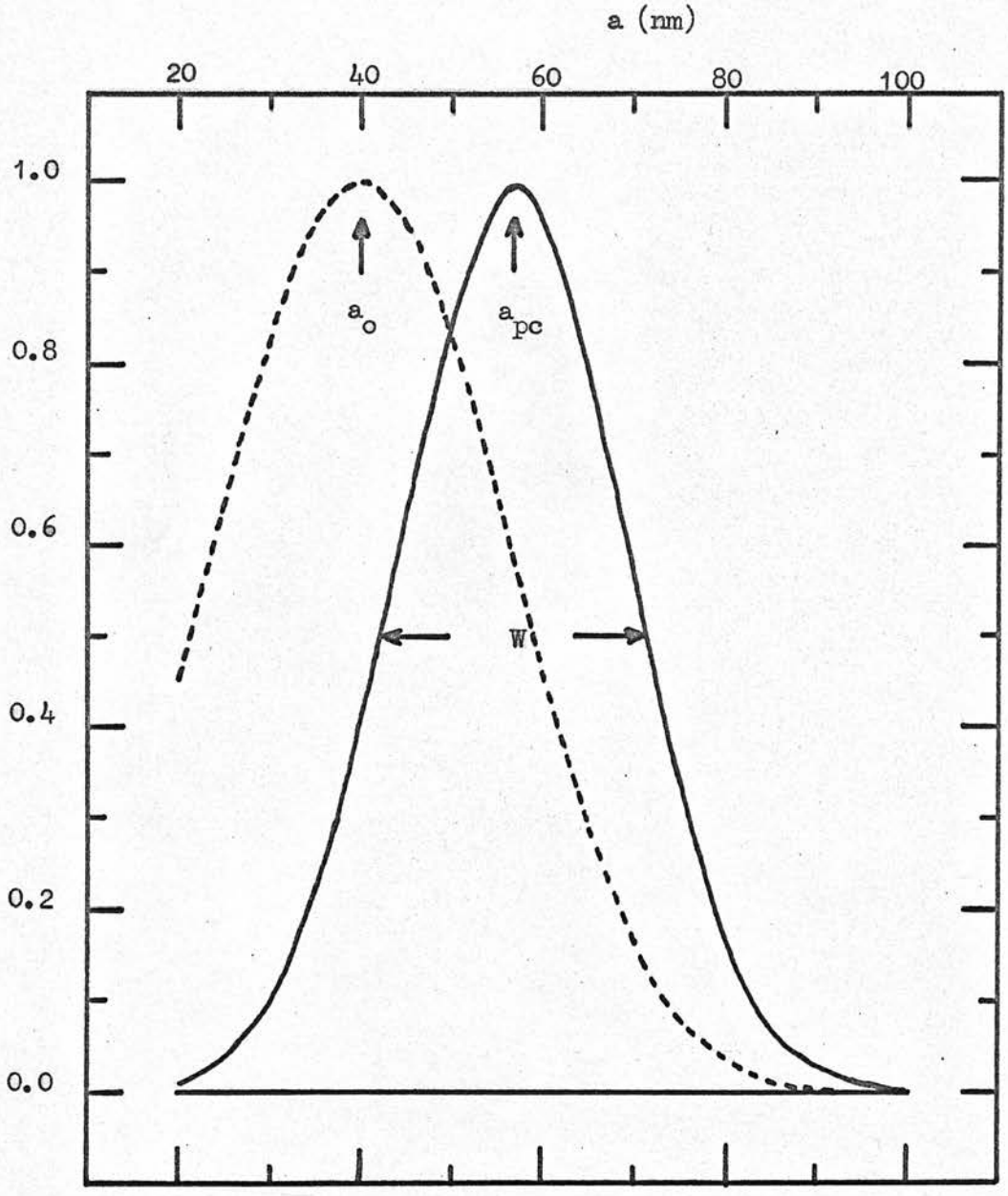

Figure 27 Curves of size distribution n(a) (- - -) and extinction contribution ($n(a).C_{ext}(a)$) (⟶) for λ = 443 nm. and $n(a) \propto a^2 \exp(-0.67(a/a_o)^3)$ for graphite grains.

considered here with m_o greater than 1.33.

6.2.2 Effect on the Profile of a Size Distribution

Results analogous to those of Table X are shown in Table XII for some size distributions of graphite and silicate grains.

Columns 2 and 3 give the form of distribution used and the characteristic radius a_o. Distribution type A is that used by Greenberg (1968):

$$n(a) \propto \exp(-5(a/a_o)^3).$$

Type B is that used by Wickramasinghe and Nandy (1970b, 1971a, b):

$$n(a) \propto a^2 . \exp(-0.67(a/a_o)^3).$$

Type C is an approximation to the celebrated Oort-Van de Hulst size distribution (Oort and Van de Hulst, 1946; Van de Hulst, 1948), used by Gilra (1971) and others:

$$n(a) \propto \exp(-0.69(a/a_o)^{2.6}),$$

and type D is a slightly different distribution:

$$n(a) \propto \exp(-0.69(a/a_o)^{2.4}).$$

Columns 4 and 5 give the radius (a_{pc}) of the peak contribution to C_{ext} in the size distribution, and the full half-width (W) of the contribution curve ($n(a).C_{ext}(a)$ versus a). These quantities are explained in Figure 27. The broken line is the actual size distribution (type B for graphite) and the continuous line is the contribution curve.

There are two main conclusions to be drawn from the results of Table XII:

(1) For a given ρ, the profile is very similar for each of the different types of distribution; and all are very similar to the profile for a single particle size.
(2) The value of ρ for a size distribution is comparable with that for a particle of size equal to the peak contribution size a_{pc}. For all six distributions considered here, ρ is in fact about half its value for $a=a_{pc}$.

6.3 Profiles for '4430' for Coated Spheres.

Graphite and other types of interstellar grains may become coated with ices or solid hydrogen by accretion from the surrounding gas to such an extent that their optical properties undergo significant changes (Güttler, 1952; Wickramasinghe, 1967; Wickramasinghe and Nandy, 1968). '4430' profiles were therefore determined for some representative cases of coated spheres, with impurities in either the core or the mantle. These results are presented in Table XIII, and some are illustrated in Figure 28.

Conclusions are as follows:
(1) The general shape of the resultant line does not change when silicate or graphite grains are covered by up to three times their volume of dirty ice or solid hydrogen. In general, ρ takes a value somewhere between that for pure core-material and that for pure mantle-material (see Figure 28).
(2) A small core of dielectric (silicon carbide) or absorbing (graphitic) material introduced into silicate

Table XIII — Models for '4430' for Coated Spheres.

Fixed parameters : as for Table X.

Core	Inner radius (nm)	Mantle	Outer radius (nm)	Volume ratio (mantle/core)	Impurities in: (C, core ; M, mantle)	Nf_1 ($\times 10^5 \mu m^{-3}$)	γ_1 ($\times 10^{-3}$) (μm^{-1})	$(\lambda_{A_C} - \lambda_{A_E})$ (nm)	A_E (%)
Silicate	100	--	100	0	C	7.2	7.8	2.4	1.0
Silicate	100	Dirty Ice	126	1	C	11.0	6.1	1.4	3.1
Silicate	100	Dirty Ice	159	3	C	13.5	4.4	1.0	7.7
Silicate	100	Solid H_2	126	1	C	8.2	7.2	2.0	1.5
Silicate	100	Solid H_2	159	3	C	9.5	6.9	1.7	1.9
Graphite	50	--	50	0	C	27.5	6.8	1.7	2.1
Graphite	50	Dirty Ice	63	1	C	27.0	5.8	1.3	3.8
Graphite	50	Dirty Ice	79	3	C	27.8	4.1	1.0	8.2
Graphite	50	Solid H_2	63	1	C	28.5	6.6	1.6	2.7
Graphite	50	Solid H_2	79	3	C	30.0	6.0	1.3	3.6

(continued)

(Table XIII continued)

--	0	Silicate	100	∞	M	7.2	7.8	2.4	1.0
Silicon Carbide	10	Silicate	100	10^3	M	7.1	7.8	2.5	1.0
Graphite	50	Silicate	100	8	M	9.6	6.6	1.5	2.2
Graphite	50	Silicate	100	8	C	125	0.04	*	80

* See Figure 29, where this complicated profile is plotted out.

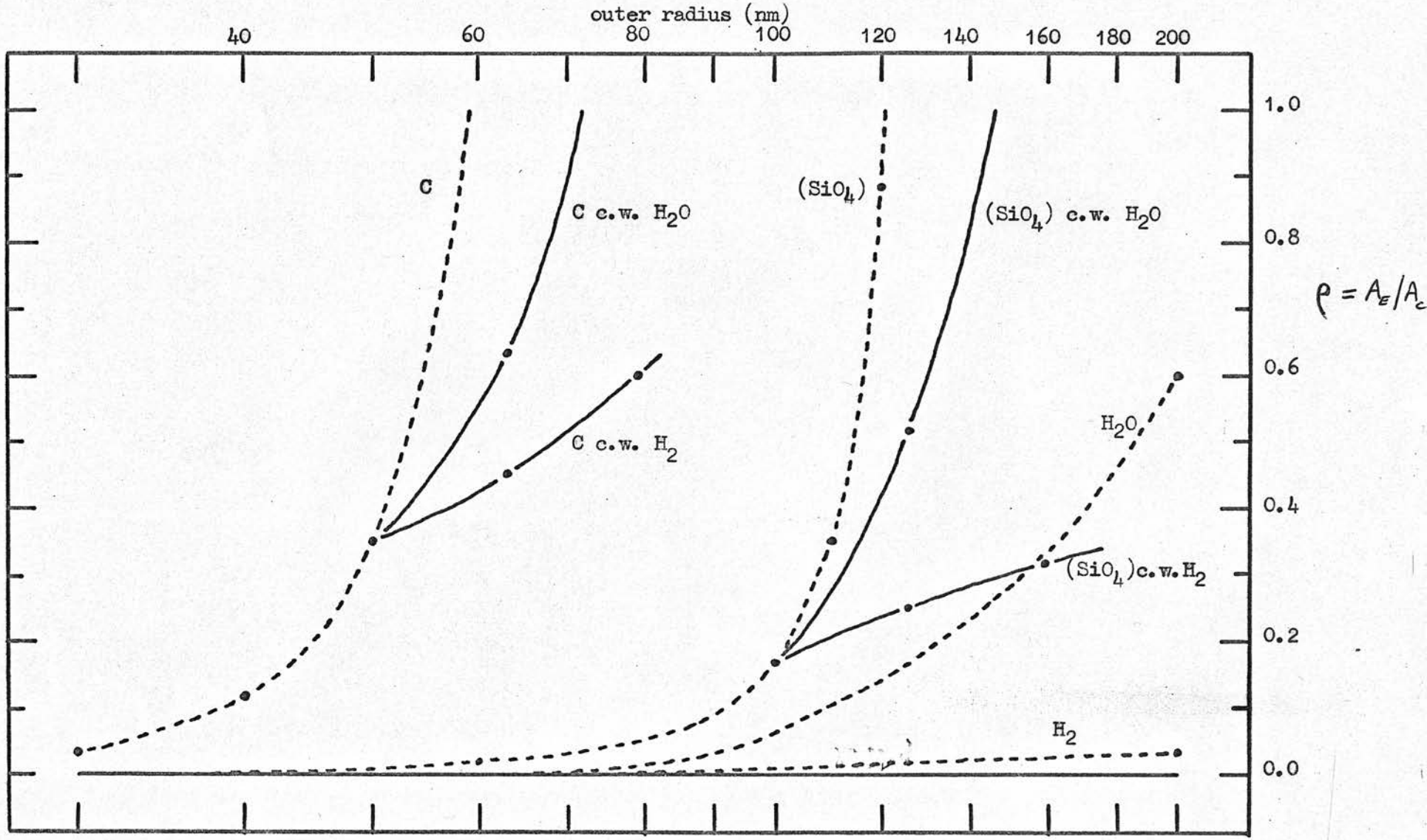

Figure 28 ρ for '4430' as a function of outer radius for coated spheres with impurities in the core. Some curves for simple spheres are included for comparison.

C refers to graphite ; (SiO_4) to silicates ; H_2O to dirty ice ; H_2 to solid hydrogen ; and 'c.w.' means 'coated with'.

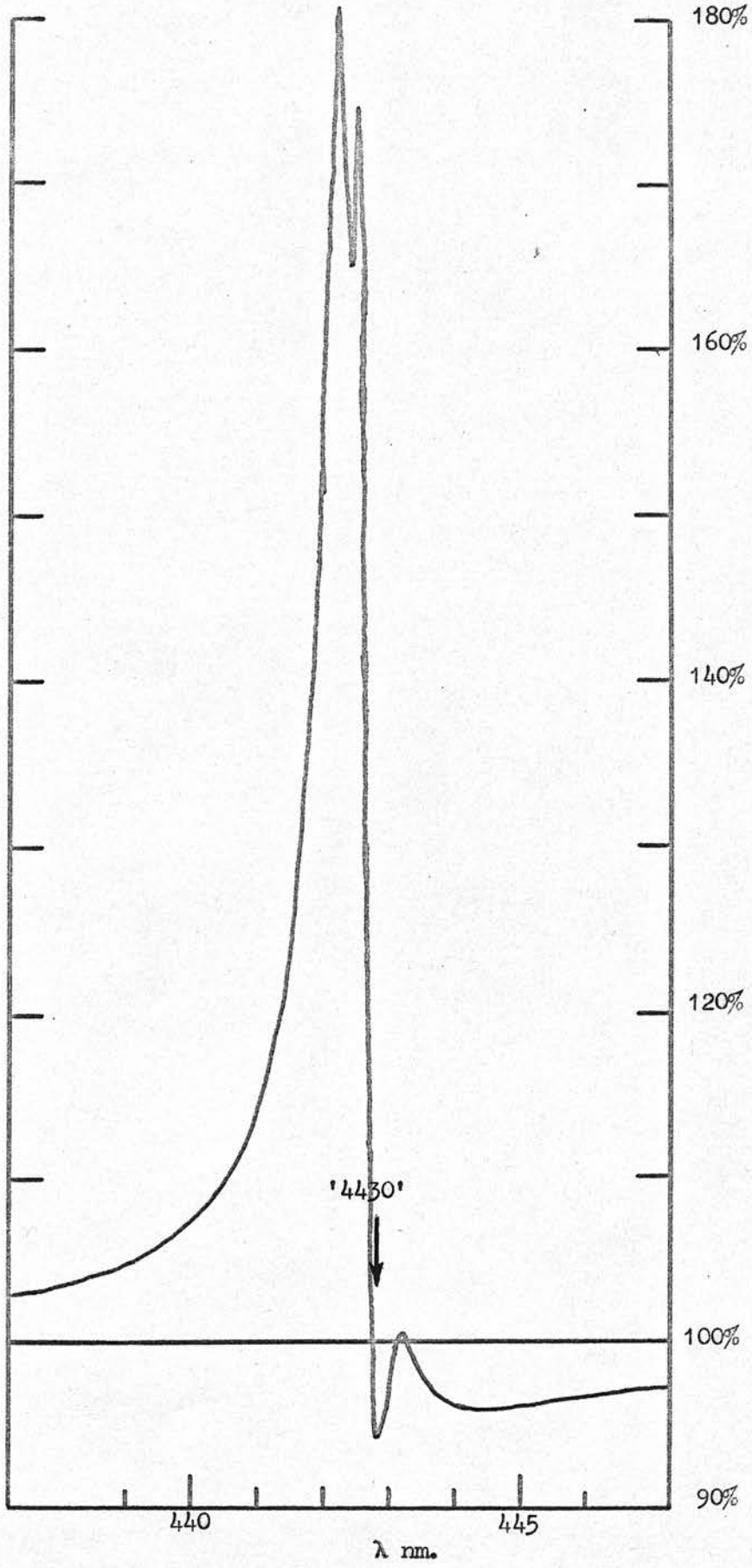

Figure 29 Profile of '4430' for 50 nm. graphite sphere coated to 100 nm. with silicate material, and with impurities in the core.

Table XIV Dependence of Profile on Distribution of Impurities in the Grain.

Fixed parameters: $m_o = 1.66$; $A_c = 6\ \%$; $\delta = 1.8$ nm. ; $\lambda_{A_c} = 443.0$ nm. ; $E_{B-V} = 0.53$ mag.

Model	Nf_1 ($\times 10^5 \mu m^{-3}$)	γ_1 ($\times 10^{-3} \mu m^{-1}$)	$(\lambda_{A_c} - \lambda_1)$ (nm)	A_E (%)	$(\lambda_{A_c} - \lambda_{A_E})$ (nm)
Impurities evenly dispersed in sphere of radius 100 nm.	7.24	7.8	0.3	1.0	2.4
Sphere of radius 100 nm., with impurities concentrated into inner half of volume.	13.5	7.5	0.3	1.3	2.0
Sphere of radius 100 nm., with impurities concentrated into outer half of volume.	15.0	8.0	0.3	0.7	2.8
Sphere of radius 100 nm., with no impurities, coated to a depth of 5 nm. with impurities only (i.e., mantle with $m_o = 1.0$ containing all the impurities).	60.0	7.7	0.2	0.9	2.4

grains does not appreciably change the profile of a line arising from impurities in the mantle.

(3) The profile assumes a very complicated shape when ρ becomes very large. (This is also true for simple spheres of very large size). Figure 29 shows such a profile, for the case of impure graphite grains thickly coated with silicate material.

6.3.1 Distribution of Impurities in the Grain.

The theory of coated spheres may also be used to investigate the profile dependence on the distribution of impurities in a grain. This is achieved by having both core and mantle of the same material but restricting the impurities to one or other region. Only spherically symmetric distributions can be considered, of course.

It transpires that ρ - and hence the degree of asymmetry of the profile - increases as the impurities are concentrated towards the centre of the grain. Some results for 100 nm. silicate spheres are presented in Table XIV. The final model quoted is a classical representation of absorption by molecules on the surface of a grain. It is interesting to see that the emission wing does not disappear. In fact, for the 100 nm. silicate grain the extinction profile is very similar to that calculated for the same impurities distributed evenly throughout the grain.

6.4 Asymmetry of the Profiles.

Unless the emission wing is very small, the theoretical

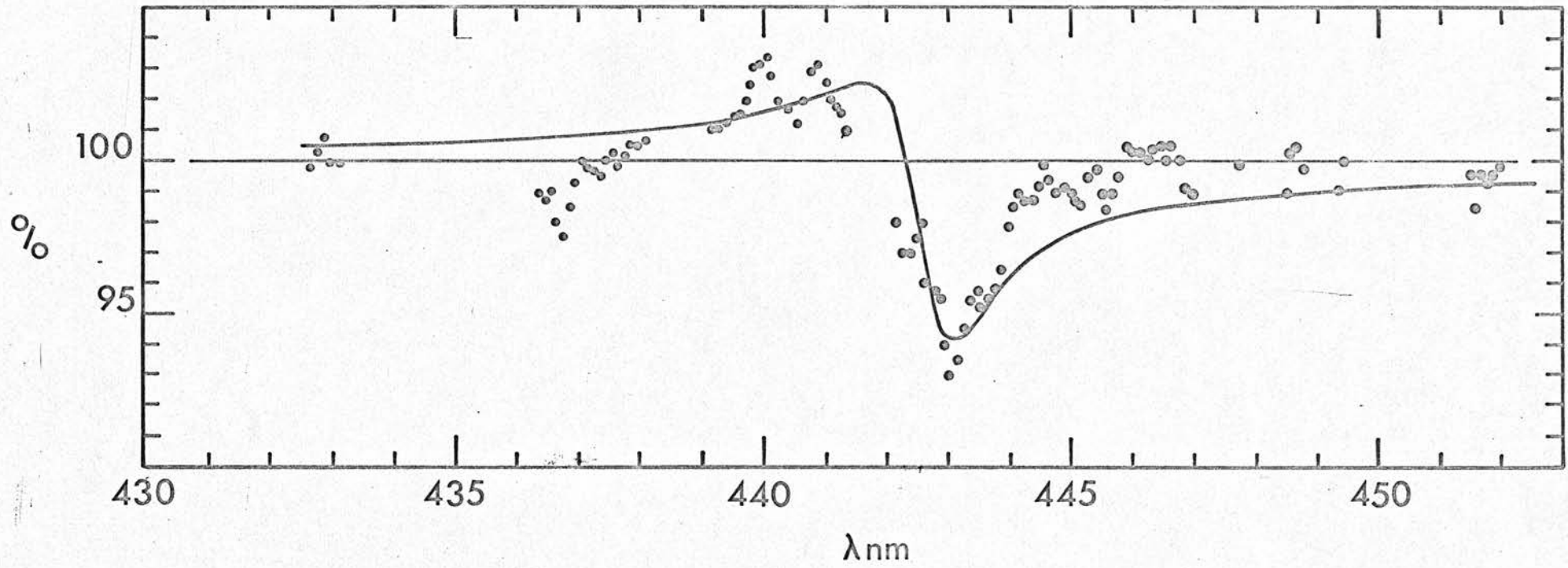

Figure 30

A theoretical profile for '4430' (for a size distribution of silicate grains) compared with observational points from Figure 13. Regions affected seriously by stellar lines have been omitted from the plotted observational points.

profiles are considerably asymmetric in both absorption and emission wings (see Figure 5). For $\rho \simeq 0.5$ they are more asymmetric than the image tube observations suggest: this is apparent in Figure 30, where the theoretical and observational profiles are compared. Regions affected by stellar lines have been omitted from the plotted observational points. The theoretical curve is for the Wickramasinghe-Nandy silicate size distribution (see Table XII).

At first sight, both emission and absorption wings in the theoretical profile seem to be too extensive to match the observations. It must be remembered, however, that it was assumed in the derivation of the observational profile (Section 3.1) that the total extent of the feature was only $\lambda\lambda 443 \pm 4.5$ nm., and that continuum was fitted to regions outside those limits. This procedure necessarily forcibly curtails any very extensive wings that may be present, although A_C and A_E would not be affected significantly. Unfortunately, increasing the interpolation region much beyond $\lambda\lambda 443 \pm 4.5$ nm. soon generates unacceptable interpolation uncertainties. This minor problem seems to be insurmountable.

Moreover, as pointed out by Wickramasinghe and Nandy (1970a), the asymmetry may in any case be different if there is photon-phonon coupling (Wickramasinghe et al., 1968) which cannot be considered on purely classical theory.

The ratio ρ would seem to be the simplest and safest criterion for comparison of theory and observation.

6.5 Impurity Concentrations.

The concentrations of impurity atoms needed to reproduce the observed line strengths are readily calculated from the Nf values of Tables X to XIV. For example, for simple spherical grains, the values of Nf_1 needed to give the mean observed ratio of '4430' absorption to colour excess (11% per magnitude) with $\rho \doteq 0.5$ can be found from the results of Tables X and XII. The corresponding impurity concentrations are then given by

$$C = \frac{N/\mathcal{N}\rho}{d/w}$$

where $\mathcal{N}$ is Avogadro's Number, d is the density of the host material, and w its mean atomic weight. The results are as follows:

for graphite, $C = 3 \times 10^{-5}/f_1$;

for silicon carbide, $C \doteq 2 \times 10^{-5}/f_1$;

for iron, $C \doteq 1 \times 10^{-5}/f_1$;

for silicates, $C = 8\text{-}9 \times 10^{-6}/f_1$;

for ices, $C = 5 \times 10^{-6}/f_1$;

and for solid hydrogen, $C \doteq 2 \times 10^{-6}/f_1$.

Similar concentrations are needed for impurities in coated grains.

We can see that even if the oscillator strength f_1 for '4430' were rather low, say 0.001, we would still need only one atom in about a hundred to be an impurity atom. On the more reasonable assumption that $f_1 = 10^{-1}$ to 10^{-2} for this the strongest of the diffuse lines, the required concentrations vary from .002 to 02% for solid hydrogen

host to .03 to 3% for graphite host.

There are some 16 elements with normal cosmic abundancies more than 3×10^{-3} than of carbon - or more than 10^{-3} that of oxygen - (Aller, 1963; Allen, 1963), including magnesium, sodium, aluminium, calcium and iron, the most common substitution atoms in silicates.

The concentrations required to give the observed '4430' strengths thus appear to put few constraints on the type of impurities possible.

It must be noted, however, that we have assumed for each type of grain in turn full responsibility for both discrete '4430' absorption and the continuous extinction. If, on the contrary, the '4430' impurities were preferentially associated with a type of grain that contributes only, say, 1 part in 100 to the visual continuous extinction, then the concentration C for that particular host species would need to be 100 times what we have calculated here.

6.6 Discussion of the Results for '4430'

The observed mean ratio of emission to absorption for '4430' (see Figure 13) can be reproduced theoretically for any of the host grain types considered here, providing that the size of the grain is right (see figure 26). The candidature of each type of grain is now discussed in the light of these 'optimum sizes'.

Solid hydrogen

Large grains of solid hydrogen - about 500 nm. in radius - are needed to give the observed value of .

Yet even larger grains are required to fit the visual extinction curve (Van de Hulst, 1948, 1949). The existence of solid hydrogen grains is probably restricted to localised, cool interstellar regions (compare Krishna Swamy and Donn, 1969, with Reddish, 1970), and cannot be responsible for more than a very small fraction of the visual extinction in the general interstellar medium. The total abundance of the hypothetical impurities in this case would thus need to be very high (see Section 6.5).

Ices

Effective particle radii of about 200 nm. are needed for ices. This is about half the dominant size in the Oort-Van de Hulst distribution that best fits the visual extinction curve (Van de Hulst, 1948). For this distribution, therefore, the emission is too strong - as Van de Hulst himself found (1949). Such large ice grains could perhaps survive in interstellar space except close to stars, but their numbers must be relatively small (Wickramasinghe, 1967; Knacke et al., 1969b; Donn and Jackson, 1970). So, as with solid hydrogen, the total impurity abundances would need to be too high.

Silicates

The observed value of ρ is reproduced for silicates of radius about 120 nm. In fact, refractive indices of silicates range from 1.55 to 1.7, and this corresponds to optimum sizes of from 110 to 130 nm. These are certainly within the range of sizes usually used for the closest Mie approximations to the interstellar extinction curve. For example, Wickramasinghe and Nandy (1970b, 1971a) find

that for graphite-silicate-iron mixtures they need silicate grains of about 150 to 180 nm. in radius for the best curve-fitting. D.P. Gilra (1971), on the other hand, finds that for graphite-silicate-silicon carbide mixtures, the required peak contribution size of silicate grains is about 80 nm. D.R. Huffman and J.L. Stapp (1971) claim a good fit to observations using bimodal size distributions for silicate grains alone: their peak contributions come from 80 and 180 nm. grains.

It seems from all this evidence that the profile of '4430' can impose tighter constraints on the particle sizes than does the continuous extinction curve. A size distribution of silicate grains must exist that is compatible with the observations of both continuous extinction and of '4430'.

There are two other points in favour of silicates as '4430' hosts. Firstly, theoretical polarisation profiles for '4430' for elongated silicate grains are not incompatible with the available observational data (Greenberg and Stoeckly, 1971; Wickramasinghe and Nandy, 1971b; Kelly, 1971). Secondly, laboratory spectra of silicate minerals with iron (Fe^{++} and Fe^{+++}) impurities show some wavelength coincidences with the broadest diffuse interstellar features (see Huffmann (1970); Manning (1970)).

Silicon carbide

Effective radii needed for silicon carbide grains are about 100 nm. Such particles form one of Gilra's (1971) proposed three main constituents, but whether they can be

formed at all in the required quantities remains doubtful. C. Friedemann (1969) calculates that the relative mass of silicon carbide to graphite ejected from the atmospheres of carbon-rich stars is only 10^{-8}. R.C. Gilman (1969) finds that silicon carbide would be the predominant condensate for only those few stars which have oxygen to carbon ratios in the range: $0.90 \lesssim O/C \lesssim 1.05$. Furthermore, from the viewpoint of total abundances, silicon carbide and silicate grains must be at least partially mutually exclusive (Gilra, 1971).

If there are numerous silicon carbide grains in interstellar space then they must therefore be much smaller than 100 nm., and so cannot provide the required '4430' profiles. The silicon carbide grains in Gilra's mixture, it may be noted, contribute very little to the shape of the extinction curve except near the Whitford-Nandy 'knee' at $2.3\mu m^{-1}$. And this 'knee' cannot be fitted really well by any Mie curves (Nandy et al., 1968; Harris, 1969).

Iron

The 'optimum' size for iron grains is about 70 nm. Such particles are much larger than those assumed to be abundant in the interstellar medium (Schalén, 1965). Wickramasinghe and Nandy (1970b, 1971a) find that the dominant iron particles in the most likely grain mixtures are certainly smaller than 30 nm. in size. Furthermore, numerous grains of larger dimensions would constitute an interstellar iron abundance anomolously high (Wickramasinghe, 1967).

Graphite

The observed value of ρ can be reproduced for graphite grains about 50 nm. in radius. Such grains are significantly smaller than the dominant ones in the curve-fitting mixtures of Wickramasinghe and Nandy, which are about 80 nm. Gilra uses grains of about 50 nm. in radius, but then he uses the m_o values of Greenaway et al. (1969) - and for these the optimum size is less than 50 nm. (see Table X).

Nevertheless it should be stated in support of graphite as candidate that even a relatively thin coating of dielectric condensate such as ice or solid hydrogen substantially reduces ρ (see Figure 28). Such a thin coating - especially if it were of solid hydrogen - would not markedly affect the extinction curves.

To summarise, graphite and silicate grains are the most likely candidates, with silicates (at the present moment) having more circumstantial evidence in their favour.

6.7 Profiles of Other Features in the Blue.

Results for the two features in the blue at λ476 and λ489 nm. are shown in Table XV for a few graphite and silicate models.

The most notable result is a reduction of up to 50% in ρ compared with the '4430' line - and the reduction is more pronounced for silicates than for graphite.

Figure 31 shows profiles for the two lines for a model that fits the '4430' observations well (the Wickramasinghe-Nandy silicate size distribution) compared with the image

Table XV — Models for '4760' and '4890', with '4430' results for comparison.

Model	m_o	λ_{A_c} (nm)	Nf_s ($\times 10^5 \mu m^{-3}$)	γ_s ($\times 10^{-3} \mu m^{-1}$)	$(\lambda_{A_c} - \lambda_s)$ (nm)	A_c (%)	A_c/E_{B-V} (% per magnitude)	δ (nm)	$(\lambda_{A_c} - \lambda_{A_E})$ (nm)	$\rho = A_E/A_c$
Graphite (a = 50 nm)	(2.46-1.42i)									
		443.0	27.5	6.8	0.4	6.0	11.3	1.8	1.7	0.35
		476.4	5.5	4.3	0.2	3.0	5.6	1.2	1.4	0.23
		488.5	12.6	8.7	0.4	3.0	6.7	2.5	3.0	0.20
Silicate (a = 110 nm)	(1.66)									
		443.0	8.70	6.7	0.5	6.0	11.3	1.8	1.7	0.35
		476.4	1.63	4.5	0.2	3.0	5.6	1.2	1.6	0.20
		488.5	3.50	9.0	0.4	3.0	6.7	2.5	3.5	0.17

(continued)

(Table XV continued)

Silicate (1.66) (size distribn. type B, a_{pc} = 121 nm. W = 51 nm.)	443.0	7.50	6.5	0.5	6.0	11.3	1.8	1.5	0.43
	476.4	1.60	4.0	0.2	3.0	5.6	1.2	1.2	0.30
	488.5	3.75	8.3	0.4	3.0	6.7	2.5	2.6	0.27
	476.4 *	2.00	4.5	0.3	3.0	5.6	1.2	1.3	0.43
	488.5 *	3.75	8.3	0.5	3.0	6.7	2.7	2.4	0.23

* These profiles were calculated using equation (5) of Section 5.2 with k = 2, so that allowance was made for the influence of '4890' on the profile of '4760' and vice versa.

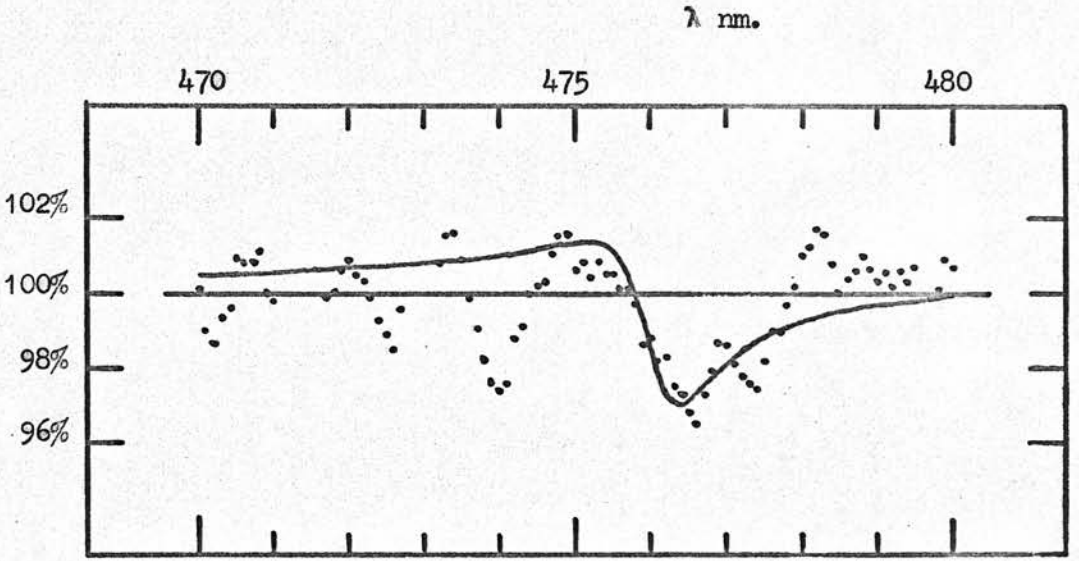

Figure 31 Theoretical profiles for '4760' and '4890' (allowing for the presence of the one in the profile of the other), for silicate size distribution 'B', compared with observational points from Figures 15 and 17.

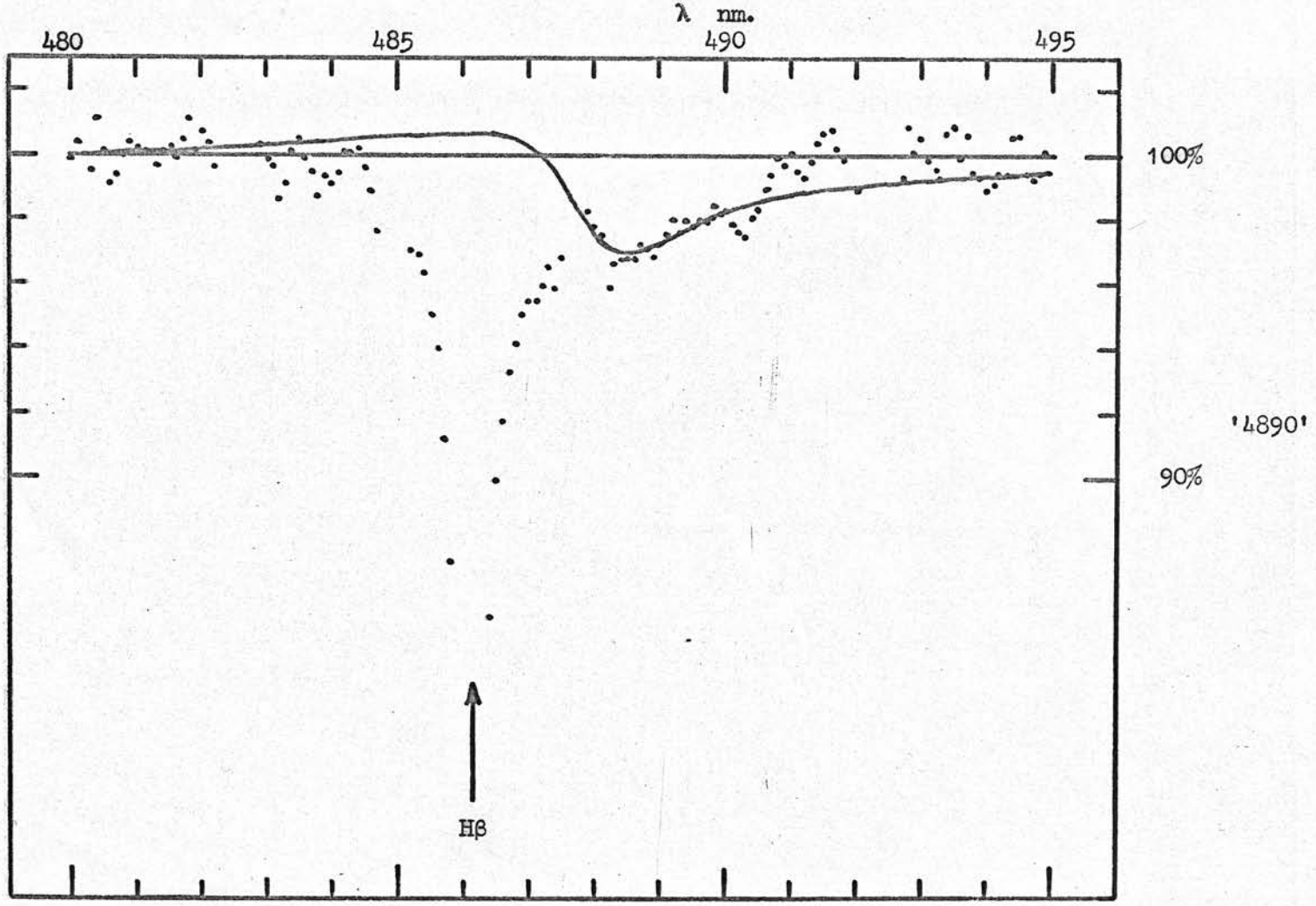

Figure 31 (continued)

tube observations of Figures 15 and 17. As with Figure 30, the stellar lines (except Hβ) have been omitted from the plotted observational points. The influence of the presence of the one line on the profile of the other was allowed for by using equation (5) (Section 5.2) with k = 2. The true observational profile for '4890' is difficult to ascertain because of the uncertain extent of the wings of Hβ, (see Section 3.3). However, since the ratio of the observed to the theoretical profiles in Figure 31 gives an approximately symmetrical Hβ line, which is expected for these six stars, the present observations at the least do not contradict the proposed theoretical explanation. The small discrepancy in the absorption wing longward of λ491 nm. is probably due to the continuum fitting procedure (see Section 6.4). The '4760' profile is in reasonable agreement with the image tube observations except near λ478 nm. The unidentified lines at λ472.6 and λ474 nm. may be interstellar (see Section 3.2) but are not taken into account here.

6.8 Profiles of Diffuse Features in the Red.

A few profiles of some of the red features, corresponding to the Cygnus OB2 spectra (see Figure 22) are described in Table XVI.

For the strongest line, λ628.3, the ratio of emission to absorption is similar to that for the blue features λλ476, 489 nm., and lower than for the λ443 nm. feature, even though the absorption is very strong. As with λ476 and λ489 nm. lines, the graphite model is marginally less favourable since any emission wing in the observed profile

Table XVI

Models for Diffuse Lines in the Red.

Model	m_o	λ_{A_c} (nm)	Nf_s ($\times 10^5 \mu m^{-3}$)	γ_s ($\times 10^{-3} \mu m^{-1}$)	$(\lambda_{A_c} - \lambda_s)$ (nm)	A_c (%)	A_c/E_{B-V} (% per mag.)	δ (nm)	$(\lambda_{A_c} - \lambda_{A_E})$ (nm)	$\rho = A_E/A_c$
Graphite (2.46-1.42i) (a = 50 nm)		628.3	3.33	0.18	0.0	45	25	0.4	0.2	0.26
Graphite (2.7 -1.4i)** (a = 50 nm)		628.3	3.08	0.23	0.0	45	25	0.4	0.2	0.26
Silicate (1.66) (a =110 nm)		628.3	1.03	0.28	0.0	45	25	0.4	0.2	0.20
Silicate (1.66) (size distrbn. type B a_{pc}=121nm. W = 51 nm.)		617.6 *	1.90	6.20	0.3	11	6.1	2.5	4.2	0.14
		620.3 *	0.13	0.23	0.0	14:	8:	0.3:	***	***
		626.9 *	0.18	0.40	0.1	7.6	4.2	0.4	0.3	0.26
		628.3 *	0.80	0.35	0.0	47.5	26	0.4	0.25	0.10

* Combined profile, calculated using equation (5) of Section 5.2 with k = 4.

** Greenaway et al. (1969)

*** Indeterminate, because of distortion by the λ 617.6 nm. line.

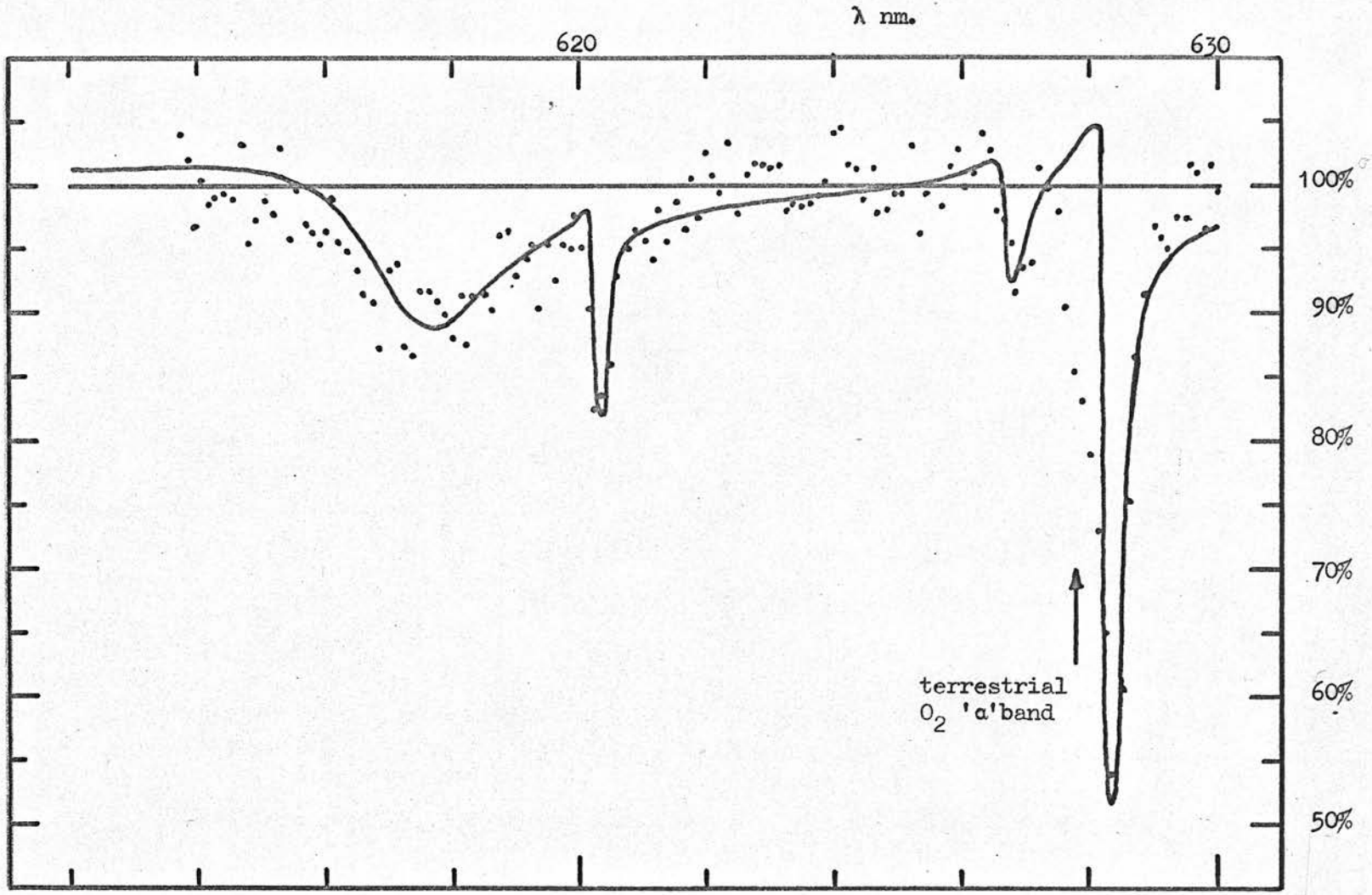

Figure 32 Theoretical profile (combined) for four lines in the red, compared with observational points from Figure 21.

is probably small (see Figure 22).

These results are based on the assumption that λ628.3 nm. is an isolated line, but the features in the red are really too close together for the dispersion equation with k = 1 to be strictly valid. Therefore, a combined profile of the four lines at λ617.6, 620.3, 626.9, and 628.3 nm., was calculated for the usual silicate size distribution, using equation (5) (Section 5.2) with k = 4.

This is compared with the observations in Figure 32. The emission wing to the λ628.3 nm. line is now even smaller, due to the presence of the λ626.9 nm. line. At the resolution used in the observations (200 pm.), this emission wing may easily be hidden by the strong atmospheric oxygen band. Indeed, the presence of an apparent emission wing may even explain why Merrill et al. (1937) could not successfully correct the equivalent width of the λ628.3 nm. line for this O_2 band. There is good agreement with the other profiles in Figure 32.

It seems plausible that all the observed features can be due to the same impurities in the same type of grains. Whilst for '4430' either silicate or coated graphite hosts could provide the observed profile, the shapes of the other lines may imply a silicate preference, because (compared with '4430') ρ is lower for silicates.

6.9 The Complete Extinction Curve

Figure 33 shows a theoretical extinction curve for the Wickramasinghe-Nandy size distribution of silicate

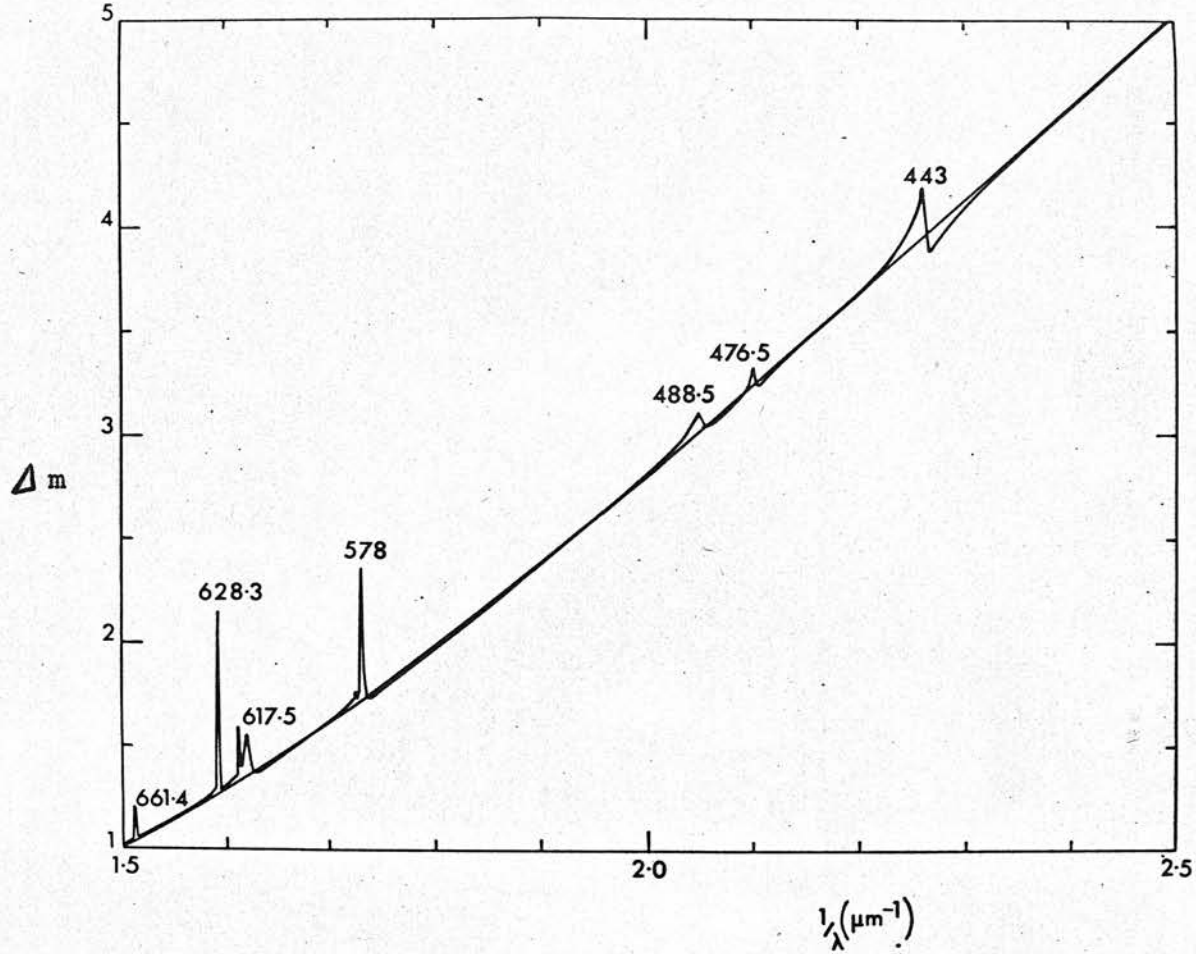

Figure 33

Theoretical extinction curve for silicate size distribution 'B', with and without eleven impurity lines.

grains. Eleven impurity lines, corresponding to eleven 'established' diffuse lines and bands, have been included. (Some of them are however too close together to be separated with the resolution of .002μm^{-1} used here). The strengths of the red lines are as seen in Cygnus OB2 no. 10 (Section 4.4). The strengths of the blue lines are predicted values for the same star, calculated by extrapolation of mean line strength versus colour excess relations to E_{B-V} = 1.8 magnitudes appropriate for this star. This procedure is valid because the measured strengths of the red lines are about 'normal' for the star's colour excess (see Section 4.4).

The weakness of the emission wings on all the lines except '4430' is clearly shown on this diagram. This effect is partly due to the presence of the $\lambda\lambda$626.9 and 577.6 lines very close to the emission wings of the strong lines at λ628.3 and λ578.0 nm., but the intrinsic variation in ρ is important.

It can be concluded that none of the observed line profiles contradict the hypothesis that they are all due to the presence of the same impurities in the same type of interstellar grains. If this is indeed the case then the number concentration of impurities N is a constant, and relative oscillator strengths for the lines are given by the relative Nf_s values used to compute the curve of Figure 13. If we further assume that these eleven lines are the only important ones, in the sense that

$$\sum_{s=12}^{K} f_s \ll \sum_{s=1}^{11} f_s = 1 ,$$

then their actual f values are as shown in Table XVII,.

Table XVII

Oscillator Strengths for Eleven Diffuse Lines.

The assumption is made that $\sum_{s=1}^{11} f_s = 1.$

Wavelength of line (nm)	f
443.0	0.42
476.4	0.08
488.5	0.19
577.6	0.03
578.1	0.02
579.7	0.01
617.6	0.16
620.3	0.01
626.9	0.015
628.3	0.06
661.4	0.005

Although these have been calculated using the silicate model, approximately the same results would emerge for any model that fits the observations.

Putting $f_1 \simeq 0.4$ for '4430' in the equations for impurity concentration C of Section 6.5, we find that, for example,

$$C = 2 \times 10^{-5} / \beta_{sil} \text{ for silicates, and}$$

$$C = 8 \times 10^{-5} / \beta_{gra} \text{ for graphite.}$$

Here, β_{sil} and β_{gra} are the gractional contributions to the depression of a stellar continuum at λ443 nm. from <u>continuous</u> extinction by silicate, and by graphite grains, respectively. It should be noted that if the β values change significantly between λ440 and λ660 nm. then the f-values of Table X would have to be adjusted accordingly, but this effect is neglected here.

Values of β_{sil} and β_{gra} are still rather uncertain. But the results of Gilra (1971) and of Wickramasinghe and Nandy (1971a) are consistent with both β_{sil} and β_{gra} being in the range 0.1 to 0.5. If, for example, $\beta_{sil} \simeq 0.4$, then if the impurities responsible for the diffuse features are situated in silicate grains, their concentration is $C \simeq 5 \times 10^{-5}$, or only one impurity atom for every 20,000 others in each grain.

7. Theoretical Profiles for Spheroids (Approximate Theory).

7.1 The 'Second Range of Validity' of the Rayleigh Approximation.

There is no exact theory available for calculating interstellar extinction by ellipsoidal particles. However, full use does not seem to have been made of the first order approximate theory due to Lord Rayleigh (1871, 1897), especially when only short wavelength ranges are required, as in the present study.

The Rayleigh approximation is normally valid only if the particle size is small compared with the wavelengths of light both outside and inside the particle. For spheres the conditions are $2\pi a \ll \lambda$ and $2\pi |m|. a \ll \lambda$.

But M.J. Jaycock and G.D. Parfitt (1962) and W. Heller (1965) have shown that for some values of a, m, and λ, fortuitous cancelling out of errors leaves a 'second range of validity' of the Rayleigh approximation. This happens because as thesize parameter $x = 2\pi a/\lambda$ is increased from very small values, the Rayleigh extinction cross-section C_{ext}^{R} at first increases more slowly than the exact (Mie) value C_{ext}^{M}, but at larger values of x the former increases more rapidly and eventually overtakes C_{ext}^{M}. It is close to this cross-over point of the two curves C_{ext}^{R} and C_{ext}^{M} that the 'second range of validity' occurs.

In Figure 34 are plotted on the m-x plane the errors incurred in assuming C_{ext}^{R} is accurate. This diagram

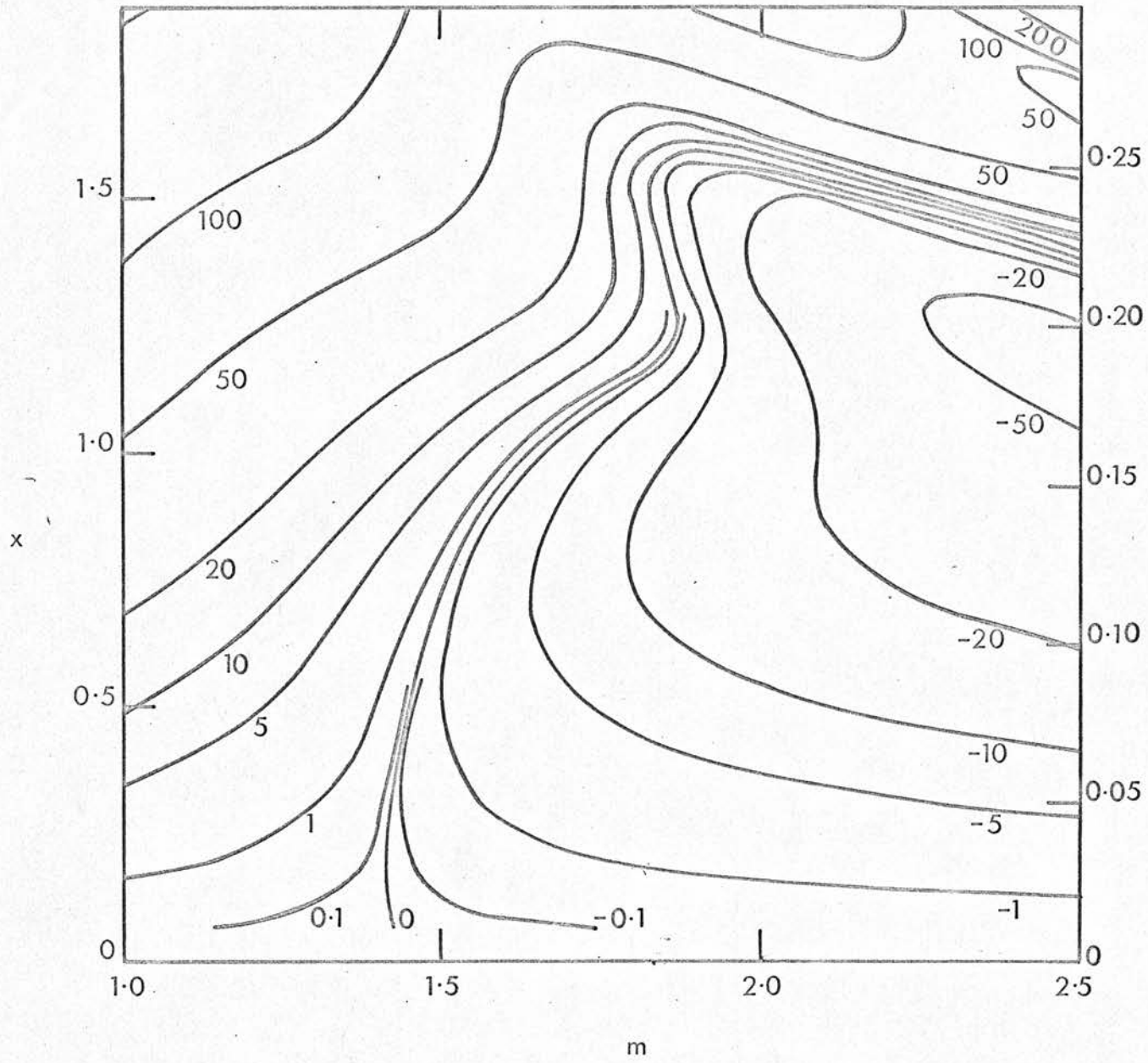

Figure 34

Percentage Rayleigh Discrepancies, as a function of size parameter (x) and refractive index, for dielectrics.

refers to dielectrics with refractive indices in the range $1.0 \leq m \leq 2.5$. The contours are lines of equal 'percentage Rayleigh discrepancy',

$$D = \frac{(C_{ext}^{R} - C_{ext}^{M})}{C_{ext}^{M}} \times 100\%$$

These were derived using a computer program specially written for this purpose.

The results are in good agreement with those of Jaycock and Parfitt, and also with those of Heller's calculated from his own Mie computations. However, Heller's Rayleigh discrepancies for $m > 1.6$, which were all based on very early manual computations by other workers, do <u>not</u> agree with the present results. Since the Mie programs used here have been doubly checked as regards accuracy (see Section 5.1), it must be concluded that Heller's results for $m \gtrsim 1.6$ are in error.

Our interest in Figure 34 is this: Is there a region of 'validity' for any values of m and x corresponding to interstellar grains near λ = 443 nm? Further, is the accuracy good enough over a sufficient range of x to allow us to consider ellipsoidal particles? The answer is yes for silicates, for values of x up to about 1.2. For λ = 443 nm., this condition becomes $r \lesssim 85$ nm., where r is the longest semi-axis of the ellipsoid.

In fact, for values of m between 1.5 and 1.9 the Rayleigh approximation could be used to advantage at significantly larger values of a/λ than the usual upper limit of 0.05: but the other interstellar

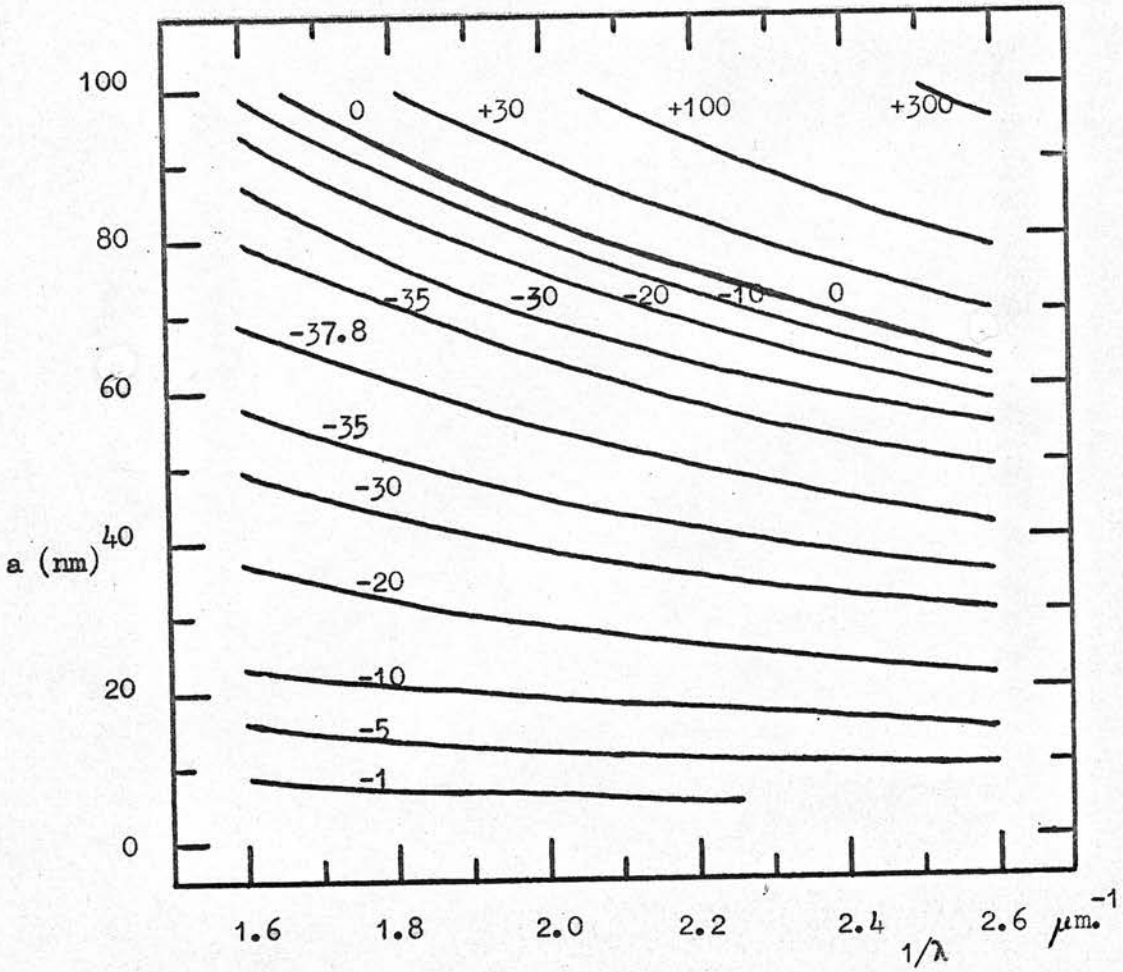

Figure 35

Percentage Rayleigh Discrepancies as a function of radius and wavenumber, for m = 2.46 - 1.42 i (graphite).

'dielectrics' (ices, solid hydrogen and silicon carbide) all have refractive indices outwith this range.

The Rayleigh discrepancies for a typical highly absorbing material, namely graphite (m = 2.46 - 1.42i), are plotted on the radius - wavenumber plane in Figure 35. The accuracy in this case will be somewhat poorer than for silicates, but since we only need a very short range in λ^{-1} near 2.3 μm^{-1}, radii near 70 nm. could be used to advantage.

The two examples described in the next Section illustrate the optimum use of the 'second range of validity' of the Rayleigh approximation.

7.2 Results for Spheroids

Consider first a prolate silicate spheroid with semi-axes a = 85 nm., and b = c = a/2 = 42.5nm. This has the same volume as a sphere of radius about 53.5 nm. Changes in m over an impurity line will be small enough not to violate significantly further the validity of the Rayleigh equations. The profiles for an isolated line at λ443 nm. using the impurity parameters of Table X for 60 nm. radius silicate spheres, are plotted in Figure 36. The procedure described in Section 5.2 was followed again, except that Rayleigh C_{ext} values for spheroids replaced the exact C_{ext} values for spheres. Also plotted is the polarisation profile for perfect alignment of the prolate spheroids.

The quantity plotted is $p^{(impure)}$ as a percentage of $p^{(pure)}$, where

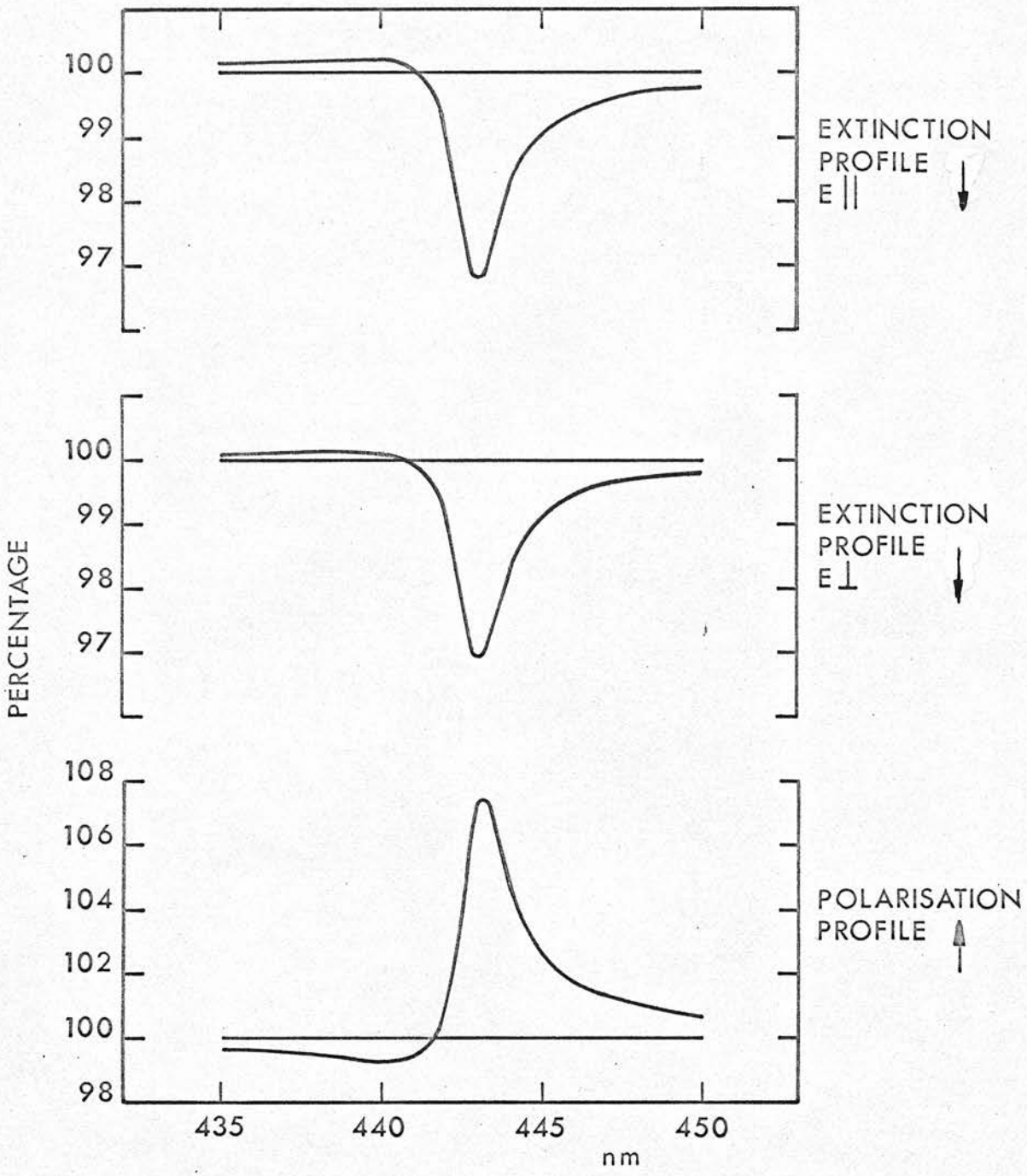

Figure 36 Extinction and polarisation profiles for '4430' for a prolate silicate spheroid with a = 2b = 85 nm. C_{ext} (//)/C_{ext} (⊥) was about 1.8

$$p^{(impure)}/p^{(pure)} = 0.921 \exp\ (\Delta m_p^{(pure)} - \Delta m_p^{(impure)},$$

$$\frac{\Delta m_p^{(pure)}}{\Delta m^{(pure)}} = 2\,\frac{|(C_{ext(E//)} - C_{ext\ (E\perp)})|}{(C_{ext(E//)} + C_{ext\ (E\perp)})}\ ,$$ (see Greenberg and Shah, 1966),

and $\Delta m^{(pure)}\ (\lambda = 443\ nm) \simeq \Delta m^{(pure)}(\lambda = B) \simeq 4E_{B-V}$,

assuming a value of 3 for the 'ratio of total to selective absorption', A_V/E_{B-V}.

Here $\Delta m^{(pure)}$ and $\Delta m_p^{(pure)}$ are the extinction and polarisation in magnitudes for grains with no impurities.

Considering the accuracy of these calculations, the following purely qualitative conclusions can be drawn:

(1) The extinction profiles for both 'perpendicular' and 'parallel' positions of the electric field vector with respect to the grain axis are very similar to the corresponding profiles for spheres of the equivalent volume radius.

(2) The polarisation profile is similar to the extinction profiles; that is to say, there is an excess polarisation peak at almost precisely λ 443 nm., and corresponding to the 'emission' wing there is a polarisation deficiency to the violet of λ 443 nm.

(3) The excess polarisation is greater than the excess extinction, <u>but not much greater</u> even for perfect alignment.

These general results agree with those from exact calculations (J.M. Greenberg and R. Stoeckly (1971) and A. Kelly (1971)) for infinite silicate cylinders of radius $\simeq$ 50 nm.

The second and third results seem to throw some doubt on the assumption that the same impurities in the same grains are responsible both for the excess extinction and for the excess polarisation at '4430' - at least, for the star 55 Cygni. The observations of Nandy and Seddon (1970) show a polarisation excess for this star of the order of 50%. Wickramasinghe and Nandy (1971b) have found that an Nf_1 value of 3×10^{19} cm^{-3} is needed to reproduce the observed profile, even assuming perfect alignment of cylinders. This is equivalent to $Nf_1 = 10^7 \mu m^{-3}$ (see equation (4)), which for the A_c/E_{B-V} ratio of $\simeq$ 10% per magnitude appropriate to 55 Cygni would give a peak extinction at λ443 nm. of around 50%, ten times more than that observed. Mrs Kelly (1971) places the Nf_1 required for polarisation nearer $10^8 \mu m^{-3}$, which is a hundred times greater than that required for extinction. She suggests that preferential alignment of larger grains could partially explain the anomaly. Yet the situation would be even worse if the cylinders were, more realistically, imperfectly aligned.

Can graphite flakes offer a better solution?

Let us represent graphite grains by oblate spheroids (see for example, Wickramasinghe, 1967) with b/a = 2, with $m_b = 2.46 - 1.42\ i$, as used in Chapter 6, and $m_a = 1.54 - 0.002\ i$ (Greenaway et al., 1969; and with the conductivities in the ratio $\sigma_b / \sigma_a = 10^3$).

Rayleigh calculations will be of sufficient accuracy for present purposes for $m = 2.46 - 1.42\ i$ when $b \simeq 75$ nm. (Figure 35), and for $m = 1.54$ when $a \lesssim 70$ nm. (Figure 34).

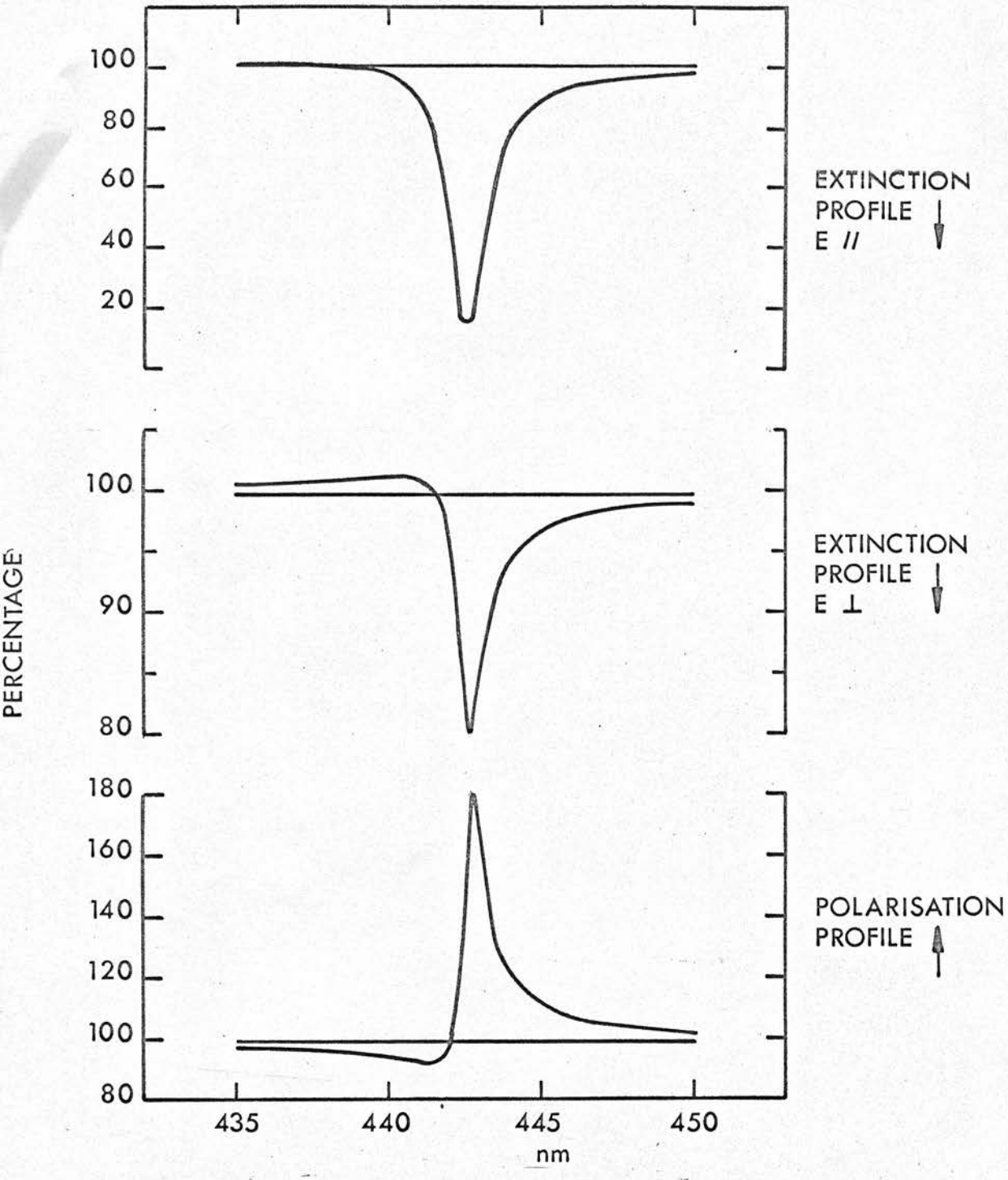

Figure 37 Extinction and polarisation profiles for '4430' for an oblate graphitic spheroid with b = 2a = 74 nm. $C_{ext}(//)/C_{ext}(\perp)$ ranges from $\simeq$ 0.02 in the continuum to $\simeq$0.09 at the centre of the line.

Figure 37 shows the results for an oblate graphitic spheroid with b = 2a = 74 nm. The impurity parameters inserted are those given in Table X for 60 nm. graphite spheres.

Both extinction profiles indicate values of appropriate to a mixture of small quartz spheres and 60 nm. graphite ones, as is to be expected from the refractive indices used. Even though the value of Δ_{mp}/Δ_m for perfectly aligned pure grains now reaches almost its maximum value of 2, the peak polarisation excess p_c is still only four times the peak excess extinction A_c, and in general the results are similar to those for prolate spheroids of silicate material. Since to account for the observed continuous polarisation of $p/A_V = 0.034$ (Hiltner, 1956) we need only the equivalent of one in thirty or so graphite flakes perfectly aligned, with the rest randomly oriented (Wickramasinghe, 1967), the p_c value of Nandy and Seddon may be no better explained by graphite flakes than by silicate cylinders. But more detailed comparisons should probably be deferred until further observational results are available:

As far as the extinction profiles are concerned, these preliminary results suggest that no adjustments to the overall conclusions of Chapter 6 are necessary - at least, for spheroids with the ratio of major to minor axes less than about 2.

Conclusions.

The confirmation of the presence of an 'apparent emission wing' (that is, a region of decreased total extinction) in the observational profile of '4430', together with the observation of an analogous region in a relative profile of '6180', supports the theory that the diffuse features are impurity absorptions of interstellar grains.

Application of the general classical theory of extinction by small particles containing impurities to the present problem has shown that both continuous and discrete (diffuse line) extinctions could have their origin in the same grains. The earlier results of Van de Hulst and of Greenberg, namely, that (relatively) much smaller particles were needed for the discrete extinctions, have been shown to hold only for icy grains.

For the particular concentrations of impurities needed to reproduce the observed strengths and profiles of the diffuse features, it seems that the profiles may well be essentially independent of the shape of the host grain -- whether it be spherical, spheroidal or cylindrical.

It has been concluded from the detailed calculations for spheres that none of the observed profiles of diffuse features are at variance with the hypothesis that they arise from the same impurities in the same species of grain.

Acknowledgements.

I wish to express here my thanks to Professor H.A. Brück for his continued interest in, and support for, this research ; to my supervisors, Mrs. M.T. Brück and Dr. K. Nandy, for their general help and encouragement and for many fruitful discussions ; and to Dr. P.W.J.L. Brand for an introduction to the Spectracon and its entourage. I am particularly grateful to Dr. V.C. Reddish for his comments on the Cygnus OB2 association, and to Dr. K. Nandy and Mrs. A Kelly for discussions of dispersion and extinction theory. I am also indebted to Mr. P. Standen, Mr. D. Jackson and others at the Royal Greenwich Observatory, Herstmonceux, for hospitality, explanations and assistance at the Isaac Newton Telescope; and to many at Edinburgh for help with experimental and computing problems. I thank the Robert Cormack Bequest Committee of the Royal Society of Edinburgh for a three year Fellowship in support of this research.

Appendix I

Equivalent Widths of Stellar Lines.

The Table gives estimates of equivalent widths that were obtained as a by-product of the reduction of image tube spectra (Chapter 2). The measures are given in picometres (hundredths of an Ångstrom). Errors are mostly of the order of 2 to 5 pm., but entries followed by a colon are less accurate, with errors of 10 or 15 pm.

Values for some B5 and A2 stars, taken from the literature, are included for comparison. The literature on equivalent widths for late B type stars is scarce: this Table helps to bridge the gap between B8 and A2. The stars are listed in the same order as in Table IV (Section 3.1).

	λ (nm) :		414.4	423.3	426.7	429.0	429.6
			He I	Fe II	C II	Ti II	Fe II Ti II
1.	Mean of 3 stars (BT)	B5I	37	4	22	--	--
2.	HD 208501	B8Ib	18	12	7:	--	--
3.	HD 12301	B8Ib	12	--	8:	--	--
4.	β Orionis	B8Ia+	13	5:	10	--	--
5.	β Orionis (U; HW)	B8Ia+	15	10	15	--	--
6.	HD 199478	B8Ia	18:	--	11	--	--
7.	HD 14322	B8Ib	23	--	9	--	--
8.	HD 39970	A0Ia	--	30:	--	0:	10
9.	HD 40589	B9Iab	6:	28:	--	--	--
10.	HD 21291	B9Ia	1:	29	--	--	--
11.	HD 202850	B9Iab	10	29	--	--	--
12.	HD 21389	A0Ia	--	25:	--	5	0:
13.	HD 21389 (BT)	A0Ia	--	30	8	--	--
14.	HD 20041	A0Ia	--	35:	--	2	5
15.	α Cygni (G)	A2Ia	--	51	2	17	42

References

BT Butler and Thompson (1961)

G Gröth (1961)

HW Hiltner and Williams (1946)

U Underhill (1948)

	430.3	430.8	431.4	438.5	438.8	439.1	447.1	448.1	450.8	451.5
	Fe II Ti II	Ti II	Fe II Sc II Ti II	Fe II Mg II	He I	Mg II	He I	Mg II	Fe II	Fe II
1.	2	--	--	1:	58	3:	82	43	--	--
2.	6	--	--	9	24	9	48	40	--	--
3.	13	--	--	5	22	3	39	31	--	--
4.	6	--	--	6	19	6	33	39	--	--
5.	8	--	--	5	25	5	39	49	--	--
6.	8	--	--	8:	21	7	41	43	--	--
7.	10:	--	--	6:	17	--	43	45	--	--
8.	32	7	6	--	--	--	--	46	9	9
9.	23	--	--	--	--	--	--	49	12	7
10.	21	--	1:	--	--	--	--	50	4:	14:
11.	28	5:	8:	21	12	9	23	60	24:	20:
12.	28	3	12	--	--	--	--	53	12	4
13.	--	--	--	--	--	--	11	57	--	--
14.	32	5	8	--	--	--	--	53	14:	12
15.	77	18	51	33	5	14	5:	68	36	33

	452.1	453.4	454.1	454.9	455.3	455.6	455.8	456.3	456.8
	Fe II	Fe II Ti II	Fe II	Fe II Ti II	Si III	Fe II	Cr II	Ti II	Si III
1.	--	--	--	(	21	)	--	--	7
2.	--	--	--	8	11	0	--	--	6
3.	5	--	--	0	8	--	--	--	1
4.	13	--	--	3	15	5	--	--	--
5.	15	--	--	15	8	5	--	--	5
6.	9	--	--	7	11	--	--	--	8:
7.	12	--	--	2:	15:	--	--	--	--
8.	29	7	8:	21	--	9	0:	0:	--
9.	26	4	14	12	--	2	0	0	--
10.	25	10	4	12	--	0	0	0	--
11.	32	10	18	29	--	8:	5	13:	--
12.	30	12:	18	19	--	10	9	6:	--
13.	--	--	--	--	--	--	--	--	--
14.	33	11	13	31	--	12	9	16:	--
15.	74	33	21	59	--	48	35	22	--

	457.2	457.6	458.3	461.9	462.9	463.4	466.7	471.3	492.2	492.4
	Ti II	Fe II	Fe II	Fe II Cr II	Fe II	Cr II Fe II	Fe II	He I	He I	Fe II
1.	--	--	--	--	--	--	--	23	77	2
2.	--	--	--	--	--	--	--	28	--	--
3.	--	--	--	--	--	--	--	20	--	--
4.	--	--	--	--	--	--	--	12	--	--
5.	--	--	--	--	--	--	--	15	--	--
6.	--	--	--	--	--	--	--	16	40:	10:
7.	--	--	--	--	--	--	--	20	--	--
8.	4	0:	27	9	18	12	9	9	--	49
9.	0:	0:	22	5	10:	10:	2	--	--	--
10.	0:	0:	27	5	12:	18:	3	10:	15:	26
11.	5:	8:	33	2	23:	12	5	13	13:	44
12.	1	4	25	4	12:	18	4	6	--	44
13.	--	--	32	--	--	--	--	10	--	64
14.	6	3	26	5	16	16	5	10	--	45
15.	26	21	67	37	35	32	14	6	--	59

Appendix II

(i) 'Diffuse Interstellar Features in the Spectrum of the Most Heavily Reddened Star'

by G.E. Bromage ;

from 'Nature' 230, 172 (1971).

(ii) 'Interstellar Bands'

by G.E. Bromage, Mary T. Brück and K. Nandy ;

from 'Astronomische Nachrichten' 293, 39 (1971).

Diffuse Interstellar Features in the Spectrum of the Most Heavily Reddened Star

THE Cygnus OB2 stellar association contains the most heavily reddened early type star known[1,2]. If all interstellar grains were to be removed from the line of sight to this eleventh magnitude star, it would rival Sirius as the brightest in the sky, its B–V colour excess being 3.7 magnitudes[3].

A photographic spectrum of the star, at 200 pm (=2 Å) resolution, has been obtained with the Cassegrain spectrograph of the Isaac Newton telescope. The dispersion used

was 6 nm mm^{-1}; and the wavelength range, 570–675 nm. The spectrum is compared here with that of star number 10 (BD +41° 3804) in the same association, for which two spectra were obtained (with the same instrument).

Microdensitometer traces of spectra of Cygnus OB2 No. 10 and No. 12 are reproduced in Figs. 1 and 2 respectively. Relative intensity scales, marked in percentages, have been inserted at representative points along the traces.

These spectra show the second strongest diffuse interstellar features in the red so far recorded, only the broad feature near 618 nm seen in supernova spectra[4] being stronger.

The computed equivalent widths of the interstellar features, of Hα and of the stellar He I lines, together with central intensities and half-widths for the diffuse features, are presented in Table 1. All measurements of the "6284" line have been corrected for the blend with the terrestrial O_2 "α band", and those of Hα in No. 12 for the blend with the stellar C II lines at 657.8 and 658.3 nm. Also, in calculating the half-widths of the diffuse features, I have allowed for instrumental broadening, by applying a first order correction, assuming gaussian profiles. The relative inaccuracy of the measurements for No. 12 shortward of 600 nm stems from the low density of the spectrum in this region: it is a consequence of the extreme reddening of this star that only one short section of its visible spectrum can be correctly exposed at a time.

is linear over this short wavelength range. Relative to this continuous curve, then, Fig. 3*a* shows the profile of "6180". An extensive apparent emission wing to the violet is indicated.

Fig. 3*b* shows that both the strength and the profile of "6180" are the same for the two stars Cygnus OB2 No. 10 and No. 12.

Table 1 shows that all diffuse interstellar features are of almost equal strength for the two stars. Yet No. 12 is twice as reddened as No. 10. This discrepancy is remarkable, considering that the stars are in the same association, and that most of the dust responsible for the reddening lies within the association[3]. It is strong evidence that the diffuse line absorbers cannot be closely associated equally with the various species in the dust population. On the other hand, a common source for all the diffuse features is suggested by the common ratio of intensities for the two stars. (Wampler[7] has found a similar but less pronounced discrepancy in the central depths of "4430", compared with the reddening, for Cygnus OB2 stars.) Because there exist normal linear relationships between strengths of the diffuse features and interstellar reddening, on a galactic scale (and the correlations are seldom very striking[7–10]) it seems that the features are deficient in No. 12 rather than overabundant in No. 10.

The "mean wavelengths" of the unidentified diffuse lines, quoted in Table 1, are those measured relative to the stellar

Table 1 Spectral Features of the Heavily Reddened Star in Cygnus OB2

Name	Mean wavelength (nm)	Identification	Equivalent width Cyg. OB2 No. 10 (pm)	Equivalent width No. 12 (pm)	Central depth Cyg. OB2 No. 10 (%)	Central depth No. 12 (%)	Mean half-width (pm)
5,780	577.6±0.2 578.08±0.06	Unidentified, interstellar	100: 170: 269±5	280±30	6 36 41	30:	1,600±300 360±50
5,797	579.66±0.08	" "	58±3	50±20	14	10:	300±50
6,180	617.6 ±0.2	" "	360: 60: 421±10	370: 60: 432±15	12	11	2,500±300
6,203	620.35±0.03	" "			14	13	290±50
6,270	626.90±0.03	" "	35±3	37±5	9	7	280±50
6,284	628.33±0.03	" "	272±10	278±15	45	48	370±50
6,614	661.35±0.04	" "	29±2	25±3	12	10	≤200
	Wavelength						
D_1	589.59	Na I, interstellar	85±10	50±20			
D_2	589.00	"	76±8	70±20			
Hα	656.28	H I, stellar +circumstellar?	+16±5	−503±20	0:	−60	
D_3	587.56 (blend)	He I, stellar	140±3	40±20			
—	667.82	"	91±3	76±3			

An unambiguous determination of the effective stellar continuum position was possible for all lines except "5780" and "6180". The former seems to be superimposed upon a broader feature centred on 577.6 nm (see especially Fig. 1) and I have therefore interpolated the continuum over the interval λλ576–581 nm.

The "6180" absorption resembles the broad features in the blue at λ443 and λ489 nm. The errors of the measurements of "6180" quoted in Table 1 are chiefly due to the uncertain interpolation of the stellar continuum: the results have been calculated assuming continuum is regained at λ614 and λ622 nm. But there is evidence[5,6] from automated spectrophotometry of image-tube spectra that "4430" has an apparent emission wing to the violet of the main absorption.

As a test for possible extensive wings in "6180", I have determined the ratio of the spectral energy distribution in pairs of stars (*a*) Cyg. OB2 No. 10 and κ Cas., and (*b*) Cyg. OB2 No. 12 and No. 10. In each case, the spectra were taken on the same night and processed together. The results are shown in Fig. 3, where magnitude differences (normalized) are plotted against wavenumber. Only the continuum and the "6180" feature were considered. "6180" is virtually cancelled out for pair (*b*), leaving only the continuous reddening curve, which

He I lines, and averaged for the two stars. The positions of four of the diffuse lines (those at λλ 620.3, 626.9, 628.3, 661.4) could be measured accurately for both stars: all four have wavelengths slightly less in No. 12 than in No. 10, with a mean difference of 80±50 pm (or 30±20 km s^{-1}). This could be an indication of either real differences in wavelength, or else of a relative radial velocity: if the latter is true, the line-carriers are moving away from No. 12 faster than from No. 10—or, alternatively, towards No. 10 faster than towards No. 12. The rest wavelengths of the lines are not known, so we cannot yet decide which of these alternatives is true.

Two further results are interesting in this connexion. The interstellar sodium *D* lines in No. 10 have a velocity relative to the He I stellar lines of 0±20 km s^{-1}. This means that there is no significant mean difference in wavelength for the six diffuse lines in No. 10 (relative now to the *D* lines) from Merrill and Wilson's[8] mean values. Also, the core of the strong Hα emission in No. 12 has a velocity of +65±15 km s^{-1} relative to He I λ667.8 nm. This result suggests there is an infall of matter into this very young star but, without comprehensive measures of the star's radial velocity, such an infall can only be specified as relative to the effective He I absorption region in the star.

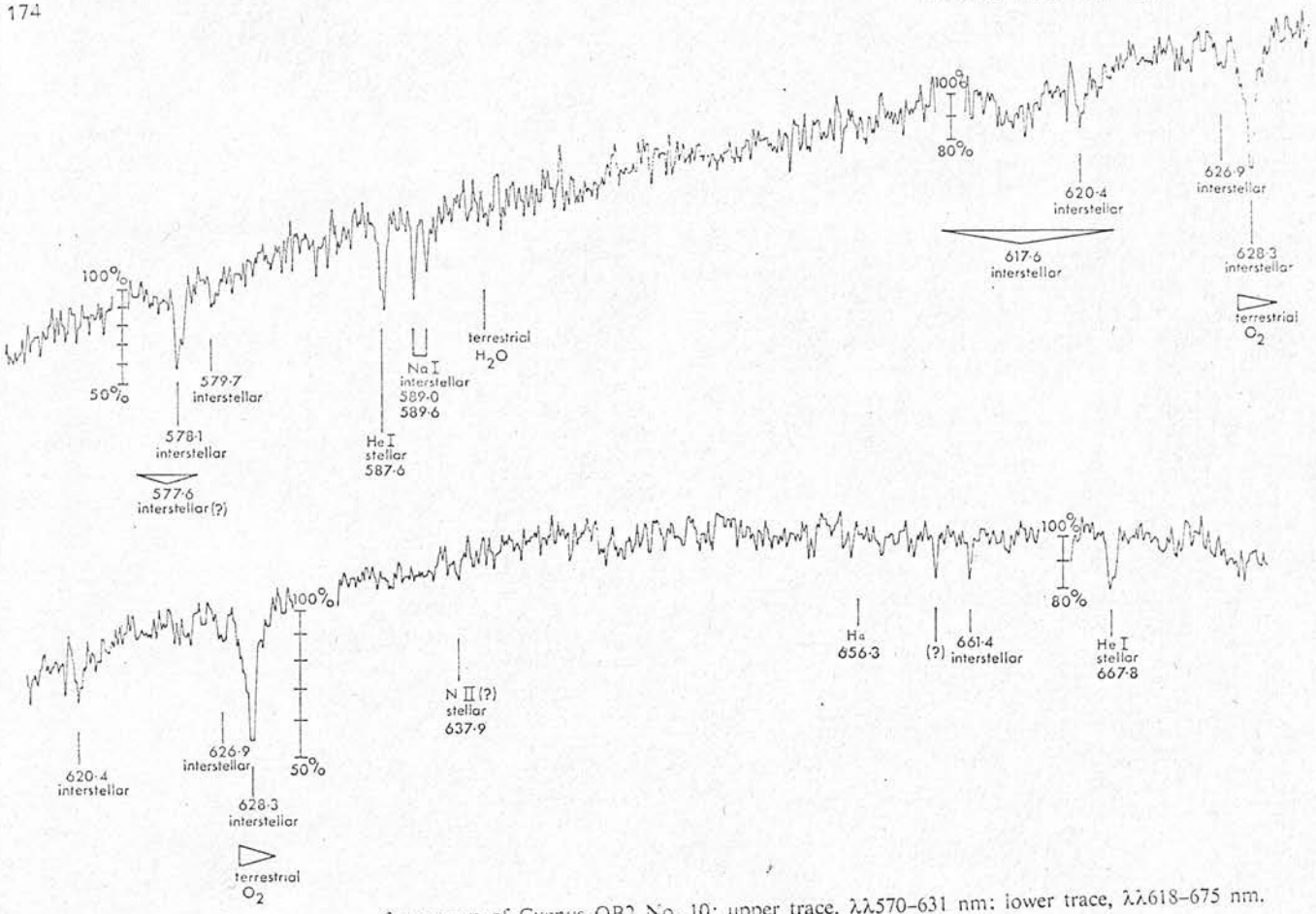

Fig. 1 Microdensitometer traces of spectrum of Cygnus OB2 No. 10: upper trace. λλ570–631 nm: lower trace, λλ618–675 nm.

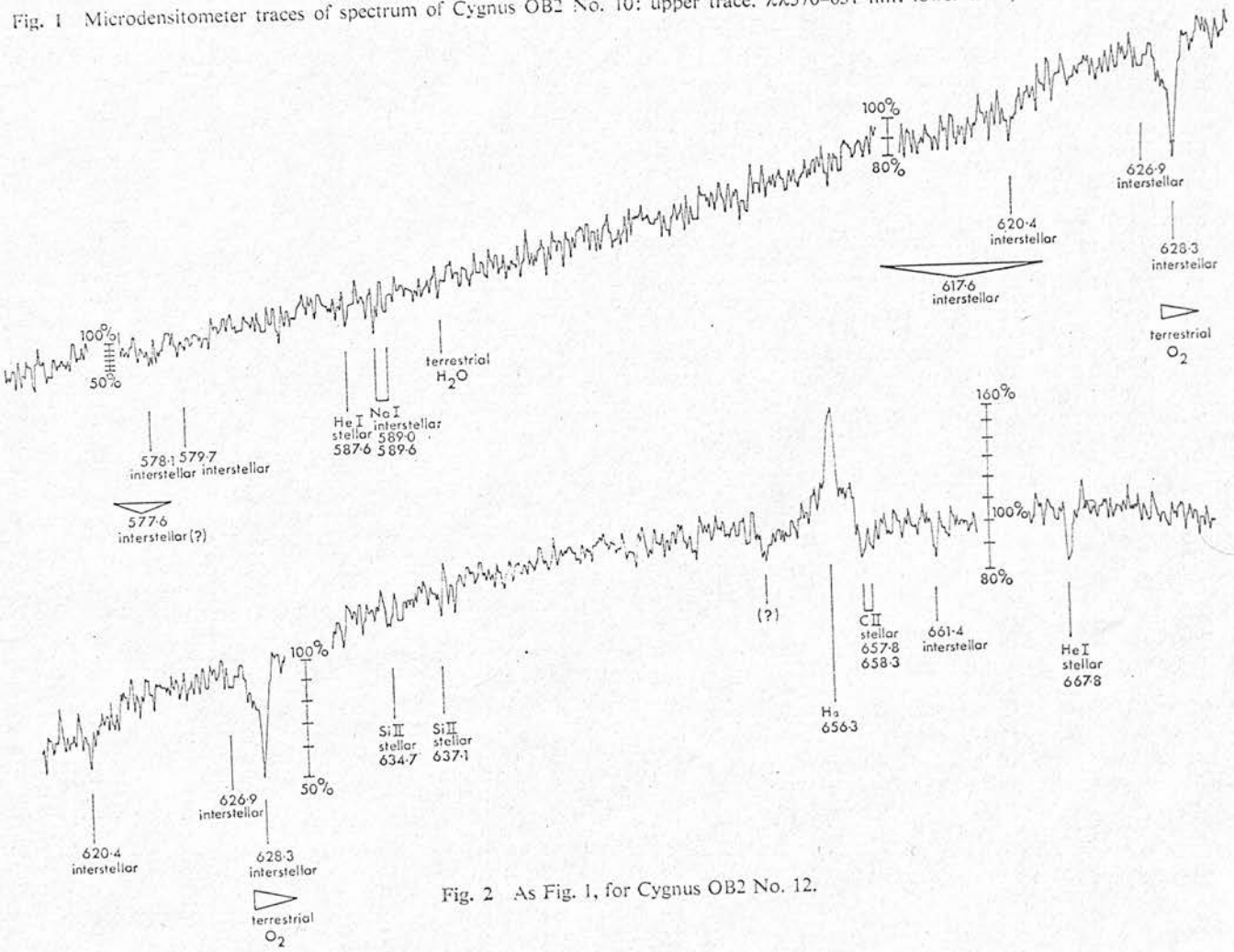

Fig. 2 As Fig. 1, for Cygnus OB2 No. 12.

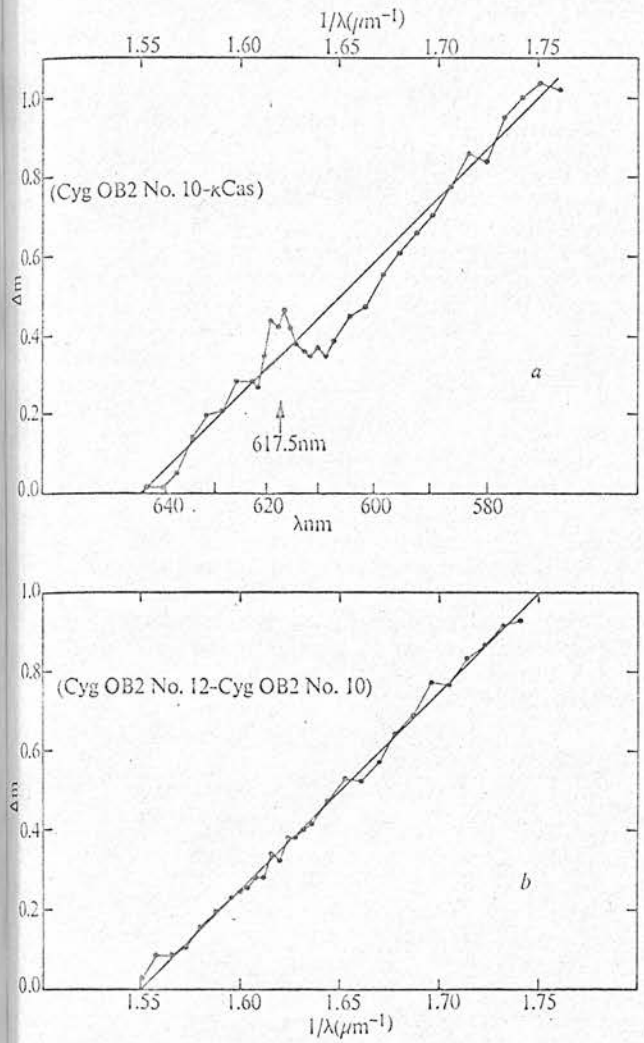

Fig. 3 The reddening curve in the region of the "6180" feature, for Cygnus OB2 No. 10 and No. 12.

The Hα emission seems to be closely stellar in origin. The spectrum of No. 12 was obtained using an extended object slit, and the star was not "trailed". Hα emission does not extend significantly beyond the stellar image. Taking the distance to the star as 2.1 kpc (ref. 3), the projected seeing and guiding disk is 0.06 pc in diameter and the slit length 0.5 pc. I conclude that there is no detectable circumstellar Hα emission between 0.03 and 0.25 pc from Cygnus OB2 No. 12, whereas a halo extending to at least 1 pc is expected for a mid-B type star such as this. The threshold of detection was about 3% of the stellar continuum intensity.

G. E. Bromage

Department of Astronomy,
University of Edinburgh

Received February 10, 1971.

1 Morgan, W. W., Johnson, H. L., and Roman, N. G., *Pub. Astron. Soc. Pacific*, 66, 85 (1954).
2 Schulte, D. H., *Astrophys. J.*, 128, 41 (1958).
3 Reddish, V. C., Lawrence, L. C., and Pratt, N. M., *Pub. Roy. Obs. Edin.*, 5, 111 (1966).
4 Seddon, H., *Nature*, 222, 757 (1969).
5 Brück, M. T., and Nandy, K., *Nature*, 220, 46 (1968).
6 Bromage, G. E., Brück, M. T., and Nandy, K., *Astron. Nachr.*, 293 (in the press).
7 Wampler, E. J., *Astrophys. J.*, 144, 921 (1966).
8 Merrill, P. W., and Wilson, O. C., *Astrophys. J.*, 87, 9 (1938).
9 Deeming, T. J., and Walker, G. A. H., *Z. Astrophys.*, 66, 175 (1967).
10 Buscombe, W., and Kennedy, P. M., *Mon. Not. Roy. Astron. Soc.*, 139, 417 (1968).

Astron. Nachr., Bd. 293 H. 1—2 (1971)

Interstellar Bands

G. E. Bromage, Mary T. Brück and K. Nandy (Edinburgh)

(Paper submitted to the IAU Colloquium "Interstellar Dust" Jena, August 1969)

The presence of an apparent emission wing in the interstellar absorption band at $\lambda = 4430$ Å is confirmed. The observed profile of the band is in qualitative agreement with recent theoretical predictions.

Investigations of the interstellar bands at 4430 Å, 4760 Å and 4890 Å are at present in progress at the Royal Observatory, Edinburgh using an image intensifier attached to the Cassegrain spectrograph of the 36-inch Telescope at a dispersion of 40 Å/mm. In a pilot study the profile of the 4430 band was derived by two methods, (a) by differencing spectrograms of pairs of stars of similar spectral type, one with weak and the other with strong 4430 features, and (b) by automated spectrophotometry of image tube spectra. The profile obtained by the first method from three pairs of stars indicates an asymmetric profile; the precision of this method depends on the accuracy of the MK types and the number of the pairs of stars studied. The 4430 profile following from the second method also shows an asymmetric feature as well as an apparent emission to the blue of the normal 4430 profile. The details of the automated spectrophotometric technique and the preliminary results have been reported elsewhere (Brück and Nandy, 1968; Brück et al., 1969).

The earlier observations have now been extended to 20 supergiants with spectral types ranging from Bo to Ao. The present results concern four B8 supergiants using the unreddened star Rigel (HD 34085) for comparison. The magnitudes and colour excesses of these stars are listed in Table 1

Table 1. The B8 stars observed: general data

HD	B	E_{B-V}	Sp. type	No. of spectra
12301	5.96	0.47	B8Ib	3
14322	7.09	0.44	B8Ib	2
199478	6.13	0.56	B8Ia	2
208501	6.53	0.83	B8Ib	4
34085	0.05	0.06	B8Ia	4

The method of reduction is as follows. Each spectrum on the image tube film is sampled at equal intervals of 12.5 μm along the direction of dispersion and the densities are recorded on tape by a digitized Joyce Loebl densitometer. The dispersion curve for each spectrum is obtained by a computerised search for strong spectrum lines and their subsequent identification. A given profile is fitted to each of the lines to calculate their equivalent widths, and a set of orthogonal polynomials is then fitted to the remaining spectral data to represent the continuum. The reduction programme for automatic spectrophotometry has been developed by Thompson (1966). For the present investigations, a region to either side of λ 4430 Å of total width 90 Å, and smaller ones around Hγ and Hδ have been omitted in the determination of the continuum. Finally, the spectra rectified to the computed continuum as unity, are plotted by means of an automatic graph plotter.

The mean 4430 profile and the intensity distribution in the neighbouring spectral region obtained from the four reddened stars are shown in Figure 1. Figure 2 shows the intensity distribution in the same region for the mean of the four spectra of Rigel. The apparent emission appears in Figure 1 at about 4405 Å, with intensity nearly half that of the absorption at 4430 Å. Since the bump near 4430 Å does not appear in Figure 2, it seems very unlikely that the emission feature in the curve of Figure 1 is instrumental.

It was first suggested by van de Hulst (1957) that a resonant absorber dispersed throughout the material of a grain may give rise to interstellar absorption bands and he predicted that for particle radii comparable with optical wavelengths the absorption profile could be asymmetrical and accompanied by an apparent emission feature to the blue of the band.

The calculations of van de Hulst were restricted to $m \approx 1$; Greenberg (1968) has extended these calculations to size distributions of homogenous ice grains. Recently Hoyle and Wickrama-

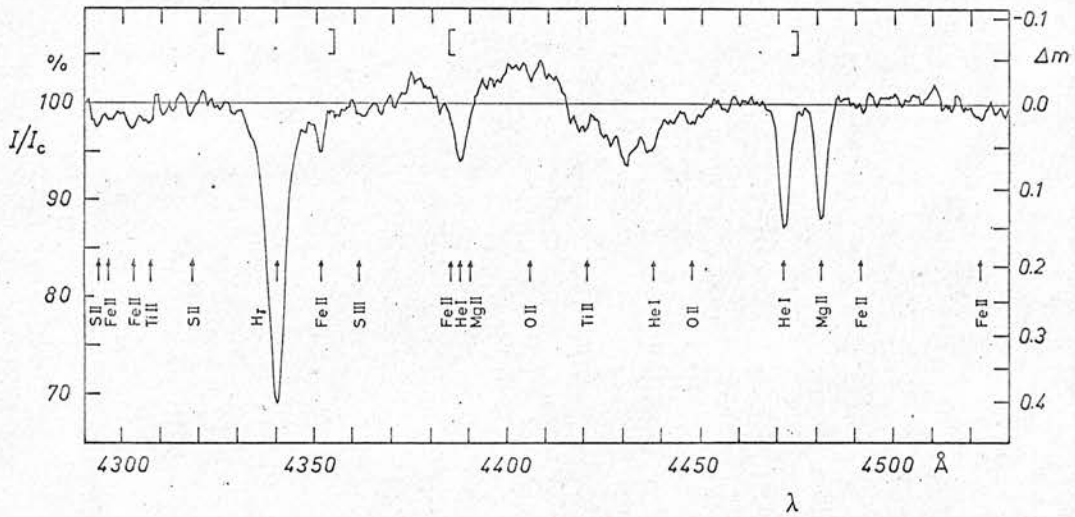

Fig. 1. The mean 4430 profile and the intensity distribution in the neighbouring spectral region for the four reddened B8 supergiants. Brackets denote regions omitted for continuum fitting.

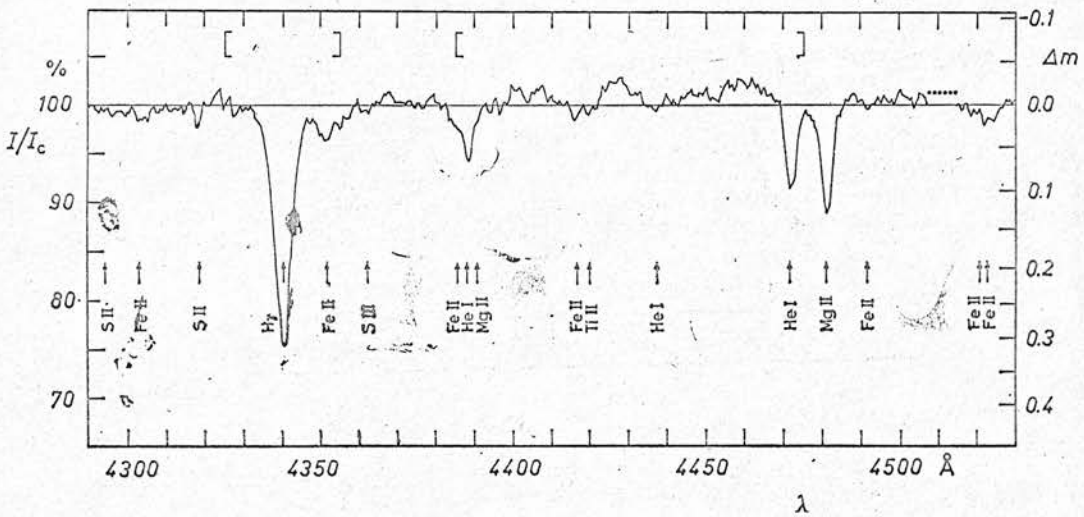

Fig. 2. The intensity distribution in the same region as in Figure 1 for Rigel.

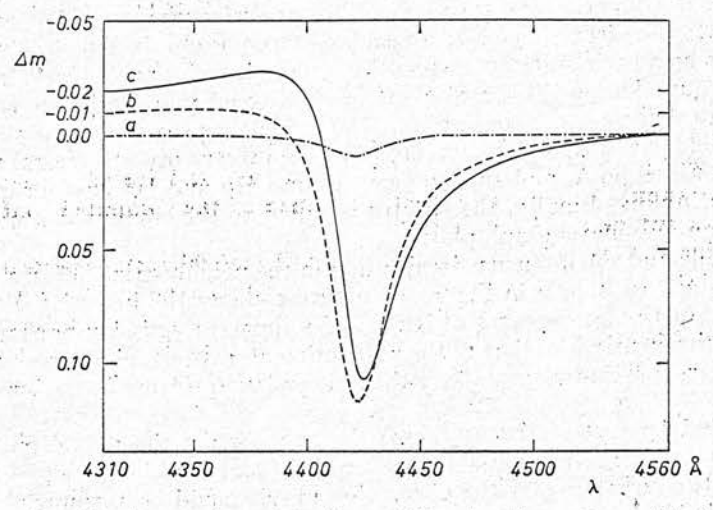

Fig. 3. Profile of the 4430 band for three grain models (a) graphite of radius 0.06 μm; (b) silicate of radius 0.07 μm; (c) solid H_2 of radius 0.35 μm.

singhe (1969) have suggested that interstellar grains may consist of a mixture of silicate particles of radii 0.07 μm and graphite particles of radii 0.05—0.07 μm. Wickramasinghe and Nandy (1969) have extended the original calculation of van de Hulst to three grain models (a) graphite particles of radii 0.06 μm with an impurity concentration of 40 per cent, (b) silicate particles of radii 0.07 μm with an impurity concentration of 10 per cent, and (c) solid hydrogen grains of radii 0.35 μm with an impurity concentration of 2 per cent. The results for these three models are shown in Figure 3. It is interesting to note that for graphite particles the central depth of the band is very small even for high concentration. For models (b) and (c) satisfactory profiles are obtained, but the ratio of the depth of the emission wing to that of the main absorption is smaller than what is actually observed. Furthermore, both models (b) and (c) show a fairly long tail to the emission wing, which has not been observed in the present studies of the 4430 band.

References

M. T. Brück and K. Nandy, Nature 220.46 (1968).
M. T. Brück, K. Nandy, and H. Seddon, Physica 41.128 (1969).
J. M. Greenberg, Nebulae and Interstellar Matter, volume 7 of Stars and Stellar Systems, p. 221 (1968).
F. Hoyle and N. C. Wickramasinghe, Nature 223.459 (1969).
H. C. van de Hulst, Light scattering by small particles London, (1957).
G. I. Thompson, Publ. R. Obs. Edinburgh 5.245 (1966).
N. C. Wickramasinghe and K. Nandy, Astrophys. and Space Sci. 6.154 (1969).

References

Aden, A.L., and Kerker, M., 1951, J.Appl. Phys. 22, 1242.

Allen, C.W., 1963, 'Astrophysical Quantities', Athlone Press, London.

Aller, L.H., 1963, 'The Atmospheres of the Sun and Stars', Ronald.

Apt, H.A., Meinel, A.B., Morgan, W.W., and Tapscott, J.W., 1968, 'An Atlas of Low-Dispersion Grating Stellar Spectra'.

Arakawa, E.T., Hamm, R.N., Hanson, W.F., and Jelinek, T.M., 1966, in 'Optical Properties and Electronic Structure of Metals and Alloys', ed. Abelès, North-Holland.

Baker, E.A., 1949, Pub. Roy. Obs. Edin. 1, 15.

Beals, C.S., 1942, M.N.R.A.S. 102, 96.

Beals, C.S. and Blanchet, G.H., 1938, M.N.R.A.S. 98, 398.

Binnendijk, L., 1952, Ap.J. 115, 428.

Brand, P.W.J.L., 1967, Thesis, University of Edinburgh.

Brück, M.T., and Nandy, K., 1968, Nature, 220, 46.

Burkhardt, G., 1950, Ann. Physik (6), 5, 373.

Buscombe, W. and Kennedy, P.M., 1968, M.N.R.A.S. 139, 417.

Butler, H.E. and Seddon, H., 1958, Pub. Roy. Obs. Edin. 2, 113.

Butler, H.E. and Seddon, H., 1960, Pub. Roy. Obs. Edin. 2, 187.

Butler, H.E. and Thompson, G.I., 1961, Pub. Roy. Obs. Edin. 2, 225.

Cannon, A.J., 1901, Ann. Harv. College Obs., 28, part 2.

Cayrel, R., and Schatzman, E., 1954, Ann. Ap. 17, 555.

Cernuschi, F., Marsicano, F. and Codina, S., 1967, Ann. Ap. 30, 1039.

Choyke, W.T. and Patrick, L., 1968, J. Opt. Soc. Am. 58, 377.

Chromey, F.C., 1960, J. Opt. Soc. Am. 50, 730.

Code, A.D., 1958, P.A.S.P. 70, 407.

Cudaback, D.D., Gaustad, J.E., and Knacke, R.F., 1971, Ap. J. 166, L49.

Debye, P., 1909, Ann. Physik (4), 30, 57.

Deeming, T.J. and Walker, G.A.H., 1967, Z.f.Ap. 66, 175.

De Jong, T., 1971, Astron. Ap. (in the press).

Ditchburn, R.N., 1963, 'Light', Blackie.

Donn, B., 1968, Ap.J. 152, L129.

Donn, B. and Jackson, W.M., 1970, Bull. Am. Astron. Soc., 2, 309.

Dorschner, J., 1968, Astron. Nachr., 290, 171.

Duke, D., 1951, Ap.J. 113, 100.

Duley, W.W., 1968, Nature, 218, 153.

Duley, W.W., 1969, Physica, 41, 134.

Duley, W.W. and Graham, W.R.M., 1969, Nature, 224, 785.

Eddington, Sir A.S., 1937, Observatory, 60, 99.

Eyster, E.H., 1937, Ap.J. 86, 486.

Fenn, R. and Oser, H., 1965, Appl. Opt. 4, 1504.

Field, G.B., Goldsmith, D.W., and Habing, H.J., 1969, Ap.J. 155, L149.

Friedemann, Chr., 1969, Astron. Nachr. 291, 177.

Gaustad, J.E., 1963, Ap.J. 138, 1050.

Giese, R.H., 1961, Z.f.Ap. 51, 119.

Gilbert, L.A., 1962, Fuel, 41, 351.

Gilman, R.C., 1969, Ap.J. 155, L185.

Gilra, D.P., 1971, Nature, 229, 237.

Greenaway, D.L., Harbeke, G., Bassani, F. and Tosatti, E., 1969, Phys. Rev. 178, A1340.

Greenberg, J.M., 1968, in 'Stars and Stellar Systems', VII, 'Nebulae and Interstellar Matter', Chicago, p.221.

Greenberg, J.M. and Shah, G., 1966, Ap.J. 145, 63.

Greenberg, J.M. and Stoeckly, R., 1970, in 'Ultraviolet Stellar Spectra and Related Ground-based Observations', I.A.U. Symposium no.36, ed. Houziaux and Butler, Reidel, p.24.

Greenberg, J.M. and Stoeckly, R., 1971, Nature Phys. Sci. 230, 15.

Greenstein, J.L. and Aller, L.H., 1950, Ap.J. 111, 328.

Gröth, H.G., 1961, Z.f.Ap. 51, 206.

Güttler, A., 1952, Ann. Physik, 11, 65.

Harris, J., 1969, Nature, 223, 1046.

Hartmann, J., 1904, Ap.J. 19, 268.

Heger, M.L., 1919, Lick Obs. Bull. 10, 141.

Heger, M.L., 1921, Lick Obs. Bull. 10, 146.

Heller, W., 1965, J.Chem. Phys. 42, 1609.

Herbig, G.H., 1963, Ap.J. 137, 200.

Herbig, G.H., 1966, Z.f.Ap. 64, 512.

Herbig, G.H., 1967, in 'Radio Astronomy and the Galactic System', I.A.U. Symposium no. 31, ed. van Woerden, p.85.

Herzberg, G., 1955, Mem. Soc. R. Sci. Liege (4), 15, 291.

Herzberg, G., 1965, J.Opt.Soc.Am. 55, 229.

Herzberg, G., 1967, in 'Radio Astronomy and the Galactic System', I.A.U. Symposium no. 31, ed. van Woerden, p.91.

Herzfeld, K.F. and Wolf, K.L., 1925, Ann. Physik, 78, 35.

Hiltner, W.A., Ap.J.Suppl. 2, 389, (1956).

Hiltner, W.A. and Williams, R.C., 1946, 'Photometric Atlas of Stellar Spectra', Univ. Michigan Press.

Hobbs, L.M., 1971, Ap.J. 166, 333.

Hoffleit, D., 1964, Catalogue of Bright Stars, Yale Univ. Obs.

Hoyle, F. and Wickramasinghe, N.C., 1962, M.N.R.A.S., 124, 417.

Hoyle, F. and Wickramasinghe, N.C., 1967, Nature, 214, 969.

Hoyle, F. and Wickramasinghe, N.C., 1970, Nature, 226, 62.

Huffmann, D.R., 1970, Nature, 228, 843.

Huffmann, D.R., and Stapp, J.L., 1971, Nature Phys. Sci. 229, 45.

Isobe, S., 1970, Pub. Astr. Soc. Japan, 22, 429.

Jaycock, M.J. and Parfitt, G.D., 1962, Nature, 194, 77.

Johnson, F.M., 1965, in 'Interstellar Grains', NASA SP-140, p.229.

Johnson, F.M., 1970, Electro-optical Systems Report 4022 = NASA CR-1667.

Johnson, H.L., 1965, in 'Stars and Stellar Systems', VII, 'Nebulae and Interstellar Matter', Chicago, p.167.

Johnson, H.L. and Morgan, W.W., 1954, Ap.J. 119, 344.

Kattawar, G.W. and Plass, G.N., 1967, Appl. Opt. 6, 1377.

Kellmann, S.A., 1970, P.A.S.P. 82, 1368.

Kelly, A., 1971, Ap. Space Sci. (in the press).

Kerker, M., 1969, 'Scattering of Light and Other Electromagnetic Radiation', Academic Press.

Kerker, M., Kratohvil, J.P., and Matijevic, E., 1962, J. Opt. Soc. Am. 52, 551.

Knacke, R.F., Gaustad, J.E., Gillett, F.C., and Stein, W.A., 1969a, Ap.J. 155, L189.

Knacke, R.F., Cudaback, D.D. and Gaustad, J.E., 1969b, Ap.J. 158, 151.

Krishna Swamy, K.S. and Donn, B., 1969, Nature, 224, 788.

Kristenson, H. and Rudkjøbing, M., 1965, J. Observateurs 48, 107.

Lenham, A.P. and Treherne, D.M., 1966a, in 'Optical Properties and Electronic Structure of Metals and Alloys', ed. Abelès.

Lenham, A.P. and Treherne, D.M., 1966b, Observatory, 86, 36.

Lindblad, B., 1935, Nature, 135, 133.

Manning, P.G., 1970, Nature, 227, 1123.

McGee, J.D., Khogali, A., Ganson, A. and Baum, W.A., 1966, Adv. Electr. Electron Phys. 22, 11.

McGee, J.D., McMullen, D., Bacik, H. and Oliver, M., 1969, Adv. Electr. Electron Phys. 28, 61.

McKellar, A., 1940, P.A.S.P. 52, 187 and 312 ; 53, 233.

Merrill, P.W., 1930, Ap.J., 72, 98.

Merrill, P.W., 1934, P.A.S.P. 46, 206.

Merrill, P.W., 1936, Ap.J. 83, 126.

Merrill, P.W. and Humason, M.L., 1938, P.A.S.P. 50, 212.

Merrill, P.W., Sanford, R.F., Wilson, O.C., and Burwell, C.G., 1937, Ap.J. 86, 274.

Merrill, P.W. and Wilson, O.C., 1938, Ap.J. 87, 9.

Mie, G., 1908, Ann.Physik, 25, 377.

Möglich, F., 1927, Ann. Physik, 83, 609.

Moore, C.E., 1959, Revised Multiplet Table of Astrophysical Interest.

Morgan, W.W., 1939, Ap.J. 90, 632.

Morgan, W.W., 1944, Astron. J. 51, 21.

Münch, L. and Morgan, W.W., 1953, Ap.J. 118, 161.

Nandy, K., 1964, Pub. Roy. Obs. Edin., 3, 142.

Nandy, K., 1968, Pub. Roy. Obs. Edin., 6, 169.

Nandy, K., Seddon, H., Wolstencroft, R.D., Ireland, J., and Wickramasinghe, N.C., 1968, Nature, 218, 1236.

Nandy, K., and Seddon, H., 1970, Nature, 227, 264.

Oort, J.M. and Van de Hulst, H.C., 1946, Bull. Astr. Neth., 10, 187.

Platt, J.R., 1956, Ap.J., 123, 486.

Rayleigh, Lord, 1871, Phil. Mag. 41, 107, 274, and 447.

Rayleigh, Lord, 1897, Phil. Mag. 94, 28.

Reddish, V.C., 1967, M.N.R.A.S., 135, 251.

Reddish, V.C., 1970, Mem. R. Soc. Sci. Liege, 19, 67.

Reddish, V.C., 1971, Nature, 232, 40.

Reddish, V.C., Lawrence, L.C. and Pratt, N.M., 1966, Pub.Roy.Obs.Edin.5, 111.

Rudkjøbing, M., 1969, Ap. Space Sci., 3, 102 ; 5, 68.

Runciman, W.A., 1970, Nature, 228, 843.

Russell, H.N., 1922, Proc. Nat. Acad. Sci. 8, 115.

Russell, H.N., 1935, M.N.R.A.S., 95, 635.

Saha, M.N., 1937, Nature, 139, 840.

Schalén, C., 1939, Uppsala Astr. Obs. Ann., 1, no.2.

Schalén, C., 1965, Arkiv f. Astron., 4, no.1.

Schulte, D.H., 1958, Ap.J. 128, 41.

Seddon, H., 1967, Nature, 214, 257 ; 215, 495.

Seddon, H., 1968, Nature, 217, 932.

Seddon, H., 1969, Nature, 222, 757.

Shah and Vardya, 1971, Ap. Space Sci. (in the press).

Sharpless, S., 1957, P.A.S.P., 69, 239.

Smyth, M.J. and Brand, P.W.J.L., 1969, Adv. Electr. Electron Phys. 28,737.

Stoeckly, R. and Dressler, K., 1964, Ap.J. 139, 240.

Svoloupolos, S.N., 1963, P.A.S.P. 75, 73.

Swings, P., 1937, M.N.R.A.S. 97, 212.

Swings, P. and Öhman, Y., 1939, Observatory, 62, 150.

Taft, E.A. and Phillip, H.R., 1965, Phys. Rev., 138, A197.

Thompson, G.I., 1966, Pub.Roy.Obs.Edin. 5, 245.

Thompson, G.I., 1971, Pub. Roy.Obs.Edin.7, 19.

Underhill, A.B., 1948, Ap.J. 107, 349.

Underhill, A.B., 1966, 'The Early Type Stars', Riedel.

Unsöld, A., 1963, Z. f.Ap. 56, 221.

Unsöld, A., 1964, Pub. Roy. Obs. Edin. 4, 35.

Van de Hulst, H.C., 1946, Rech. Astr. Obs. Utrecht, 11, part 1.

Van de Hulst, H.C., 1948, Harvard Obs. Monographs, no.7, p.73.

Van de Hulst, H.C., 1949, Rech. Astr. Obs. Utrecht, 11, part 2.

Van de Hulst, H.C., 1957, 'Light Scattering by Small Particles', Wiley.

Walker, G.A.H., 1963, M.N.R.A.S., 125, 141.

Walker, G.A.H., and Hodge, P., 1966, Pub.Dom.Astr.Obs. 12, 401.

Walker, G.A.H., Hutchings, J.B. and Younger, P.F., 1970, in 'Ultraviolet Stellar Spectra and Related Ground-based Observations', I.A.U. Symp. 36, ed. Houziaux & Butler, Riedel, p.52.

Wampler, E.J., 1963, Astron. J. 68, 81.

Wampler, E.J., 1966, Ap.J. 144, 921.

Whitney, C.A., 1964, Astron. J. 69, 564.

Wickramasinghe, N.C., 1967, 'Interstellar Grains', Chapman and Hall.

Wickramasinghe, N.C., Ireland, J., Nandy, K., Seddon, H., and Wolstencroft, R.D., 1968, Nature., 217, 412.

Wickramasinghe, N.C. and Krishna Swamy, K.S., 1969, M.N.R.A.S.144, 41.

Wickramasinghe, N.C. and Nandy, K., 1968, Nature, 219, 1347.

Wickramasinghe, N.C. and Nandy, K., 1970a, Ap. Space Sci., 6, 154.

Wickramasinghe, N.C. and Nandy, K., 1970b, Nature, 227, 51.

Wickramasinghe, N.C. and Nandy, K., 1971a, Nature Phys. Sci. 229, 81.

Wickramasinghe, N.C. and Nandy, K., 1971b, Nature Phys. Sci. 229, 234.

Wickramasinghe, N.C. and Reddish, V.C., 1968, Nature, 218, 661.

Wilson, R. , 1956, Pub.Roy.Obs.Edin. 2, 3.

Wilson, R., 1958a, Ap.J. 128, 57.

Wilson, R., 1958b, Pub.Roy.Obs.Edin.2, 61.

Wilson, R., 1964, Pub.Roy.Obs.Edin. 4, 67.

Wolff, N.J. and Ney, E.P., 1969, Ap.J. 155, L181.

Wolstencroft, R.D., Ireland, J., Nandy, K. and Seddon, H., 1969, M.N.R.A.S. 144, 245.

Wright, W.H., 1921, Lick Obs. Bull., 10, 108.

York, D.G., 1971, Ap.J. 166, 65.
